UNIVERSIDADE FEDERAL DE SANTA CATARINA
CENTRO TECNOLÓGICO
PROGRAMA DE PÓS-GRADUAÇÃO EM ENGENHARIA QUÍMICA

Thuany Naiara Silva Laurintino

High-pressure phase equilibrium data and coprecipitation of methionine and ethyl cellulose in carbon dioxide + ethanol + acetic acid

Florianópolis
2023

Thuany Naiara Silva Laurintino

High-pressure phase equilibrium data and coprecipitation of methionine and ethyl cellulose in carbon dioxide + ethanol + acetic acid

Tese submetida ao Programa de Pós-Graduação em Engenharia Química da Universidade Federal de Santa Catarina como requisito para a obtenção do título de Doutora em Desenvolvimento de Processos Químicos e Biotecnológicos.

Orientador: Prof. Dr.José Vladimir de Oliveira
Coorientador: Prof. Dr. Ariovaldo Bolzan,
Dr. Evertan Rebelatto

Florianópolis
2023

Ficha de identificação da obra elaborada pelo autor,
através do Programa de Geração Automática da Biblioteca Universitária da UFSC.

Laurintino, Thuany Naiara Silva
HIGH-PRESSURE PHASE EQUILIBRIUM DATA AND COPRECIPITATION OF METHIONINE AND ETHYL CELLULOSE IN CARBON DIOXIDE + ETHANOL + ACETIC ACID / Thuany Naiara Silva Laurintino ; orientador, José Vladimir de Oliveira, coorientador, Ariovaldo Bolzan, coorientador, Evertan Antônio Rebelatto, 2022.
125 p.

Tese (doutorado) - Universidade Federal de Santa Catarina, Centro Tecnológico, Programa de Pós-Graduação em Engenharia Química, Florianópolis, 2022.

Inclui referências.

1. Engenharia Química. 2. phase behaviour. 3. gas antisolvent. 4. methionine. 5. ethyl cellulose. I. de Oliveira, José Vladimir . II. Bolzan, Ariovaldo. III. Rebelatto, Evertan Antônio IV. Universidade Federal de Santa Catarina. Programa de Pós-Graduação em Engenharia Química. V. Título.

Thuany Naiara Silva Laurintino

High-pressure phase equilibrium data and coprecipitation of methionine and ethyl cellulose in carbon dioxide + ethanol + acetic acid

Esta tese de doutorado foi avaliada e aprovada pelos seguintes membros:

Profª. Dra. Ana Paula Serafini Immich Boemo
UFSC/PósENQ
Prof Dr. Marcelo Lanza
UFSC/PPGEAL
Dr. Gean Pablo Silva Aguiar
Sebrae/SC

Certificamos que esta é a versão original e final do trabalho de conclusão que foi julgado adequado para obtenção do título de doutor em Engenharia Química.

ICP-Edu
Documento assinado digitalmente
Debora de Oliveira
Data: 27/04/2023 11:31:21-0300
CPF: ***.453.929-**
Verifique as assinaturas em https://v.ufsc.br

_____

Profª. Dra. Débora de Oliveira
Coordenação do Programa de Pós-Graduação

ICP-Edu
Documento assinado digitalmente
Jose Vladimir de Oliveira
Data: 27/04/2023 11:40:31-0300
CPF: ***.858.198-**
Verifique as assinaturas em https://v.ufsc.br

_____

Prof. Dr. José Vladimir de Oliveira
Orientador

Florianópolis, 2023

Dedico este trabalho aos meus avós, Amauri e Diva, aos meus pais, Serafim e Veralúcia, e a minha irmã Thaíris, por todo amor, dedicação e incentivo.

AGRADECIMENTOS

À Deus, pela proteção, força e paz interior. Por me encorajar nos momentos em que tudo parecia impossível e colocar pessoas tão especiais no meu caminho.

À toda minha família, a quem devo tudo o que eu sou. Em especial, aos meus pais, Serafim e Veralúcia, e a minha irmã Thaíris, por todos amor, dedicação, ensinamento e incentivo.

Aos meus avós, Amauri e Diva, pelo exemplo de amor, serenidade e dedicação. Obrigada por me incentivarem e vibrarem a cada vitória conquistada.

Aos professores Dr. Vladimir de Oliveira e Dr. Ariovaldo Bolzan, pela orientação, dedicação e incentivo. Obrigada por serem tão prestativos e atenciosos! Vocês são exemplos, não só como excelentes profissionais, mas como pessoas também. Obrigada por todos os conselhos e ensinamentos!

Ao Evertan Rebelatto, pela coorientação, dedicação, conhecimento compartilhado e incentivo. Obrigada por não medir esforços para ajudar! Obrigada por me acompanhar nos vários experimentos ao longo do dia e por sempre buscar formas diferentes para facilitar o entendimento dos assuntos complexos, até desenhando, se fosse preciso. Meu muito obrigada por tudo!

Aos membros da banca examinadora, por terem aceitado o convite para contribuírem valiosamente com este trabalho.

Aos amigos do Laboratório de Termodinâmica e Tecnologia Supercrítica (LATESC) e Laboratório de Controle de Processos (LCP). Obrigada pela companhia, conversas e ensinamentos compartilhados. Pelo apoio nas horas difíceis, por todo o carinho.

A Patricia Oliveira e ao Jônatas Lopes por toda ajuda ao longo de todo o processo experimental. Obrigada pelo incentivo e auxílio no entendimento dos fenômenos envolvidos! Obrigada por me acompanharem na rotina complexa dos experimentos. Obrigada por tudo!

À CAPES e FAPESC pelo apoio financeiro.

Enfim, agradeço a todos que torceram, oraram e contribuíram para que este trabalho se tornasse realidade. Meu muito obrigada!

“Nem tudo é fácil na vida. Mas, com certeza, nada é impossível. Precisamos acreditar, ter fé e lutar para que não apenas sonhemos, mas também tornemos todos esses desejos realidade."

Cecília Meirelles

RESUMO

Para potencial aplicação na liberação controlada de partículas de metionina, o presente trabalho visou encapsular este aminoácido em etilcelulose pela técnica de gas antissolvente, utilizando dióxido de carbono como antissolvente e etanol e ácido acético como solventes. Além disso, para obter condições ótimas de precipitação, o estudo do comportamento de fases do sistema em altas pressões e a modelagem termodinâmica foi realizada utilizando a equação de estado de Peng-Robinson. Os dados de transição de fase foram obtidos pelo método visual sintético, com célula de visualização de volume variável, na faixa de temperatura de 308-328 K. Para os sistemas quaternários, os solutos foram previamente solubilizados em duas concentrações diferentes, 0,1 e 0,2 mg/mL para metionina e 2,5 e 5,0 mg/mL para etilcelulose, em uma solução de etanol e ácido acético com razão em massa de etanol para ácido acético de 1:1. Uma mistura de solventes é usada porque a metionina tem uma alta solubilidade em ácido acético, mas baixa solubilidade em etanol. Assim, foram observadas transições de fase líquido-vapor, caracterizadas como bolhas na presença ou ausência de uma fase sólida. A fase sólida foi observada em frações de massa de 0,9383 (0,1 mg/mL) e 0,7251 (0,2 mg/mL) para metionina e 0,9530 (2,5 mg/mL) e 0,8997 (5,0 mg/mL) para etilcelulose, nas três temperaturas avaliadas (308-318-328 K). Em relação a encapsulação da metionina em etilcelulose com etanol e ácido acético como solvente de mistura, a influência da razão metionina/polímero (1:3, 1:2 e 1:1), temperatura (308, 313 e 318 K) e pressão (10, 12 e 14 MPa) em termos de tamanho de partícula, morfologia das partículas, porcentagem de material encapsulado, eficiência de encapsulamento e rendimento de precipitação foram avaliados. Foram obtidas eficiências de encapsulamento de até 99,72%, para as quais a relação metionina/polímero do sistema mostrou um efeito negativo (nível de confiança de 95%). Os coprecipitados apresentaram resultados excelentes e pioneiros em termos de proteção da metionina e possível liberação controlada.

Palavras-chave: comportamento de fases; encapsulação; gas antissolvente; dióxido de carbono supercrítico; metionina; etilcelulose.

RESUMO EXPANDIDO

Introdução

A técnica envolvendo o CO_2 supercrítico como antissolvente é adequada para formar micro ou nanopartículas poliméricas visando a proteção de uma substância bioativa. Nesse processo, o poder de solubilização do material polimérico (material encapsulante) e do composto ativo (material a ser encapsulado) no solvente primário é reduzido pela expansão da solução ativa devido à adição do fluido supercrítico. A metionina, aminoácido essencial, apresenta grande importância no organismo humano, pois atua na metilação intracelular, servindo como a única fonte do doador de metila universal S-adenosil-metionina. Além disso, essa importância atinge os animais ruminantes, já que é considerada um aminoácido limitante para vacas leiteiras. Nesse caso, a metionina deve ser protegida contra a degradação microbiana do rúmen. Os revestimentos precisam ser formulados com materiais inteligentes, mostrando sensibilidade ao pH. Nesse contexto, a etilcelulose se destaca por ser sensível ao pH, atóxica, estável e biocompatível. Até o presente momento, nenhuma pesquisa descreveu o comportamento de fases dos sistemas quaternários envolvendo dióxido de carbono, etanol, ácido acético e soluto (metionina ou etilcelulose) em altas pressões, visando uma aplicação direta ao processo de encapsulamento da metionina, usando etilcelulose como agente encapsulante e o processo GAS.

Objetivos

A presente tese visa encapsular a metionina pela técnica GAS usando dióxido de carbono como antissolvente e etanol e ácido acético como solventes. Deste modo, este trabalho busca estudar o equilíbrio líquido-vapor a alta pressão de diferentes sistemas quaternários, aplicar a modelagem matemática nos dados experimentais utilizando a equação cúbica de estado de Peng-Robinson e verificar a influência da relação metionina/polímero, temperatura e pressão na coprecipitação de metionina em etilcelulose usando a técnica GAS.

Metodologia

Os dados experimentais de equilíbrio de fase foram obtidos pelo método sintético, em temperaturas de 308 a 328 K e pressões de 6,19 a 11,15 MPa. Foram avaliados sistemas quaternários envolvendo CO_2, etanol, ácido acético e soluto (metionina ou etilcelulose). Transições de fase do tipo vapor-líquido foram observadas, caracterizadas como bolhas na presença ou ausência de fase sólida. Além disso, foi aplicado um planejamento experimental 2^3 com três pontos centrais para avaliar a influência da razão metionina/polímero (1:3, 1:2 e 1:1), temperatura (308, 313 e 318 K) e pressão (10, 12 e 14 MPa) em termos de porcentagem de material encapsulado, eficiência de encapsulamento e rendimento de precipitação. Os encapsulados foram caracterizados em termos de morfologia e diâmetro de partícula usando microscopia eletrônica de varredura (MEV), difração de raios X em pó (DRX), espectroscopia de infravermelho por transformada de Fourier (FTIR), perfis calorimétricos com calorimetria exploratória diferencial (DSC) e solvente residual.

Resultados e discussões

A partir do método sintético visual, foi possível apresentar dados pioneiros sobre o comportamento dos solutos de interesse e a visualização dos efeitos da dimerização. O aumento na concentração de soluto antecipou a presença de sólidos para frações mássicas menores de CO_2. Esse comportamento pode ser explicado pela ação do CO_2 como antissolvente. Uma fase sólida foi observada para todas as concentrações de soluto avaliadas neste estudo. A determinação da região de precipitação da metionina ou etilcelulose é importante para identificar a concentração ótima da mistura solvente/soluto, onde o CO_2 atuará fortemente como antissolvente, garantindo uma alta eficiência da técnica GAS. A modelagem termodinâmica apresentou resultados satisfatórios, onde a equação de estado de Peng-Robinson descreveu adequadamente os dados experimentais de transição de fase medidos para os sistemas quaternários. A técnica GAS foi adequada para a encapsulação da metionina, proporcionando valores de rendimento de precipitação chegando a 84 % e valores de eficiência de encapsulamento de até 99,72%. As partículas apresentaram morfologia irregular com diâmetros de 29,93 a 68,89 μm, onde os diâmetros obtidos foram significativamente menores que os dos materiais não processados correspondentes. A relação MET/ETIL revelou um efeito negativo no diâmetro das partículas (nível de confiança de 95%), ou seja, uma diminuição na relação MET/polímero (maior quantidade de etilcelulose) proporcionou coprecipitados com diâmetros maiores. Este efeito negativo também foi observado pela pressão. A temperatura mostrou um efeito positivo, assim, quando a temperatura dos experimentos foi aumentada, o diâmetro das partículas dos coprecipitados aumentou. Sobre as caracterizações das partículas formadas, as análises DRX verificaram a ausência de picos característicos da metionina devido à interferência do arranjo das moléculas de etilcelulose nas moléculas de metionina durante a precipitação, FTIR confirmou a presença de metionina e a ausência de alterações químicas no processo de coprecipitação e DSC mostrou que a etilcelulose não foi afetada pela coprecipitação supercrítica.

Considerações finais

Encapsular a metionina em etilcelulose pela técnica GAS, usando dióxido de carbono como antissolvente e etanol e ácido acético como solventes, foi realizado com sucesso. O equilíbrio líquido-vapor de alta pressão para os sistemas quaternários forneceu dados pioneiros sobre o comportamento dos solutos e a visualização dos efeitos da dimerização. A modelagem termodinâmica ajustou satisfatoriamente os dados experimentais de transição de fase. Os coprecipitados apresentaram excelentes resultados quanto à proteção da metionina e possível liberação controlada, reduzindo assim as desvantagens sofridas com o uso direto deste aminoácido. As técnicas de caracterização confirmaram a presença da metionina e a ausência de alterações químicas no processo de coprecipitação. Assim, o método de encapsulação utilizando a técnica GAS e o uso do biopolímero de etilcelulose como agente encapsulante surge como uma possível alternativa para a proteção, preservação das propriedades e controle da entrega da metionina.

Palavras-chave: comportamento de fases; encapsulação; gas antissolvente; dióxido de carbono supercrítico; metionina; etilcelulose.

ABSTRACT

For potential application to the controlled release of methionine particles, the present work aimed to encapsulate this amino acid in ethyl cellulose by the antisolvent gas technique, using carbon dioxide as antisolvent and ethanol and acetic acid as solvents. Furthermore, to obtain the optimum precipitation conditions, the phase behavior of the system at high pressures was studied, and the thermodynamic modeling was performed using the Peng-Robinson equation of state. Phase transition data were obtained by the synthetic visual method, with a variable volume visualization cell, in the temperature range of 308-328 K. For the quaternary systems, the solutes were previously solubilized in two different concentrations, 0.1 and 0.2 mg/mL for methionine and 2.5 and 5.0 mg/mL for ethyl cellulose, in a solution of ethanol and acetic acid with 1:1 mass ratio of ethanol to acetic acid. A mixture of solvents is used because methionine has a high solubility in acetic acid but low solubility in ethanol. Thus, liquid-vapor phase transitions were observed, characterized as bubbles in the presence or absence of a solid phase. The solid phase was observed in mass fractions of 0.9383 (0.1 mg/mL) and 0.7251 (0.2 mg/mL) for methionine and 0.9530 (2.5 mg/mL) and 0.8997 (5.0 mg/mL) for ethyl cellulose, at the three temperatures evaluated (308-318-328 K). Regarding the encapsulation of methionine in ethyl cellulose with ethanol and acetic acid as a mixture solvent, the influence of methionine/polymer ratio (1:3, 1:2, and 1:1), temperature (308, 313, and 318 K), and pressure (10, 12, and 14 MPa) in terms of particle size, morphology of the particles, percentage of encapsulated material, encapsulation efficiency, and yield of precipitation were evaluated. Encapsulation efficiencies as high as 99.72 % were obtained, for which the system methionine/polymer ratio showed a negative effect (95% confidence level). The co-precipitates showed excellent and pioneering results in terms of methionine protection and controlled release possible.

Keywords: phase behaviour; encapsulation; gas antisolvent; supercritical carbon dioxide; methionine; ethyl cellulose.

LIST OF FIGURES

LIST OF TABLES

LIST OF DIAGRAMS

SUMMARY

CONCEPTUAL DIAGRAM OF WORK

Initially, a Conceptual Diagram is presented regarding the main points and questions to be answered with the development of the proposed work entitled: precipitation of methionine and ethyl cellulose in carbon dioxide + ethanol + acetic acid systems at high pressures: phase equilibrium data and encapsulation by the antisolvent gas process.

Because?

i. Methionine is the first limiting amino acid for dairy cows;
ii. Encapsulation allows for greater bioavailability and controlled and specific release at the site of maximum absorption;
iii. Supercritical technology is an alternative to traditional encapsulation techniques.

Who has done?

i. There aren't works on the encapsulation of methionine by supercritical fluid in the literature;
ii. Scarcity of studies that present particles with rumen protection and release in the specific gastrointestinal tract.

What is the hypothesis?

i. Is it possible to encapsulate the methionine using techniques employing CO_2 as an antisolvent?
ii. Will encapsulated methionine show better properties compared to the unprocessed version?
iii. Is it possible to achieve a controlled release in the desired environment?

How to make?

i. Evaluate the phase behavior of the system selected to encapsulate the methionine;
ii. Study the methionine encapsulation process using supercritical technologies, such as the GAS technique;
iii. Evaluate the properties of the particles formed and the encapsulation efficiency.

THESIS METHODOLOGICAL SEQUENCE FLOWCHART

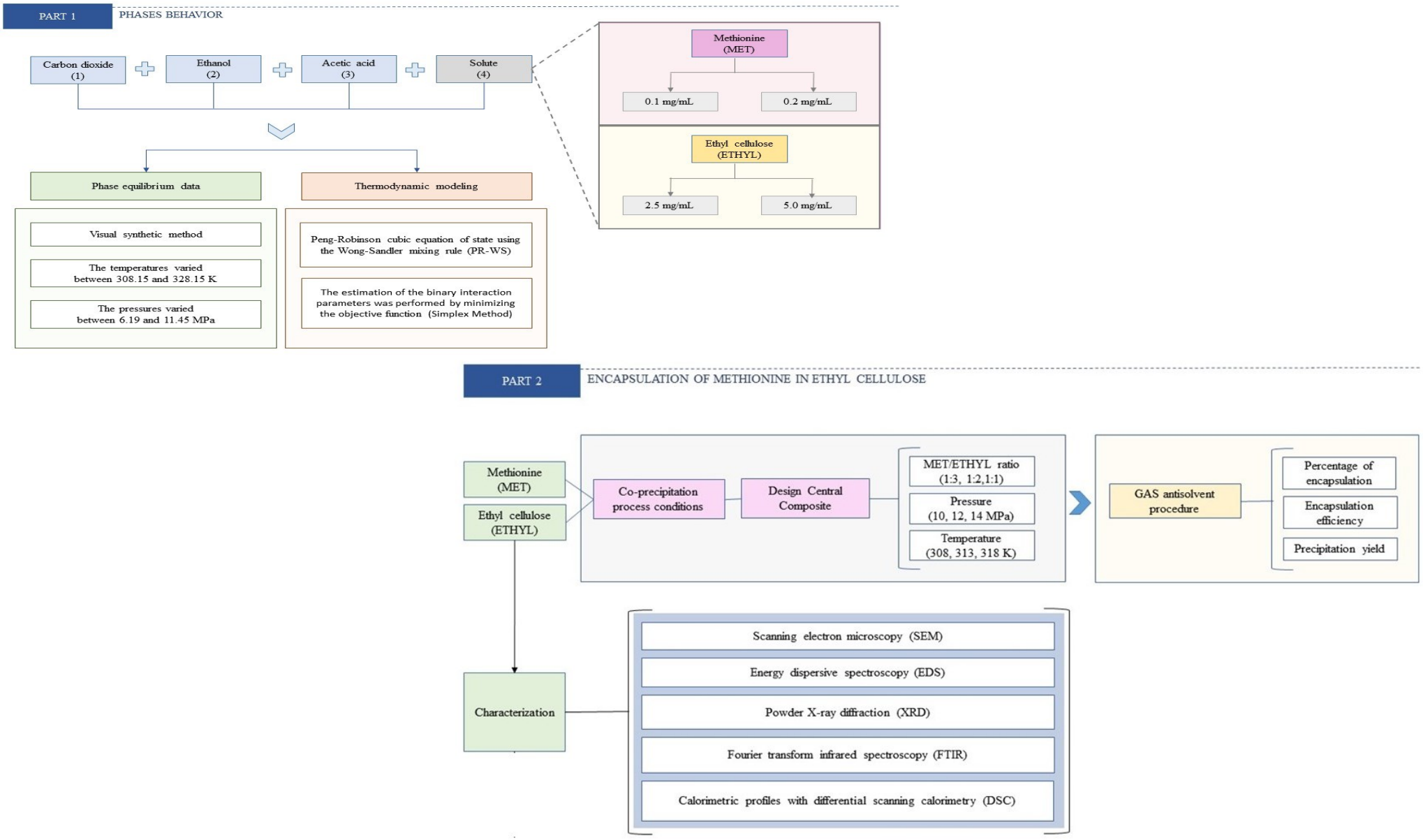

CHAPTER 1 - INTRODUCTION

The technology involving the formation of particles on the nanometer and/or micrometer scale presents high growth in different industrial sectors, with competition in the search for high-quality and increasingly innovative products. These particles may have a structure of capsules or spheres. In the spheres, the bioactive substance is dissolved in the polymer matrix. In capsules, the drugs are confined in a cavity, like a core-shell, where they can isolate and protect the encapsulated material from the external environment using an inert layer. Both particulate systems present high efficiency in the controlled release of actives in specific locations (JONG; BORM, 2008; MORA-HUERTAS, 2010).

Different techniques can be used to form particles. Some traditional methods, such as spray drying (atomization), lyophilization, and recrystallization by organic solvent, have limitations since they don't control the size of the particles formed and may involve excessive use of organic solvents, requiring post-processing steps. In addition, the conditions applied in traditional techniques may cause thermal and chemical degradation of the solute, which is not desirable.

Thus, techniques involving supercritical fluids are used as alternatives to traditional processes. Besides allowing the formation of particles with desired sizes, morphology, and distribution of particles, supercritical technology is considered a sustainable, environmentally correct, and efficient technique. Supercritical processes can be classified according to the function of the supercritical fluid in the process, divided into three main categories: solvent, solute, or antisolvent.

The technique involving supercritical CO_2 as an antisolvent is suitable for forming polymeric micro or nanoparticles aiming at the protection of a bioactive substance. In this process, the solubilization power of the polymeric material (encapsulating material) and the active compound (material to be encapsulated) in the primary solvent are reduced through the expansion of the active solution due to the addition of the supercritical fluid.

Several materials can be encapsulated, such as methionine, for example. Methionine is an amino acid of great importance for lactating dairy cows, as it directly affects the quality and quantity of milk these animals produce. Thus, this amino acid needs to be supplied in the diets efficiently so that the absorption is satisfactory,

guaranteeing the advantages related to its presence in the organisms of these ruminants.

Knowing the importance of methionine for dairy cows, where methionine is the first limiting amino acid for protein synthesis and the rumen constitutes an obstacle to the safe delivery of this amino acid, techniques with supercritical fluids can be used to encapsulate this amino acid efficiently. Thus, encapsulation seeks to prevent the polymeric coating from being degraded in the rumen, favoring the release of methionine in the specific gastrointestinal tract for rapid absorption.

However, for the proper application of the precipitation process using the GAS technique, mainly in systems involving mixtures of components, it is necessary to know the phase equilibrium so that optimal precipitation conditions can be selected, enabling the encapsulation process and optimizing the choice of operational variables, obtaining particles with preferred size and morphology.

Furthermore, the thermodynamic behavior of the studied systems can be represented in mathematical language through equations of state. Among the different types of equations, the cubic equations of the Van der Waals type, especially the Peng-Robinson (PR) equations, are highlighted since they can predict the behavior of phases considering two molecular forces: repulsive, related to the size of the molecules, and attractive, related to the interaction between one molecule and another. The PR equation is considered a reliable equation, capable of describing the thermodynamic behavior of different systems under different conditions of temperature, pressure, and composition (WEI; SADUS, 2000; MEDEIROS; ARREDONDO, 2008).

In the present work, a synthetic static method is used to collect measurement data on the behavior of the carbon dioxide + ethanol + acetic acid + solute system, where the solute can be methionine or ethyl cellulose. The literature did not describe the equilibrium behavior of these quaternary mixtures. The objective is to collect and model measurement data in a range that could be applied directly to methionine encapsulation, using ethyl cellulose as an encapsulating agent and the GAS process.

1.1 OBJECTIVES

1.1.1 General objective

Encapsulate methionine by the GAS technique using carbon dioxide as an antisolvent and ethanol and acetic acid as solvents.

1.1.2 Specific objectives

In line with the general objective, the following specific objectives were established:

1. Study the high pressure liquid-vapor equilibrium of different systems;
    a) Experimentally determine phase equilibrium data for the following quaternary systems;:
        - CO_2 (1) + ethanol (2) + acetic acid (3) + methionine (4);
        - CO_2 (1) + ethanol (2) + acetic acid (3) + ethyl cellulose (4);
    b) Evaluate the influence of the interaction of the compounds involved in the systems;
    c) Check the interference of different concentrations of solutes on the behavior of phases;
    d) Determine the region and conditions of solid precipitation.
2. Thermodynamic modelling;
    a) Fit the experimental data of the quaternary systems using the Peng-Robinson cubic equation of state using the Wong-Sandler mixing rule (PR-WS).
3. Encapsulate methionine using the GAS technique;
    a) Check the influence of pressure, temperature and mass ratio between methionine and the encapsulation agent variables in the process;
    b) Determine the percentage of encapsulation (PE) and encapsulation efficiency (EE) of methionine in the polymer matrix;
    c) Evaluate the characteristics of the particles formed in terms of morphology, particles diameter, X-ray diffraction (XRD), Fourier transform infrared spectroscopy (FTIR) and Differential scanning calorimetry (DSC).

1.1.3 Structure of the thesis

This thesis is divided into chapters, which present the development of this work. Chapter I comprises the introduction, general objective, and specific objectives developed in carrying out the thesis and its structure.

Chapter II presents a literature review, addressing relevant aspects of methionine as an agent to be encapsulated, supercritical technologies targeting encapsulation processes, thermodynamic behavior, and mathematical modeling for the phase equilibrium of different systems.

Chapter III e IV describes the methodology applied and results obtained to study methionine's phase behavior and encapsulation.

Chapter V presents the conclusions of the work.

CHAPTER 2 - LITERATURE REVIEW

This chapter aims to address aspects found in the literature, as well as contextualize the main interests and relevance of the work. Next, a brief literature review will be presented, highlighting aspects related to the main characteristics of the agent to be encapsulated (methionine), encapsulation processes using supercritical technology, phase equilibrium, and thermodynamic modeling.

2.1 AGENT TO BE ENCAPSULATED - METHIONINE

2.1.1 Ruminant animals

Food is responsible for ensuring the energy needed for the vital processes of animals, maintaining the cellular and metabolic mechanism, growth, and reproduction, for example. The digestive system is essential for these processes to occur satisfactorily, making food compounds available to the body (ALVES et al., 2016).

Ruminant animals are characterized by having digestive tracts adapted to symbiotic microorganisms, adopting specialized gastrointestinal chambers for hosting these microorganisms. Normally, these chambers correspond to a part of the gastrointestinal tract, comprised of the esophagus and stomach, which precedes the intestine (RIVERA, 2006).

The digestive tract of ruminant animals can be divided into four segments in terms of structure and function: the rumen, reticulum, omasum, and abomasum (Figure 1). The first three parts are called the pre-stomach, and the last part is related to the stomach itself (SILVA et al., 2013).

Figure 1 – Stomach compartments of a ruminant animal.

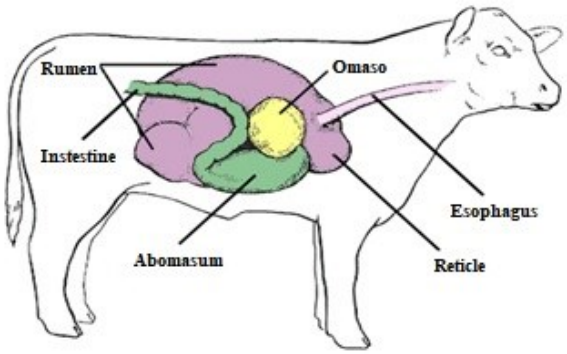

Source: Adapted from Proyecto Conocer la agricultura y la ganadería (2016).

When ruminant animals are newborns, the abomasum corresponds to the largest compartment of the stomach, and the development of the pre-stomach occurs from the ingestion of coarse food. However, when animals become adults, the rumen corresponds to the largest compartment of the pre-stomach (JUNIOR et al., 2016).

According to Schmidt-Nielsen (2002), in a compacted form, the stomach compartments of ruminant animals have the following functions:

1. Rumen – favors waterlogging and fermentation of fibrous foods. In addition, it allows the material present in its interior to be continuously mixed due to its mobility.
2. Reticulum – works like a pump, regulating the flow of liquid in and out of the rumen. This flow is of great importance, as it directs ingesta to the interior of the rumen, regulates its passage to the omasum, provides moisture to the ruminal contents, and bathes the cardio before regurgitation.
3. Omasum – works by grinding and grinding the rumen content, which can be deposited in its folds.
4. Abomasum – provides digestion of degraded and concentrated material. It corresponds to the acidic compartment of the stomach of ruminant animals.

Among ruminant animals, cows can be highlighted mainly due to their use for milk production. In Brazil, the milk production chain has high economic and social importance. In the ranking of world producers, Brazil is in third place, with more than 30 billion liters per year. And, according to projections made by the Ministry of Agriculture, Livestock, and Supply, milk production in Brazil will increase from 35.4 billion liters of milk in 2020 to values between 42.9 and 47.7 billion liters in 2030, representing an increase in annual rate terms of between 1.9 and 2.8 % (MAPA, 2020).

In addition to milk production, according to the long-term projections prepared by MAPA (2020), other points related to the production chain of milk and dairy products will show significant increases in the next ten years, such as consumption, imports, and exports. These data can be verified in Figure 2.

Figure 2 – Projection of the milk production chain (2020-2030).

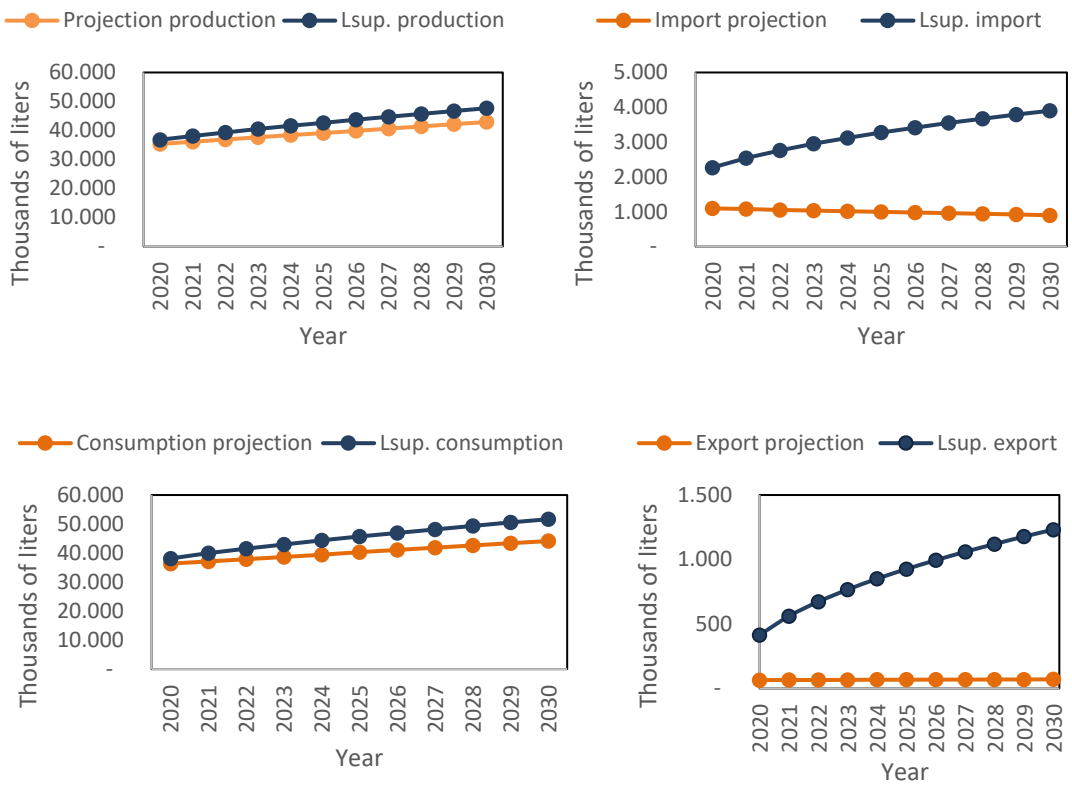

Source: Adapted from MAPA (2020).

In this way, knowing the diversity involved in the milk production chain sector and its importance for the Brazilian market, several investments can be made to optimize the cows' milk production, providing even greater advances through applying different technologies.

2.1.2 Fermentation of food in the rumen

The rumen corresponds to the stomach compartment of ruminant animals that involves food retention and microbial fermentation. Thus, the action of symbiotic microorganisms makes it possible to convert fibrous and low-quality foods into valuable nutrients.

The animal's diet partially determines the end products of fermentation. According to the feed provided to ruminants, metabolic activity can be altered by dietary changes, which can offer new substrates to microorganisms, generating different end products in fermentation. Therefore, the proportions of nutrients in the diet influence the quality of the final product obtained by fermentation. These products

will continue in the gastrointestinal tract, bringing or not benefits to the ruminant animal (BERGMAN, 1990; VALADARES FILHO; PINA, 2006).

Inside the rumen and reticulum, bacteria and protozoa are responsible for fermentation, where bacteria participate in the metabolism of 80% and protozoa of 20%, approximately. These microorganisms produce volatile short-chain fatty acids, carbon dioxide, and methane. In addition, they are involved in the hydrolysis of proteins, breaking peptides into shorter chains until free amino acids are obtained, causing significant consequences for dairy cows, which will address in the next topic (SOCHA et al., 2005; CERMAKOVA et al., 2012).

2.1.3 Degradation of ruminal protein

Proteolysis in the rumen depends on several factors, such as protein type, rumen pH, dietary starch content, and digesta passage rate. Proteolytic enzymes have an optimal pH value between 5.5 and 7.0 (MORAIS JUNIOR, 2013).

Amino acids are nutrients used for the growth of ruminal microorganisms. To bypass rumen degradation, amino acids are incorporated into microbial protein and become sources of amino acids taken up by the host animal. Generally, carrier proteins avoid ruminal degradation and direct amino acids to specific regions since they are absorbed in only some parts of the gastrointestinal tract (NATIONAL RESEARCH COUNCIL, 2001; PIEPENBRINK, 2004).

When passing the rumen, the transport proteins are submitted to extracellular proteolysis, carried out by the endopeptidases under acidic conditions. The product resulting from the digestion of proteins corresponds to a mixture of free and short-chain amino acids (oligopeptides), which will later be degraded into small peptides and some free amino acids (dipeptides and tripeptides). Then, these peptides will be hydrolyzed by intracellular peptidases, resulting only in free amino acids, which will be sent to the blood for absorption (WANG, 2010).

A balanced intake of amino acids and proteins is crucial, especially for ruminant animals. To address the amino acid deficiency, high-protein diets or preparations containing specific amino acids, such as methionine and lysine, are fed to these animals. Furthermore, when considering lactating dairy cows, methionine is the first limiting amino acid for protein synthesis, and the rumen constitutes an obstacle

to the safe delivery of this amino acid to the absorption site (NRC, 2001; PINHO, 2016; SIKORA et al., 2007).

Thus, the development of a post-ruminal transport system, mainly with limiting amino acids, can effectively reduce the loss of these nutrients along the gastrointestinal tract and obtain greater absorption in specific sites, such as the abomasum and/or small intestine. Therefore, it will be possible to get highly productive dairy cows, helping small and large dairy producers and positively moving the dairy industries.

2.1.4 Limiting amino acid (methionine)

It is known that proteins have many vital roles and are formed by amino acids in their structure, where these are classified as essential and non-essential. Essential amino acids are those not synthesized or synthesized in insufficient amounts by the body, and non-essential amino acids can be synthesized by animal tissue. The amino acids essential are arginine, histidine, isoleucine, leucine, lysine, methionine, phenylalanine, threonine, tryptophan, and valine (FROTA, 2014).

Methionine and lysine are considered limiting amino acids for dairy cows and are always present in their diets. Generally, methionine is used as a supplement for ruminant animals in its DL-methionine form or supplied from its analogs. The supplements provided need to have two essential characteristics: protection against microbial degradation of the rumen and bioavailability.

Coatings need to be formulated with smart materials, showing sensitivity to pH. The developed structure needs to maintain its integrity at ruminal pH (pH 5.4) and provoke its rupture at abomasal pH (pH 2.9), involving an immediate absorption and a quick response regarding the biological effect. In addition, the effective coating will depend on the technique and conditions used to carry out the process.

2.1.5 Methionine deficiency in the human diet

In addition to the importance in animals, amino acids are crucial for humans, as they are involved in several important biological processes such as metabolism, growth, and immunity (HE et al., 2011). These nutrients obtained from food act by maintaining an adequate nutritional status for the regulation of metabolic, physiological and neuronal homeostasis, as well as for the prevention of various diseases (STOVER et al., 2017; TRUMBO, 2008).

Methionine, a precursor of succinyl-CoA, homocysteine, cysteine, creatine, and carnitine, is an essential sulfur-containing amino acid that is catabolized and recycled in a series of metabolic reactions termed the methionine cycle. Briefly, methionine is converted to the universal methyl donor S-adenosyl-methionine (SAM), which upon donation from its methyl group, is converted to S-adenosyl-homocysteine (SAH). SAH is hydrolyzed to generate homocysteine, which is then converted to cysteine via the transsulfuration pathway back into methionine (SANDERSON et al., 2019).

One of the most prominent functions of methionine is its contribution to intracellular methylation by serving as the sole source of the universal methyl donor S-adenosyl-methionine (SAM); SAM is a necessary substrate for all methylation reactions, including those that phospholipid integrity, the activity of signaling pathways and polyamine biosynthesis. Beyond mediating these SAM-dependent reactions, methionine contributes to essential metabolic pathways that regulate nucleotide biosynthesis and intracellular redox balance (SANDERSON et al., 2019). The methionine cycle is extremely important in epigenetics for the methylation of DNA, RNA, and histones due to generating the universal cellular donor of methyl (MORELLATO et al., 2021).

Methionine also maintains cellular redox status by providing homocysteine as a substrate for the transsulfuration pathway, producing the antioxidant glutathione (GSH). The subsequent reversible oxidation of GSH to oxidized glutathione (GSSG) effectively combats cellular damage caused by reactive oxygen species (HOSIOS; HEIDEN, 2018). Further contributing to its role as a regulator of cellular oxidative stress, methionine also functions as a source of sulfur for producing the critical signaling molecule hydrogen sulfide (HINE et al., 2015). Finally, methionine is particularly important in autophagic processes (SUTTER et al., 2013) and protein synthesis via multiple mechanisms (MAZOR et al., 2018).

The levels of methionine obtained in the diet can greatly affect cellular metabolism, establishing a link between nutrition and the metabolism of tumor cells, causing tumor-specific metabolic alterations that can be influenced by the diet (SANDERSON et al., 2019).

Aissa et al. (2014) found that dietary methionine deficiency and supplementation can induce molecular abnormalities in the liver associated with the

development of non-alcoholic fatty liver disease, including altered expression of one-carbon and lipid metabolism genes leading to lipid accumulation in the liver. The authors observed that a methionine-deficient diet could substantially alter the one-carbon cellular metabolic pathway in the liver, causing marked elevations in hepatic metabolism.

Furthermore, Aissa et al. (2022) found that a methionine-deficient diet has the power to interfere with the expression of genes related to fat metabolism in liver cells. Several molecular alterations can be triggered by the absence of methyl group donors, favoring the development of different diseases, such as non-alcoholic fatty liver disease (NAFLD) in humans. The effects of diets with improper concentrations of methionine, especially methionine-deficient diets, on developing liver pathologies may involve the dysregulation of several microRNAs that play a significant role in hepatic homeostasis.

Methionine-deficient diets have been used to study the mechanisms of fatty liver disease and its progression. These diets recapitulate the phenotypes seen in humans with NAFLD (non-alcoholic fatty liver disease), including an accumulation of triglycerides in the liver (HEBBARD; GEORGE, 2011). In some cases, hepatic steatosis is an early manifestation of liver dysfunction that sometimes progresses to steatohepatitis, fibrosis, cirrhosis, and liver cancer (CHEUNG; SANYAL, 2010).

However, excess methionine in the diet can alter hepatic lipid metabolism, induce oxidative stress, and cause hepatocyte damage. Thus, methionine supplementation still needs to be studied more thoroughly to determine the ideal dosage to guarantee all the benefits involved by this amino acid. Therefore, it will be crucial to identify a clinically relevant level of dietary methionine intake that can maximize health-promoting benefits while preventing the potential toxicities associated with its restriction.

2.2 ENCAPSULATION

The nanometric and/or micrometric scale particulate systems can be applied in various industrial sectors. Due to their characteristic properties and associated advantages, these systems are highlighted for being effective vectors of active substances, with excellent ability to control and direct the release of drugs. In addition,

they can significantly contribute to the stability of different bioactive through encapsulation processes (MORA-HUERTAS, 2010).

The functionality and main properties of the particles formed are related to the size, morphology, and distribution of particles and depend on the techniques used for precipitation, where they are selected according to the product's final application. Some traditional techniques are used for particle formation, such as spray drying, lyophilization, and organic solvent recrystallization. However, these conventional techniques have some limitations, such as excessive use of organic solvents, the need for post-processing steps, and thermal and chemical degradation of the solute (HONG et al., 2000; LIN et al., 2007; PRIAMO, 2011).

Techniques based on the supercritical fluid are used to produce particles to overcome the limits involved in traditional methods. In addition, these alternative processes have lower environmental impacts, lower energy consumption, less toxic waste, better use of by-products, and better quality and safety of the final product (KNEZ et al., 2014).

The main characteristics of supercritical fluids and the different encapsulation techniques are presented below, in which CO_2 is used as a solvent, solute, and antisolvent for particle formation. In addition, the main parameters involved in determining particle size, a relevant property for the application of particulate systems, will also be addressed.

2.2.1 Supercritical fluid

The choice for processes involving supercritical fluids can be justified because they are engaged in sustainable, environmentally correct, and efficient operations. In addition, they have characteristics that allow the production of products with high added value and free from chemical residues.

Another advantage is adjusting the thermophysical properties of fluids, such as diffusivity, viscosity, density, or dielectric constant, only changing the pressure-temperature binomial (KNEZ et al., 2014).

2.2.1.1 Properties of supercritical fluids

In order to understand the main foundation of a substance in its supercritical state, it is necessary to analyze Figure 3. In the diagram, each substance has a single

critical point, defined as the required temperature, Tc, and the critical pressure, Pc, in which there is no difference between the liquid and gas phases. As represented in the figure, supercritical fluids are defined as substances that have temperatures and pressures above their critical point (ESFANDIARI, 2015).

Figure 3 – Phases diagram.

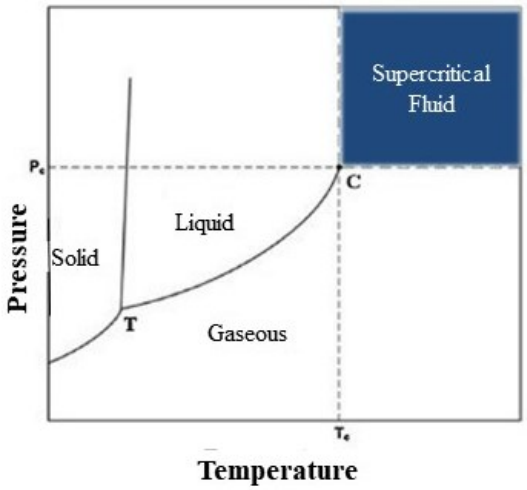

Source: Esfandiari (2015).

Analyzing the diagram, it appears that three lines delimit three regions, corresponding to the three physical states: solid, liquid, and gas. The points that lie along the lines, that is, between the states, define the equilibrium between the two phases. Vapor pressure starts at the triple point, T, and ends at the critical point, C. At the critical point, Tc corresponds to the highest temperature at which a gas can be converted to a liquid by increasing pressure. Pc corresponds to the most elevated pressure at which a liquid can be converted to a gas by increasing the temperature. In this critical shaded region, substances have gas and liquid properties.

As can be observed in Table 1, the supercritical fluid has a density close to that of liquids, a viscosity comparable to that of gases, and diffusivity with a value greater than that of liquids. Furthermore, when a fluid is above its critical conditions, such as at a pressure equivalent to four times its critical pressure, its physical properties are comparable to liquids and gases.

Table 1 – Comparison of some physical properties of gas, liquid and fluid.

Physical properties	*GAS (1atm – 30°C)*	*Supercritical fluid*		*Liquid (15-30°C)*
		T_c, P_c	T_c, $4P_c$	
Diffusion coefficient ($cm^2.s^{-1}$)	0.1-0.4	0.7×10^{-3}	0.2×10^{-3}	$(0.2\text{-}2) \times 10^{-5}$
Viscosity ($g.cm^{-1}.s^{-1}$)	$(1\text{-}3) \times 10^{-4}$	$(1\text{-}3) \times 10^{-4}$	$(3\text{-}9) \times 10^{-4}$	$(0.2\text{-}3) \times 10^{-2}$
Density ($g.L^{-1}$)	$(0.6\text{-}2) \times 10^{-3}$	0.2-0.5	0.4-0.9	0.6-0.6

Source: Santos (2012).

Different solvents are used in processes involving supercritical technology. However, critical properties, toxicity, and cost are the main factors determining the most suitable solvent. The most used solvent in technologies involving high pressures corresponds to carbon dioxide because it is cheap, innocuous, non-toxic, non-reactive, non-flammable, non-polluting, has high diffusivity, has a low critical temperature (Tc = 31.1 °C) and moderate critical pressure (P_c = 7,38 MPa) (ESFANDIARI, 2015).

2.2.2 Particle formation with supercritical fluid

Processes involving fluid in a supercritical state are an alternative to traditional methods, which present an innovative methodology for particle formation with numerous advantages. Supercritical processes can be employed in micro or nanoencapsulation processes, surface coating of an active substance particle with a polymeric material, or co-crystallization (FAGES et al., 2004).

Different methods can be employed using this technology, where classification occurs according to the role of the supercritical fluid in the process, dividing it into three main categories: solvent, solute, or antisolvent (Table 2).

Table 2 – Summary of particle formation technologies using supercritical fluids.

Function of the supercritical fluid	Abbreviation	Function of the organic solvent	Phase separation mode
Solvent	RESS	Cosolvent	Pressure/temperature induced
Solute	PGSS	-	Pressure/temperature/solvent -induced
Antisolvent	GAS	Solvent	Solvent induced
Antisolvent	SAS	Solvent	Solvent induced
Antisolvent/dispersing agent	SEDS	Solvent/non-solvent	Solvent induced

RESS, Rápida Expansão de Solução Supercrítica; PGSS, Partículas a partir de Soluções de Gas-saturado; GAS, Gas Antisolvente; SAS, Supercritical Antissolvent; SEDS, Solution Enhanced Dispersion by Supercritical Fluids)
Source: Adapted from Yeo and Kiran (2005).

The choice of the supercritical process aiming at the encapsulation of active compounds needs to be based on the solubility of the compound and the polymer matrix in the supercritical fluid. In addition, other factors must be considered, such as the particles' size, shape, and structure, the production scale, and the process's cost (SILVA; MEIRELLES, 2014).

2.2.2.1 Supercritical fluid as an antisolvent

Techniques involving the supercritical fluid as an antisolvent consist of precipitating the substrate in an organic solution. The antisolvent gas method can be highlighted among the different techniques that employ this concept.

This process has as its basic principle the recrystallization of solid compounds not soluble in supercritical fluids. Thus, this technique is suitable for forming particles of polymeric compounds due to the low solubility of most polymers in supercritical fluids or gases and for encapsulating polar components (YEO; KIRAN, 2005; SILVA; MEIRELLES, 2014).

This technique involves mixing a polymer solution with a supercritical gas or fluid (Figure 4). Thus, initially, the polymer is dissolved in a liquid organic solvent. Then a gas in a supercritical state is used as an antisolvent for the polymer, causing the particles precipitate. In addition, the formation of particles can also be observed by the

phase transition, where the output of a system from the homogeneous region (single phase) to a biphasic region (two phases) will be subjected to the separation process.

Figure 4 – (a) Schematic representation of the GAS process; (b) ternary phase diagram.

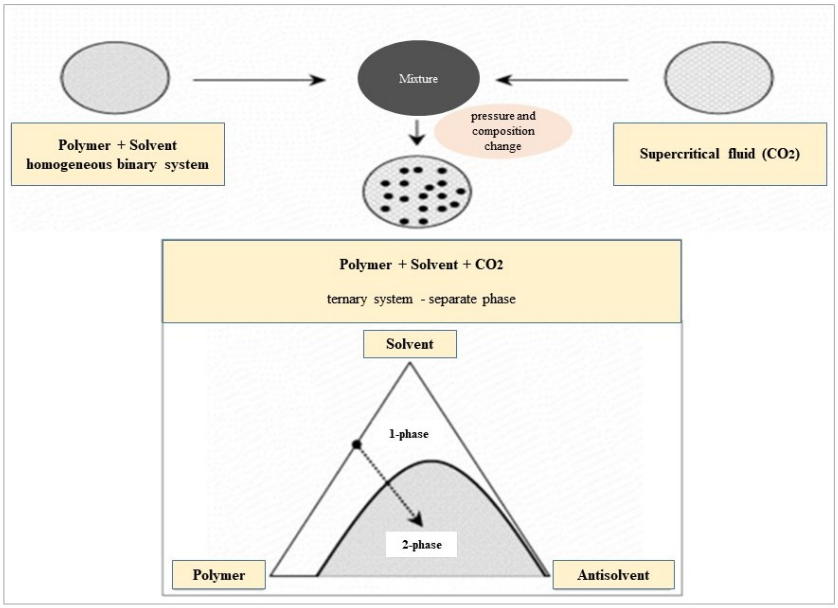

Source: Source: Adapted from Yeo and Kiran (2005).

The main difference between the GAS technique, which uses the supercritical fluid as an antisolvent, and the RESS technique, which uses the supercritical fluid as the solvent, is the formed system. The RESS technique employs a binary system formed by polymer and supercritical fluid, while the GAS technique involves a ternary system formed by polymer, organic solvent, and antisolvent gas.

Figure 5 presents the GAS process in a simplified way. As already mentioned, this process is characterized by forming an active solution, which corresponds to the solubilization of the active substance + polymer + organic solvent (primary solvent). In this technique, the solubilization power of the polymeric material (encapsulating material) and the active compound (material to be encapsulated) in the primary solvent are reduced through the expansion of the active solution due to the addition of the supercritical fluid.

Figure 5 – Simplified schematic of the GAS process.

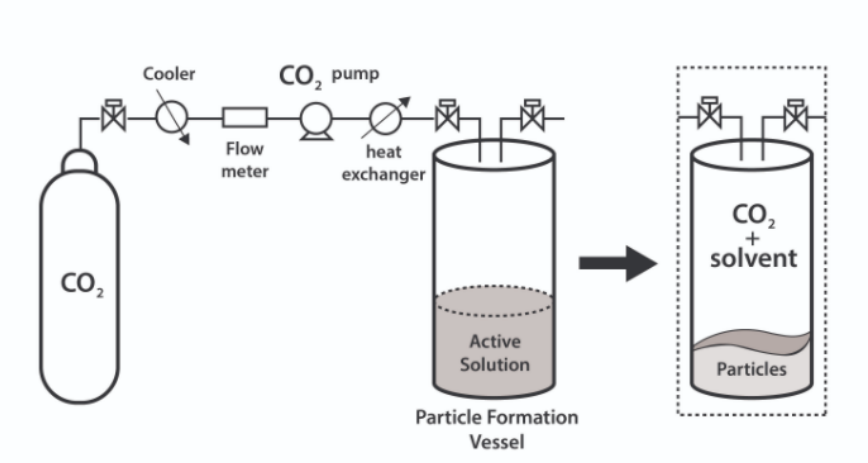

Source: SILVA; MEIRELLES, 2014.

In this way, the supercritical fluid will cause the saturation of the active solution through the mass transfer process due to the high diffusion rate, leading to a reduction in the mixture density (active solution + supercritical fluid). Density is related to the solvent power of a liquid; thus, by adding the antisolvent in the precipitation chamber, the solubility of the solute (active compound + polymer) decreases until it reaches saturation supersaturation, where the nucleation and particle formation (SILVA; MEIRELES, 2014).

2.2.3 Process parameters and particle size

Different factors directly affect the final characteristics of the encapsulated material, such as (1) properties of the chosen supercritical fluid, (2) properties of the solute, such as the bioactive compound (material to be encapsulated), polymer (encapsulating material) and organic solvent, and (3) operating conditions such as temperature, pressure, concentration, feed flow rate and antisolvent flow rate, for example (KALANI; YUNUS, 2011; SILVA; MEIRELES, 2014).

Pressure and temperature are parameters that affect the density of the supercritical fluid, where this density influences the mass transfer between the organic solvent and the supercritical fluid. Rapid mass transfer can cause high supersaturations, resulting in rapid nucleation and growth of more than one particle per primary droplet (FAGES et al., 2004).

Regarding the effects of concentration, depending on the solution's initial concentration, the particles' size can be significantly affected. In studies presented in

the literature, it is possible to observe that the supersaturation of the bioactive compound happens slowly at low concentrations, delaying precipitation and nucleation and producing smaller particles. At higher concentrations, supersaturation occurs more rapidly, with growth dominating nucleation, having larger particle sizes (REVERCHON; ADAMI, 2006; REVERCHON et al., 2008).

The chemical composition of the organic solvent also interferes significantly, where solvents of greater volatility form smaller particles due to the state of supersaturation occurring more quickly. For an effective encapsulation, the solubility of the polymer + organic solvent mixture must be greater than the solubility of the bioactive compound + organic solvent since the bioactive compound must first precipitate, followed by the polymer coating (YEO; KIRAN, 2005; KALANI; YUNUS, 2011).

The properties of the bioactive compound are related to its chemical composition, which can affect its solubility with the other compounds in the system, interfering with the formation and final size of the particle. This factor is of great importance in the GAS technique, where it is not desired that the bioactive compound be able to dissolve in the supercritical fluid. If this behavior is observed, the compound will be removed to the gas phase without any precipitation; consequently, no particles will be produced. In this way, precipitation will be rapid, the lower the solubility of the bioactive compound in the supercritical fluid (STECKEL et al., 1997; COCERO et al., 2009).

In addition, another point must be considered regarding the chemical composition of the solute and the structure of the polymer chosen as an encapsulating agent. This material, which will be used as a coating, must present characteristics such as biocompatibility, absence of toxicity, easy processing, and preservation of the properties and activity of the active compound (COCERO et al., 2009).

The polymer's properties of diffusivity and solubility in the supercritical fluid must also be considered. Among the factors that affect these properties, two are worth mentioning: (1) the molecular structure, which influences the interaction between the supercritical fluid and the molecular chains of the polymer, and (2) the morphology of the polymer, such as crystalline, semi-crystalline or amorphous (KALANI; YUNUS, 2011).

Selecting a suitable polymer is important for the desired application, where it protects the bioactive compound, preventing its degradation before the desired location and targeting absorption in specific organs.

Ethyl cellulose is a biocompatible, stable, non-toxic and hydrophobic polymer. Authors different used this polymer to form particles (DUARTE et al., 2006; LI et al., 2008; CHEN; LIU, 2008; MONTES et al., 2011; MONTES et al., 2012; DJERAFI et al., 2015; DJERAFI et al., 2017). In addition, mixtures involving ethanol and carbon dioxide are considered the best solvents for cellulosic polymers (KIRAN; POHLER, 1998; LI; MARK; HUGH, 2004).

In addition to ethanol, acetic acid can be used to improve the solubility of solutes. This solvent has unique characteristics caused by the dimerization effect since the pure solvent consists of monomers and dimers. In figure 6, it is possible to identify the degree of dimerization of pure acetic acid along a coexistence curve, that is, vapor + liquid. Thus, the liquid phase is predominantly composed of dimers, and the degree of dimerization increases with decreasing temperature.

Figure 6 – Dimerization degree. (a) of acetic acid along the coexistence curve (vapor + liquid) and (b) of acetic acid in the liquid and gas phases coexisting in the binary system with carbon dioxide.

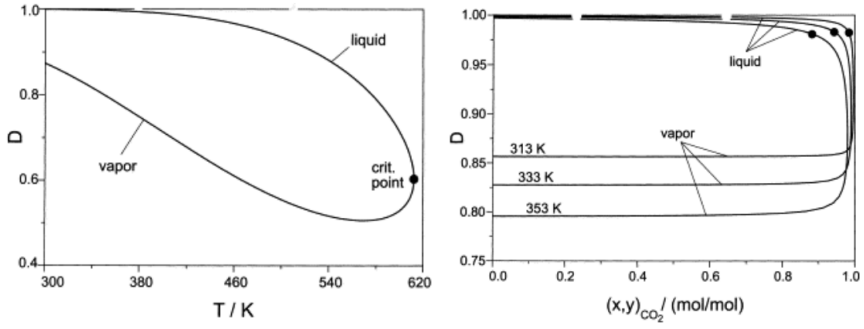

(a) **(b)**

Source: Bamberger, Sieder, and Maurer (2000); Jonasson et al. (1998).

The properties of polymers in supercritical fluids are crucial parameters for the efficiency of different processes. However, there is still a lack of experimental data, requiring further studies regarding mixtures involving polymers (encapsulating agents), solutes (agents to be encapsulated), and supercritical CO_2.

Regarding encapsulation in supercritical media, understanding the phase equilibrium of the system allows the application of optimal conditions of precipitation,

nucleation, growth kinetics, and mass transfer, for example. In this way, studying the behavior of phases is fundamental for evaluating the feasibility of encapsulation processes and optimization of the operational variables.

2.3 PHASE EQUILIBRIUM

2.3.1 Definition and calculation of phase equilibrium

A system is in equilibrium when it has a thermodynamically stable system. The constraints presented in Diagram 1 must be followed to achieve this balance.

Diagram 1 – Constraints to reach the equilibrium state.

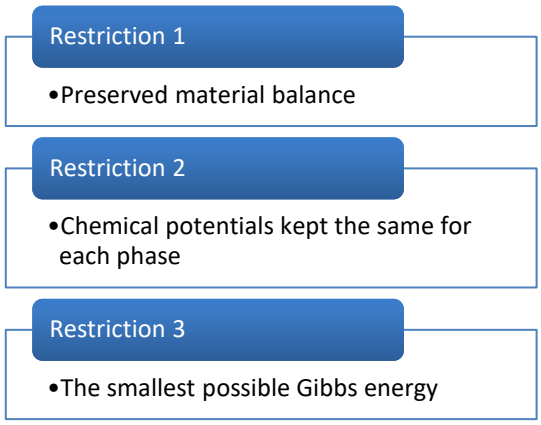

Source: Costa (2009); Filho (2020).

Knowing the phase equilibrium is essential for the numerous applications of supercritical carbon dioxide, as reliable vapor-liquid equilibrium (VLE) data is required for accurate process design and optimization. The equilibrium state can be described quantitatively by variables when the phases are considered homogeneous and free to exchange energy and matter with each other. This phase represents any homogeneous region where the intensive properties are uniform, and any modification would cause a change in the phase equilibrium (ROSA et al., 2011).

In this way, equilibrium between the phases is reached when the analyzed system conditions satisfy the thermal, mechanical, and chemical equilibrium criteria (ARCE-CASTILLO, 2005), presented in the equations 1, 2 e 3:

Thermal balance: $T^I = T^{II} = \cdots = T^{\pi}$ $(Equation\ 1)$

Mechanical balance: $P^I = P^{II} = \cdots = P^{\pi}$ $(Equation\ 2)$

Chemical balance: $\mu_i^I = \mu_i^{II} = \cdots = \mu_i^{\pi}$ $(Equation\ 3)$

The chemical potential presents abstract quantities and, therefore, can be related to physically measurable quantities, such as temperature, pressure, and composition, using the concept of fugacity introduced by Lewis.

$$\mu_i - \mu_i^0 = RT.ln\frac{f_i}{f_i^0}\ (Equation\ 4)$$

This way, the equality between the chemical potentials used for the equilibrium calculation can be expressed by the isofugacity between the phases. Considering a vapor-liquid equilibrium, the equality of fugacity between the phases in the mixture is presented in the following equation (SANDLER, 2006).

$$\hat{f}_i^L(P,T,x_i) = \hat{f}_i^V(P,T,y_i)\ (Equation\ 5)$$

Where *P* is pressure, *T* is temperature, x_i e y_i are the molar fractions of component i in the liquid (L) and vapor (V), respectively, where i represents the components of the system and $\hat{f}_i$ the fugacity of component i in each phase.

The fugacity in the liquid and vapor phases can be expressed in the equations 6 e 7 (PRAUSNITZ; LICHTENTHALER; AZEVEDO, 1999; ARCE-CASTILLO, 2005):

$$\hat{f}_i^L(P,T,x_i) = x_i\hat{\phi}_i^L P\ (Equation\ 6)$$
$$\hat{f}_i^V(P,T,y_i) = y_i\hat{\phi}_i^V P\ (Equation\ 7)$$

Where $\hat{\phi}_i$ is the fugacity coefficient of component i in the mixture obtained from PVT relationships (pressure – volume – temperature), and x_i and y_i represent the molar fractions in the liquid and vapor phases, respectively.

The study of the ELV behavior can be carried out using different approaches, such as the gamma-phi (γ-φ) approaches, generally applied for low and moderate

pressures (up to 10.0 bar), and phi-phi (φ-φ), used to high pressures (SANDLER, 2006). These approaches are represented in the following equations:

$$x_i P_i^{sat} \gamma_i = y_i \hat{\phi}_i^V P \ (Equation\ 8)$$

$$x_i \hat{\phi}_i^L = y_i \hat{\phi}_i^V \ (Equation\ 9)$$

Where x_i and y_i are the molar fractions of component i in the liquid and vapor phases, P_i^{sat} is the saturation pressure of component i at equilibrium temperature, γ_i is the activity coefficient of component i, $\hat{\phi}_i$ is the fugacity coefficient of component i in a certain phase of the mixture and P the system pressure.

Thus, the main properties that seek to describe the phase equilibrium consist of pressure, temperature, and composition. These properties can be related and presented in a diagram, representing one of the ways to express the behavior of phases. These equilibrium relationships between phases can be two-dimensional or three-dimensional (*P-T-x*). Interpretation is facilitated when two-dimensional diagrams are used: pressure–composition (constant temperature) and temperature–composition (constant pressure). These diagrams feature two curves: the bubble curve (*P-*x_i ou *T-*x_i) and the dew curve (*P-*y_i ou *T-*y_i) (SMITH; INOMATA; PETERS, 2013).

Generally, diagrams are plotted as a function of the concentration of the most volatile component. The region between the bubble and dew curves is called the vapor-liquid phase equilibrium region. The bubble curve corresponds to the transition from the liquid phase to liquid-vapor equilibrium, and the dew curve corresponds to the phase transition vapor to vapor-liquid equilibrium. Typically, these diagrams compare experimental data with predicted data obtained by thermodynamic models.

The phase equilibrium properties, mainly of systems involving mixtures of components, are essential for developing techniques that employ the supercritical fluid, as in particle formation processes, the main purpose of the present work. Thus, from the ELV phase diagram of the studied systems, it is possible to determine the best process conditions, obtaining particles with preferred size and morphology (CHIU; LEE; LIN, 2008).

2.3.2 Types of phase behavior

Scott and Van Konynenburg (1970) developed the classification for binary systems according to the complexity of equilibrium diagrams, presenting five basic types, which can be described from the Van der Waals equation. Rowlinson and Swinton (1982) introduced the sixth Type of diagram, which, unlike the diagrams proposed by Scott and Van Konynenburg, can only be described using potential functions. The six types of diagrams can occur as a function of molecular asymmetry (difference in size, polarity, and molecular functionality). In addition, except Type I, all diagrams show the occurrence of liquid-liquid immiscibility (BENDER 2014). The diagrams are shown in Figure 7.

Figure 7 – Types of phase behavior according to the classification of Scott and Van Konynenburg (1970) and Rowlinson and Swinton (1982). P-T projection of different types of systems.

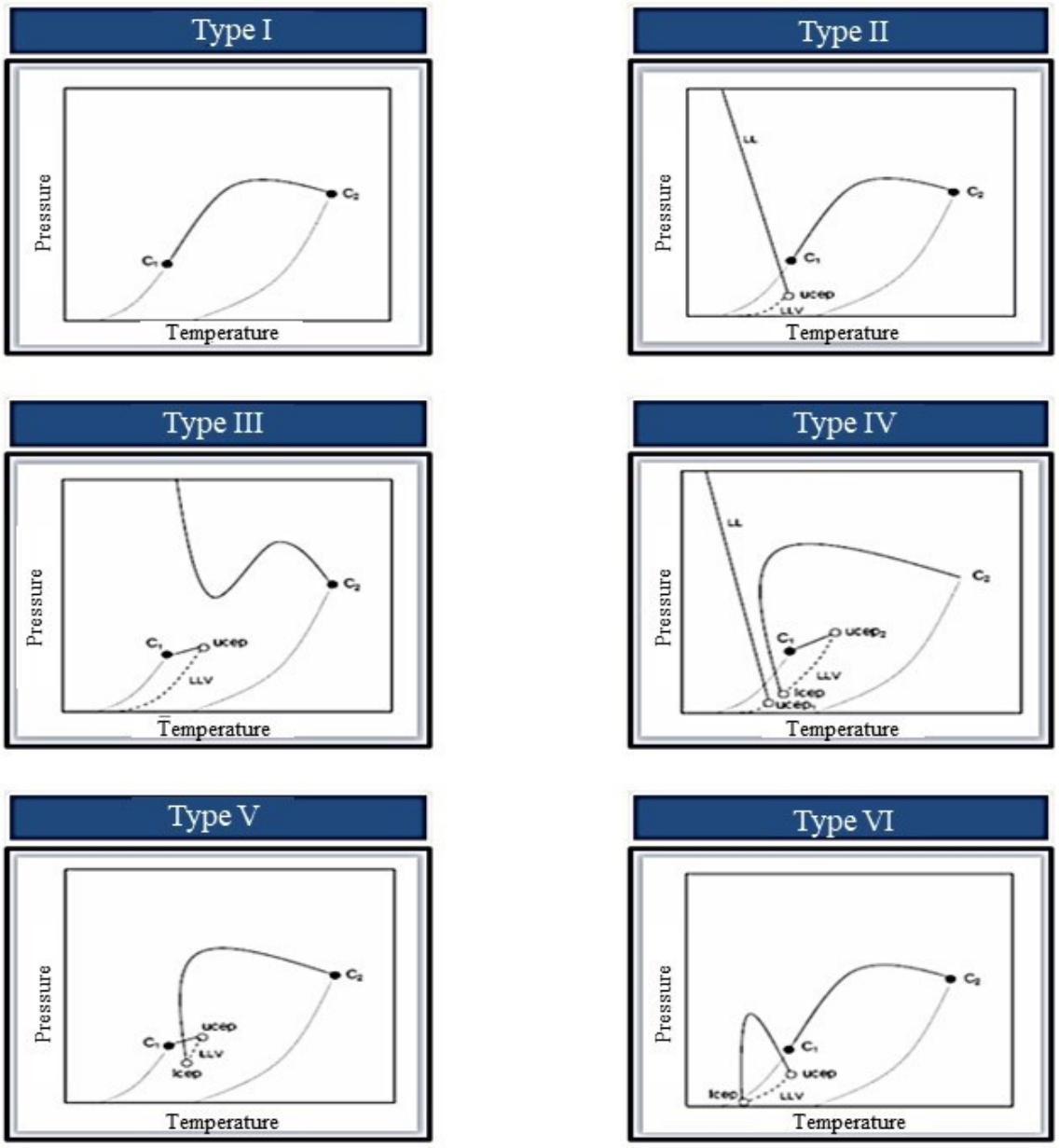

Source: Adapted from Arce-Castilho (2005).

The main concepts involved in this classification of the types of phase behavior, proposed by Scott and Van Konynenburg (1970) and Rowlinson and Swinton (1982), are described in diagram 2. In addition, examples of binary systems for the six types of diagrams are presented.

Diagram 2 – Main concepts and examples of binary systems for the different types of phase behavior, according to the classification of Scott and Van Konynenburg (1970) and Rowlinson and Swinton (1982).

Type I

- The behavior is characterized by a single critical line, where the critical points of the pure components C1 and C2 are connected continuously. Generally, type I occurs in systems that are chemically similar and/or do not show significant differences in their critical properties. Typical examples are methane + ethane and benzene + toluene (PRAUSNITZ, 1969).

Type II

- The behavior is characterized by the presence of liquid-liquid immiscibility (LL), where it is possible to observe an additional critical line at temperatures lower than the critical temperature of the most volatile component. Thus, type II presents two critical lines: the first line connects C1 and C2, identical to type I, and the second line connects an ELLV line with an upper critical end point UCEP (Upper Critical End Point), where the two liquid phases become indistinguishable. Typical examples are carbon dioxide + n-octane, ammonia + toluene (PRAUSNITZ; LICHTENTHALER; AZEVEDO, 1999).

Type III

- The behavior is characterized by two unconnected critical lines. The first arises from C1 to the UCEP of ELLV, and the second arises from C2 and advances to the high-pressure region. Generally, this system occurs in mixtures with high immiscibility, such as water + n-alkane and ethane + methanol (PRAUSNITZ; LICHTENTHALER; AZEVEDO, 1999).

Type IV

- The behavior is characterized by presenting three critical lines. The first line arises from the UCEP of an ELLV and advances to the high-pressure range, similar to type II. The second line appears at C2 and connects the Lower Critical End Point (LCEP) to an ELLV line, close to the most volatile component. The third line appears in C1 up to the UCEP of the same previous ELLV. When the pressure increases, two critical points appear; one corresponds to the ELV and the other to the ELL. Examples of typical behaviors are methane + 1-hexene and n-tridecane + CO2 systems (ARCE-CASTILHO, 2005).

Type V

- The behavior is characterized by having two critical lines that form an immiscibility triangle, similar to type IV, but without a low-temperature ELL critical line. Examples of behaviors are ethane + 1-propanol and ethane + ethanol (ARCE-CASTILHO, 2005).

Tipo VI

- The behavior is characterized by having two critical lines. The first line connects the UCEP and LCEP point of a low-temperature ELLV, forming a concave parabola, and the second line connects the critical points of the pure components, similar to type I. This type is found in mixtures with strong molecular interaction (bridge hydrogen), e.g., water + 2-butoxyethanol system (PRAUSNITZ; LICHTENTHALER; AZEVEDO, 1999).

Source: the autor (2021).

Among the concepts applied in the different types of phase behavior, the definitions of the terminal critical point (UCEP and LCEP) and the solution critical point (UCST and LSCT) need to be understood to avoid future confusion. Concerning the critical end point the upper critical end point (UCEP) and lower critical end point (LCEP) are characterized by the disappearance of a liquid phase at equilibrium liquid-liquid-vapor, caused by the increase and decrease in temperature, respectively (BENDER, 2014; REBELATTO, 2018).

Regarding critical solution points, the UCST (upper critical solution temperature) behavior describes the pressure dependence of a transition between liquid-liquid and fluid phase as the temperature increases. Thus, this behavior is observed when a heterogeneous system (two liquid phases) becomes homogeneous (a single phase) by decreasing the transition pressure with increasing temperature, $(\partial P/\partial T)x < 0$ (VAN KONYNENBURG; SCOTT, 1980; FILHO, 2020).

The LSCT (lower critical solution temperature) behavior is observed by the difference in free volume between each component in the solution. When the temperature increases, one of the components exhibits a greater relative volume expansion than the other component (free volume difference), leading to a greater negative entropy of the mixture. Thus, this behavior is visualized when a single liquid phase splits into two immiscible phases, followed by an increase in temperature, where $(\partial P/\partial T)x > 0$. When temperatures that comprise the interval between UCST and LCST, the system features complete miscibility (BENDER, 2014; FILHO, 2020).

Understanding the types of phase diagrams can help classify systems not yet present in the literature due to applying pioneering groups of compounds, such as the systems studied in the current work. From the information collected, it is possible to understand better the phenomena and the main characteristics involved in the systems, guaranteeing the execution of different processes with higher quality.

2.3.3 Experimental methods for the determination of phase equilibrium

A wide variety of experimental methods seek to determine the ELV at high pressures, which vary according to the purpose of the data (CHRISTOV; DOHRN, 2002; DOHRN; FONSECA; PEPER, 2012). According to Christov and Dohrn (2002), experimental methods for phase equilibrium at high pressures can be classified into two types: (1) analytical methods and (2) synthetic methods. In analytical methods,

also called direct sampling methods, the phases are determined by analyzing the sample. In synthetic methods, known as indirect methods, the phases are determined synthetically, where it is necessary to know the mixture's composition previously.

Synthetic methods have as a basic principle the preparation of a mixture of known precisely compositions and the observation of the phase behavior in an equilibrium cell. These methods are used in systems where phase separation is difficult or barotropic systems where the coexisting phases have the same density. In addition, synthetic methods do not require sampling, making the procedure quick and easy. However, these methods yield less information when compared to analytical methods (CHRISTOV; DOHRN, 2002; FONSECA; DOHRN; PEPER, 2011).

Another classification used to determine the phase equilibrium corresponds to the static or dynamic method division. The dynamic method involves mixing flow components, where equilibrium is performed, and effluents from both phases are collected and analyzed. Static methods use an equilibrium cell in which thermodynamic equilibrium is achieved without fluid mixing. Equilibrium properties can be measured by taking samples or visually observing phase separation or single-phase formation. In the latter case, the quantity of the components must be known exactly (KOROSI et al., 2019, REBELATTO, 2018).

2.3.3.1 Visual synthetic method

Synthetic methods can be classified into methods with or without phase transition. In synthetic phase transition methods, conditions in the equilibrium cell, such as pressure, temperature, or composition, are modified until a new phase appears or one of the existing phases disappears. Each experiment produces a point in the P-T-x phase envelope. Furthermore, these methods can be classified as visual and non-visual, Figure 8. Visual synthetic methods allow observation of the appearance of a new phase. In contrast, non-visual methods do not allow this visual observation, and identification occurs through other physical properties, such as X-rays and pressure density (BOUCHOT; RICHON, 1998; ABEDI et al., 1999; CHRISTOV; DOHRN, 2002; FONSECA; DOHRN; PEPER, 2011; DOHRN; FONSECA; PEPER, 2012).

Figure 8 – Visual synthetic method and a non-visual synthetic method. (a) the phase transition is detected non-visually by observing the change in the slope of the PV curve and visually detecting the bubble. (b) Graphic representation.

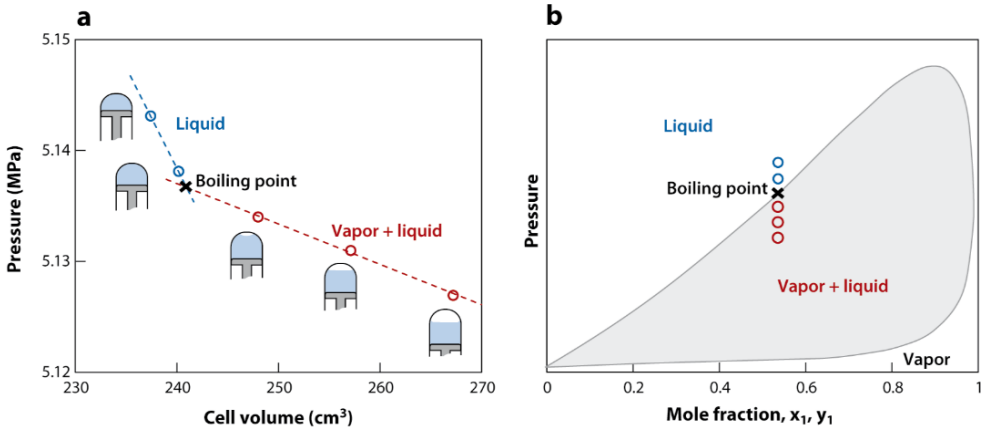

Source: Dohrn, Fonseca and Peper (2012).

As shown in figure 8, the bubble point is determined by the piston movement and the PV curve. Initially, the curve slope is quite steep until dissolved gas starts to be released from the solution, corresponding to the bubble pressure. From this point, any decrease in pressure causes an increase in volume, making the PV curve slope smoother (DOHRN; FONSECA; PEPER, 2012). The identification of phases is dependent on the skill of the observer.

Visual synthetic methods have a wide variety of applications, from simpler applications involving the determination of ELV to more complex ones, such as multiphase equilibria, solid-liquid equilibria, critical mixing curves, and phase equilibrium in polymer-solvent systems, among others (CHRISTOV; DOHRN, 2002; FONSECA; DOHRN; PEPER, 2011).

2.4 THERMODYNAMIC MODELING FOR PHASE BALANCE

The thermodynamic behavior can be expressed in mathematical language using equations of state, which are simple models for high-pressure phase equilibrium calculations. These equations of state play an important role in expanding the study of fluid phase equilibrium and fluid mixtures. They can be applied to pure components and polar and non-polar mixtures in wide temperature and pressure ranges (WEI; SADUS, 2000).

Types different of state equations can be based on molecular principles, such as virial-type and molecular-type equations, represented by chain molecules and associated fluid equations, and empirical principles, such as Van der Waals-type equations, classified into cubic and non-cubic (Figure 9).

Figure 9 – Classification of various types of equations of state. Van der Waals equations of state are those cubic and non-cubic equations that consider the compressibility factor.

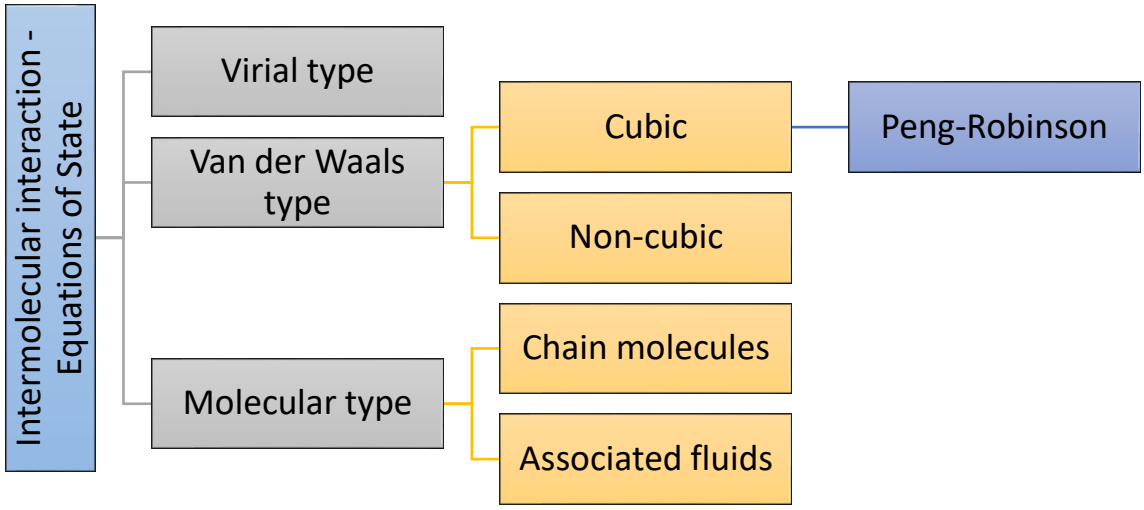

Source: Adapted from Valderrama (2003).

The application of each equation depends on the theoretical basis and practical use involved in its applications, which may have advantages and disadvantages. Among the equations of state, the cubic equations of the Van der Waals type can be highlighted, especially the Peng-Robinson (PR) equations. These equations are preferred for simulations and equilibrium calculations, as they predict the behavior of phases with mathematical simplicity, easy implementation, and low computational resources. They are suitable for binary and multicomponent systems, where only critical properties and acentric factors are used for substances (WEI; SADUS, 2000; MEDEIROS; ARREDONDO, 2008).

2.4.1 Cubic equations of state

The Van der Waals equation (1873) was the first cubic equation that sought to mathematically express the thermodynamic behavior with the consideration of two molecular forces: (1) repulsive, due to the size of the molecules, and (2) attractive, related to the interaction between one molecule and another. After this first version of equation of state, several modifications were proposed to improve predictions of volumetric, thermodynamic, and phase equilibrium properties (VALDERRAMA, 2003).

The following general equation can represent the Van der Waals type cubic equations:

$$P - \frac{RT}{v - b} + \frac{a}{v^2 + ubv + qb^2} = 0 \text{ (Equation 10)}$$

Applying the values of *u* = 2 and *q* = -1, the Peng-Robinson cubic equation (Equation 11) is obtained:

$$P - \frac{RT}{v - b} + \frac{a}{[v\,(v + b) + b\,(v - b)]} = 0 \ (Equation\ 11)$$

Where *P* is the system absolute pressure, *T* is the absolute temperature, *R* is the universal constant of ideal gases, *v* the molar volume, *a* (energy parameter, measure of attraction intermolecular forces), and *b* (co-volume parameter, estimation of the molecule size) are defined from pure component parameters. These parameters are combined using mixing rules for mixtures, binary and multicomponent systems.

For the PR equation, the coefficients *a* and *b* are obtained by equations 12 and 13.

$$a = \frac{0{,}45724\ R^2\ T_C^2}{P_C}\left[1 + (0{,}37464 + 1{,}5422\omega - 0{,}26992\omega^2)(1 - \sqrt{T_r})\right]^2 \ (Equation\ 12)$$

$$b = 0{,}07779607\frac{RT_C}{P_C} \ (Equation\ 13)$$

Where *ω* is the acentric factor, *Tc* is the critical temperature, *Pc* is the critical pressure, and *Tr* is the reduced temperature ($T_r = T/T_c$).

In this way, it is verified that the state cubic equations can be used for pure substances and mixtures. In systems with pure substances, only the critical properties of the compound will be used to determine the thermodynamic behavior of phase equilibrium, such as critical temperature, pressure, and acentric factor. In mixtures, this behavior will depend on the application of mixing rules, which will be used to determine the values of parameters *a* and *b*.

2.4.2 Estimation of binary interaction parameters (optimization)

The equations of state need a certain number of adjustable intermolecular parameters to obtain more accurate representations and predictions of the physical properties of the substances present in the systems. Typically, these parameters are obtained using regression of experimental phase equilibrium data. Thus, regression analysis consists of applying the equation of state to the calculation of a particular property, aiming to minimize the differences between the predicted and experimental values, consequently obtaining optimal values of the parameters using an acceptable optimization method (VALDERRAMA, 2003, BENDER, 2014).

Thermodynamic models present a high degree of nonlinearity concerning binary parameters, requiring the use of efficient techniques for the optimization of these parameters to obtain a smaller difference between the predicted and experimental data and a good fit of the model to the experimental data. The optimization step in the thermodynamic modeling process is based on finding values by successive iterative calculations for the parameters kij and lij that satisfy (minimize) the objective function (FO, equation 14) (BENDER, 2014; FILHO, 2020).

$$FO = \sum_{i}^{Nobs} \left(P_i^{exp} - P_i^{calc}\right)^2 \quad (Equation\ 14)$$

Where *nobs* is the number of experimental observations, P^{exp} corresponds to the bubble point pressure obtained experimentally, and P^{cal} to the predicted pressure.

The objective function provides the quality of the thermodynamic model. The lower the value of FO, the smaller the deviation between the pressures P^{exp} e P^{cal}, and the better the model fits the experimental data. This minimum value of FO is obtained by the correct k_{ij} e l_{ij}, estimated with optimization methods. Thus, the choice of the

optimization method is crucial, as it directly influences the accuracy of the parameter values found, consequently, the quality of the thermodynamic model provided.

Optimization methods can be classified into two types: (1) deterministic methods, which are dependent on the initial estimate, and may converge to local minima, and (2) stochastic methods, which are independent of initial estimates, presenting a random search within a region defined for the parameters (BENDER, 2014).

Among the deterministic and stochastic methods, the Simplex method and the PSO method (Particle Swarm Optimization) deserve to be highlighted, respectively. The Simplex method uses an iterative algorithm to find the solution that satisfies the constraints and brings the best value to the objective function. On the other hand, the PSO method is inspired by the collective intelligence of animals. It evaluates the movement of particles within the search space, using as a basis the consideration of particle modification with time, where the position is changed according to each particle's experience and the other components involved (SECCHI, 2015).

Next, the material and methods, and results obtained to study the behavior of phases and thermodynamic modeling of the quaternary systems evaluated are presented, system A {CO_2 (1) + ethanol (2) + Acetic acid (3) + methionine (4)} and system B {CO_2 (1) + ethanol (2) + Acetic acid (3) + ethyl cellulose (4)}. In addition, the material and methods, and results of encapsulation of the methionine in ethyl cellulose by the GAS process are also presented.

2.5. REFERENCES

ABEDI, S. J., CAI, H. Y., SEYFAIE, S., SHAW, J. M. Simultaneous phase behaviour, elemental composition and density measurement using X-ray imaging. Fluid Phase Equilibria, 158–160, p. 775–781, 1999.

AISSA, A. F., TRYNDYAK, V., DE CONTI, A., MELNYK, S., GOMES, T. D. U. H., BIANCHI, M. L. P., ... & POGRIBNY, I. P. Effect of methionine-deficient and methionine-supplemented diets on the hepatic one-carbon and lipid metabolism in mice. Molecular nutrition & food research, 58(7), 1502-1512, 2014.

AISSA, A. F., TRYNDYAK, V. P., DE CONTI, A., MACHADO, A. R. T., TUTTIS, K., DA SILVA MACHADO, C., ... & ANTUNES, L. M. G. Epigenetic changes induced in mice liver by methionine-supplemented and methionine-deficient diets. Food and Chemical Toxicology, 163, 112938, 2022.

ALVES, A. R. et al. Fibra para ruminantes: Aspecto nutricional, metodológico e funcional. PUBVET, v.10, n.7, p.568-579, 2016.

ARCE-CASTILLO, P. F. Modelagem do equilíbrio multifásico e de fenômenos críticos em sistemas ternários contendo dióxido de carbono + polímero + co-solvente usando equações de estado. Tese (doutorado), Universidade Estadual de Campinas, Faculdade de Engenharia Química, 2005.

BAMBERGER, A., SIEDER, G., MAURER, G. High-pressure (vapor+liquid) equilibrium in binary mixtures of (carbon dioxide-water or acetic acid) at temperatures from 313 to 353 K. The Journal of Supercritical Fluids, v. 17, p. 97-110, 2000.

BENDER, J. P. Equilíbrio de fases do monômero L,L-lactídeo em altas pressões: dados experimentais e modelagem. Florianópolis: Universidade Federal de Santa Catarina, 2014.

BERGMAN, E. N. Energy contributions of volatile fatty acids from the gastrointestinal tract in varius species. Phytological Reviews, v. 70, n. 2, p. 567-590, 1990.

BOUCHOT, C., RICHON, D. Direct Pressure-Volume-Temperature and Vapor-Liquid Equilibrium Measurements with a Single Equipment Using a Vibrating Tube Densimeter up to 393 K and 40 MPa: Description of the Original Apparatus and New Data. Ind. Eng. Chem., v. 37, p. 3295-3304, 1998.

CERMAKOVA, J., KUDRNA, V., ILLEK, J., BLAZKOVA, K., HAMAN, J. Effects of a rumen-protected form of methionine and a methionine analogue on the lactation performance of dairy cows. Czech J. Anim. Sci., v. 57, p. 410–419, 2012.

CHEN, L., LIU, Z. Microparticle formation of ethyl celullose using compressed CO_2 antisolvent precipitations. Journal of Agricultural Machinery Science, 4(3), 313-317, 2008.

CHRISTOV, M., DOHRN, R. High-pressure fluid phase equilibria Experimental methods and systems investigated (1994–1999). Fluid Phase Equilibria, v. 202, p. 153-218, 2002.

CHEUNG, O., & SANYAL, A. J. Recent advances in nonalcoholic fatty liver disease. Current opinion in gastroenterology, 26(3), 202-208, 2010.

COCERO, M. J., MARTIN, A., MATTEA, F., VARONA, S. Encapsulation and co-precipitation processes with supercritical fluids: Fundamentals and applications. The Journal of Supercritical Fluids. V. 47, p. 546-555, 2009.

COSTA, G. M. N. Estabilidade de Fases em Processos Industriais de Polimerização de Eteno a Alta Pressão. Salvador: Universidade Federal da Bahia, 2009.

DJERAFI, R., MASMOUDI, Y., CRAMPON, C., MENIAI, A., BADENS, E. Supercritical anti-solvent precipitation of ethyl celulose. The Journal of Supercritical Fluids, v. 105, p. 92-98, 2015.

DJERAFI, R., SWANEPOEL, A., CRAMPON, C., KALOMBO, L., LABUSCHAGNE, P., BADENS, E., MASMOUDI, Y. Supercritical antisolvent co-precipitation of rifampicin and ethyl celulose. European Journal of Pharmaceutical Sciences, v. 102, p. 161-171, 2017.

DOHRN, R., FONSECA, J. M. S., PEPER, S. Experimental Methods for Phase Equilibria at High Pressures. Rev. Chemical and Biomolecular Engineering, v. 3, p. 343-367, 2012.

DUARTE, A. R. C., COSTA, M. S., SIMPLICIO, A. L., CARDOSO, M. M., DUARTE, C. M. M. Preparation of controlled release microspheres using supercritical fluid technology for delivery of anti-inflammatory drugs. International Journal of Pharmaceutics, v. 308, p. 168-174, 2006.

ESFANDIARI, N. Production of micro and nano particles of pharmaceutical by supercritical carbon dioxide. Journal of Supercritical Fluids, v. 100, p. 129-141, 2015.

FAGES, J., LOCHARD, H., LETOURNEAU, J., SAUCEAU, M., RODIER, E. Particle generation for pharmaceutical applications using supercritical fluid technology. Powder Technology. V. 141, p. 219-226, 2004.

FILHO, C. A. B. Equilíbrio de fases a alta pressão de sistemas contendo dióxido de carbono, etanol, quercetina e nicotinamida. Dissertação (mestrado), Universidade Federal de Santa Catarina, Programa de Pós-Graduação em Engenharia de Alimentos, 2020.

FONSECA, J. M. S.; DOHRN, R.; PEPER, S. High-pressure fluid-phase equilibria: Experimental methods and systems investigated (2005-2008). Fluid Phase Equilibria, v. 300, n. 1–2, p. 1–69, 2011.

FROTA, H. N. Suplementação de lisina e metionina em associação ou não com óleo de soja na dieta de vacas leiteiras. Dissertação (Mestre em Zootecnia), Universidade Federal de Viçosa (UFV), Minas Gerais, 2014.

HE, Q., YIN, Y., ZHAO, F., KONG, X., WU, G., REN, P. Metabonomics and its role in amino acid nutrition research. Frontiers in Bioscience-Landmark, 16(7), 2451-2460, 2011.

HEBBARD, L., & GEORGE, J. Animal models of nonalcoholic fatty liver disease. Nature reviews Gastroenterology & hepatology, 8(1), 35-44, 2011.

HINE, C., HARPUTLUGIL, E., ZHANG, Y., RUCKENSTUHL, C., LEE, B. C., BRACE, L., … MITCHELL, J. R. Endogenous hydrogen sulfide production is essential for dietary restriction benefits. Cell, 160(1-2), 132-144, 2015.

HONG, L., GUO, J. Z., GAO, Y., YUAN, W. K. Precipitation of microparticulate organic pigment powders by a supercritical antisolvent process. Industrial & Engineering Chemistry Research, v. 39, p. 4882-4887, 2000.

HOSIOS, A. M., VANDER HEIDEN, M. G. The redox requirements of proliferating mammalian cells. Journal of Biological Chemistry, 293(20), 7490-7498, 2018.

JONASSON, A., PERSSON, O., RASMUSSEN, P., SOAVE, G. S. Vapor-liquid equilibria of systems containing acetic acid and gaseous components. Measurements and calculations by a cubic equation of state. Fluid Phase Equilibria, v. 152, p. 67-94, 1998.

JONG, W. H., BORM, P. J. A. Drug delivery and nanoparticles: applications and hazards. International Journal of Nanomedicine, v. 3, p. 133-149, 2008.

JUNIOR, M. B. C. et al. A influência da dieta no desenvolvimento ruminal de bezerros. Nutritime, v. 13, n. 06, 2016.

KALANI, M., YUNUS, R. Application of supercritical antisolvent method in drug encapsulation: a review. International Journal of Nanomedicine. Vol. 6, pags 1429-1442, 2011.

KIRAN, E., POHLER, H. Alternative solvents for cellulose derivatives: miscibility and density of cellulosic polymers in carbon dioxide + acetone and carbon dioxide + ethanol binary fluid mixtures. The Journal of Supercritical Fluids, v. 13, p. 135-141, 1998.

KNEZ, Z.; MARKOCIC, E.; LEITGEB, M.; PRIMOZIC, M.; KNEZ HRNCIC, M.; SKERGET, M. Industrial applications of supercritical fluids: A review. Energy, v. 77, p. 235-243, 2014.

KOROSI, M., BERI, J., SEDON, A., KOMBA, K., SZEKELY, E. New vapour-liquid equilibrium data on the ternary system carbon dioxide e methanol e dimethyl sulphoxide. Fluid Phase Equilibria, v. 497, p. 113-139, 2019.

LI, D., MARK, A., HUGH, M.C. Solubility behavior of ethyl cellulose in supercritical fluid solvents. The Journal of Supercritical Fluids, v. 28, p. 225-231, 2004.

LI, B., ZHANG, Y., ZHANG, W., HUA, Z. Supercritical CO_2 spray drying of ethyl celulose (EC) for preparing particles. Drying Technology: Na International Journal. 26:4, 464-469, 2008.

LIN, C., NG, K. M., WIBOWO, C. Producing nanoparticles using precipitation with compressed antisolvent. Industrial & Engineering Chemistry Reserarch, v. 46, p. 3580-3589, 2007.

MAPA. Ministério da Agricultura, Pecuária e Abastecimento. Projeções do agronegócio: Brasil 2019/20 a 2029/30 (projeções de longo prazo). 11ª edição, 2020.

MAZOR, K. M., DONG, L., MAO, Y., SWANDA, R. V., QIAN, S. B., STIPANUK, M. H. Effects of single amino acid deficiency on mRNA translation are markedly different for methionine versus leucine. Scientific reports, 8(1), 1-13, 2018.

MEDEIROS, M; ARREDONDO, P. T. Cubic Two-State Equation of State for Associating Fluids. Industrial & Engineering Chemistry Research, v. 47, p. 5723-5733, 2008.

MONTES, A., GORDILLO, M. D., PEREYRA, C., MARTINEZ DE LA OSSA, E. J. Co-precipitation of amoxicillin and ethyl celullose microparticles by supercritical antisolvent process. The Journal of Supercritical Fluids, v. 60, p. 75-80, 2011.

MONTES, A., GORDILLO, M. D., SCHINDHELM, S., PEREYRA, C., MARTINEZ DE LA OSSA, E. J. Supercritical antisolvent precipitation of ethyl celullose. Particulate Science and Technology, v. 30, p. 424-430, 2012.

MORA-HUERTAS, C. E., FESSI, H., ELAISSARI, A. Polymer-based nanocapsules for drug delivery. Int J Pharm. vol. 385, pág. 113-142, 2010.

MORAIS JUNIOR, N. N. Suplementação de vacas leiteiras com análogo de metionina e proteína de soja. Tese. Minas gerais, 2013.

MORELLATO, A. E., UMANSKY, C., PONTEL, L. B. The toxic side of one-carbon metabolism and epigenetics. Redox Biology, 40, 101850, 2021.

NATIONAL RESEARCH COUNCIL - NRC. Nutrient requirements of dairy cattle. 7.ed. Washington: National Academic Press, 2001. 381p.

PIEPENBRINK, M. S., A. L. MARR, M. R. WALDRON, W. R. BUTLER, T. R. OVERTON, M. VAZQUEZ-ANON, AND M. D. HOLT. 2004. Feeding 2-hydroxy-4(methylthio)-butanoic acid to periparturient dairy cows improves milk production but not hepatic metabolism. J. Dairy Sci. 87:1071–1084.

PINHO, S. C. M. OS Aminoácidos lisina e metionina na nutrição e na alimentação da vaca leiteira. Relatório de Estágio, Universidade do Porto, 2016.

PRAUSNITZ, J.M. Molecular thermodynamics of fluid-phase equilibria. Ch. 5, Prentice Hall, Inc., Englewood Cliffs, NJ, 1969.

PRAUSNITZ, J. M.; LICHTENTHALER, R. N.; AZEVEDO, E. G. Molecular Thermodynamics of Fluid-Phase Equilibria. 3. ed. New Jersey: Prentice Hall, 1999.

PRIAMO, W. L. Encapsulamento de β-caroteno em PHBV com dióxido de carbono e avaliação da liberação *in vitro*. Tese (doutorado), Universidade Federal de Santa Catarina, Programa de Pós-graduação em Engenharia de Alimentos, 2011.

PROYECTO CONOCER LA AGRICULTURA Y LA GANADERÍA. Los cuatro estómagos de la vaca (2016). Disponível em: http://www.conocerlaagricultura.com/2016/03/los-cuatro-estomagos-de-la-vaca.html, Acessado em: 02/05/2019.

REBELATTO, E. A. Equilíbrio de fases de sistemas contendo dióxido de carbono, ωpentadecalactona e cossolventes em altas pressões: dados experimentais e modelagem termodinâmica. Florianópolis: Universidade Federal de Santa Catarina, 2018.

REVERCHON, E., ADAMI, R. Nanomaterials and supercritical fluids. The Journal of Supercritical Fluids. 37, 1-22, 2006.

REVERCHON, E., ADAMI, R., CAPUTO, G., DE MARCO, I. Spherical microparticles production by supercritical antisolvent precipitation: Interpretation of results. The Journal of Supercritical Fluids. 47, 70-84, 2008.

RIVERA, A. R. Estudo da fermentação ruminal por bovinos consumindo feno de tifton 85 e concentrado com aditivos. Dissertação de mestre em zootecnia, Faculdade de Ciências Agrárias e Veterinárias – Unesp, Campus de Jaboticabal, 2006.

ROSA, A. J.; CARVALHO, R. S.; XAVIER, J. A. D. Engenharia de reservatórios de petróleo. 1ª. ed. Rio de Janeiro: Interciência, 2011.

ROWLINSON, J. S.; SWINTON, F. L. Liquids and Liquid Mixtures. 3. ed. London: Butterworth-Heinemann, 1982.

SANDERSON, S. M., GAO, X., DAI, Z., LOCASALE, J. W. Methionine metabolism in health and cancer: a nexus of diet and precision medicine. Nature Reviews Cancer, 19(11), 625-637, 2019.

SANDLER, S. I. Chemical, biochemical and engineering thermodynamics. 4th ed. Hoboken: John Wiley and Sons, 2006.

SANTOS, D. N. E. Extração com dióxido de carbono supercrítico e estudo da composição dos extratos de sementes de pitanga (Eugenia uniflora L.). Dissertação (mestrado). Faculdade de Zootecnia e Engenharia de Alimentos. Universidade de São Paulo. Pirassununga, 2012.

SCOTT, R. L.; VAN KONYNENBURG, P. H. Static properties of solutions. Van der Waals and related models for hydrocarbon mixtures. Discussions of the Faraday Society, v. 49, p. 87, 1970.

SCHMIDT-NIELSEN, K. Fisiologia animal: Adaptação e meio ambiente. Medicina e Sacede edition, 2002.

SECCHI, A. R. Otimização de processos (COQ 897). Programa de Engenharia Química, Universidade Federal do Rio de Janeiro, 2015.

SILVA, O. V, et al. Características químicas e fisiológicas da fermentação ruminal de bovinos em pastejo – revisão de literatura. Revista Científica Eletrônica de Medicina Veterinária – issn: 1679-7353, 2013.

SILVA, E. K., MEIRELES, M. A. A. Encapsulation of foods compounds using supercritical Technologies: Applications of supercritical carbon dioxide as na antisolvent. Food and Public Health, 4(5), 247-258, 2014.

SMITH, R., INOMATA, H., PETERS, C. Introduction to supercritical fluids – A spreadsheet-based approach. Supercritical Fluid Science and Technology Series, v. 3. Amsterdam: Elsevier, 2013.

SOCHA, M. T., PUTNAM, D. E., GARTHWAITE, B. D., WHITEHOUSE, N. L., KIERSTEAD, N. A., SCHWAB, C. G., DUCHARME, G. A., ROBERT, J. C. Improving

intestinal amino acid supply of pre – and postpartum dairy cows with rumen – protected methionine and lysine, J. Dairy Sci., v. 88, p. 1113-1126, 2005.

STECKEL, H., THIES, J., MULLER, B. W. Micronizing of steroids for pulmonary delivery by supercritical carbono dioxide. International Journal of Pharmaceutics. Vol. 152, pags. 99-110, 1997.

STOVER, P. J., DURGA, J., FIELD, M. S. Folate nutrition and blood–brain barrier dysfunction. Current opinion in biotechnology, 44, 146-152, 2017.

SUTTER, B. M., WU, X., LAXMAN, S., TU, B. P. Methionine inhibits autophagy and promotes growth by inducing the SAM-responsive methylation of PP2A. Cell, 154(2), 403-415, 2013.

SÝKORA, T.; RABIŠKOVÁ, M.; TŘINÁCTÝ, J.; VETCHÝ, D.; HÄRING, A.; DVOŘÁK, P. Postruminal Delivery System for Amino Acids and Proteins in Cattle. ACTA VET. BR, 76: 547-552, 2007.

TRUMBO, P. R. Challenges with using chronic disease endpoints in setting dietary reference intakes. Nutrition reviews, 66(8), 459-464, 2008.

VALADARES FILHO, S. de C.; PINA, D. dos S. Fermentação ruminal. Nutrição de ruminantes. Jaboticabal: FUNEP, 2006.

VALDERRAMA, J.O. The state of the cubic equations of state. Ind. Eng. Chem. Res., v. 42, p. 1603-1618, 2003.

VAN KONYNENBURG, P. H.; SCOTT, R. L. Critical Lines and Phase Equilibria in Binary Van Der Waals Mixtures. Philosophical Transactions of the Royal Society A: Mathematical, Physical and Engineering Sciences, v. 298, n. 1442, p. 495–540, 18 dez. 1980.

WANG, C., LIU, H. Y., WANG, Y. M., YANG, Z. Q., LIU, J. X., WU, Y. M., YAN, T., YET, H. W. Effects of dietary supplementation of methionine and lysine on milk production and nitrogen utilization in dairy cow. Journal of Dairy Science, vol. 93, n. 8, pág. 3661-3670, 2010.

WEI, Y. S., SADUS, R. J. Equations of state for the calculation of fluid-phase equilibria. AIChe Journal, v. 46, p. 169-196, 2000.

YEO SD, KIRAN E. Formation of polymer particles with supercritical fluids: a review. J Supercrit Fluids, v. 34, p. 287–308, 2005.

CHAPTER 3 - PRECIPITATION OF METHIONINE AND ETHYL CELLULOSE IN CARBON DIOXIDE + ETHANOL + ACETIC ACID SYSTEMS AT HIGH PRESSURES: PHASE EQUILIBRIUM DATA FOR THE GAS ANTISOLVENT PROCESS

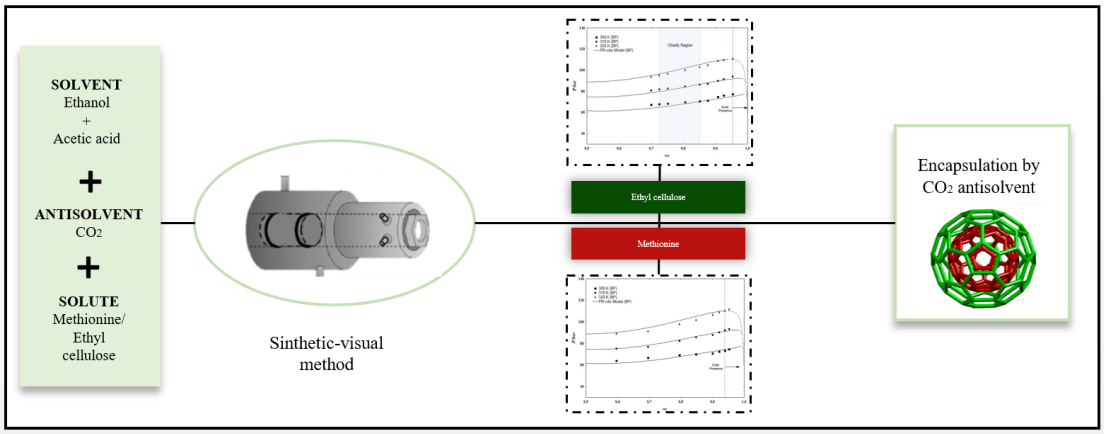

ABSTRACT

This work reports experimental data on the phase transitions in the quaternary system involving carbon dioxide, ethanol, acetic acid and solute (methionine or ethyl cellulose) at high pressures. Experimental data were obtained by the synthetic method, with a variable volume visualization cell, in the temperature range of 308.15-328.15 K and pressures from 6.19 to 11.15 MPa. For the quaternary systems, the solutes were previously solubilized at two different concentrations, 0.1 mg/mL [0.0110 % mass fraction] and 0.2 mg/mL [0.0221 % mass fraction] for methionine and 2.5 mg/mL [0.2757 % mass fraction] and 5.0 mg/mL [0.5514 % mass fraction] for ethyl cellulose, in a 1:1 mass ratio solution of ethanol to acetic acid. Vapor-liquid-type phase transitions were observed, characterized as bubbles in the presence or absence of solid phase. A solid phase was observed for all solute concentrations evaluated in this study. Determination of the region of precipitation of methionine or ethyl cellulose is important to identify the optimal concentration of the solvent/solute mixture, where CO_2 will act strongly as an antisolvent, ensuring a high efficiency of the GAS technique. Thermodynamic modeling presented satisfactory results, where it adequately described of experimental phase equilibrium data, neglecting the acetic acid dimerization effect.

Keywords: phase behavior; precipitation; CO_2 antisolvent; solubility; methionine; ethyl cellulose.

3.1 INTRODUCTION

Methionine ($C_5H_{11}NO_2S$) is an essential amino acid, i.e., amino acid that need to be obtained from the diet because they cannot be synthesized by the organism. This amino acid corresponds to an important source of sulfur and acts mainly in protein synthesis, in which is considered a limiting factor for the productivity of dairy cows [1,2]. Methionine is used as a supplement for ruminant animals to improve dairy production, however, it suffers ruminal degradation when incorporated into the diet, becoming available in sufficient quantity and quality for absorption [3].

Because of ruminal degradation, the incorporation of methionine in protective matrices is necessary for its effective use as supplement. Although many matrices achieve good stability in the rumen, they do not guarantee sufficient availability of this amino acid to ruminants. Thus, formulated methionine should be prepared with smart materials, showing sensitivity to pH, i.e., it should maintain its integrity at ruminal pH and provoke its rupture at abomasal pH. These characteristics promote immediate absorption and a quick response regarding the biological effect [4].

For rumen-protected methionine in encapsulated systems, it is desirable to use a polymeric matrix with biocompatible and/or biodegradable characteristics [5,6]. The coating material must also provide a suitable medium for preserving the properties and the activity of the active substance and be easy to process with the precipitation technique. In this context, ethyl cellulose is one of the most used encapsulating materials because is non-toxic, stable and biocompatible [6,7]. The low solubility of ethyl cellulose in CO_2 and its relatively high solubility in organic solvents provide suitable conditions to preferably employ high pressure process for particle formation and design of improved controlled delivery systems [8].

Because CO_2 is accessible, innocuous, non-toxic, non-reactive, non-flammable, non-polluting, and has a low critical temperature and pressure, it is used to produce particles aiming to overcome the drawbacks involved in traditional techniques. CO_2-based methods involve sustainable, environmentally correct and efficient processes, which characteristics allow to obtain products with high added value and free from chemical residues [9, 10].

In processes involving CO_2 as an antisolvent, two conditions must be respected: (1) the organic solvent and carbon dioxide in a supercritical state (antisolvent) must be miscible under the process conditions; (2) the solute to be

precipitated has to be soluble in an organic solvent and insoluble in the mixture formed by the organic solvent and the antisolvent. Thus, it is necessary to employ conditions that allow the rapid formation of a solution between the organic solvent and the supercritical fluid, inducing the precipitation of the solute. Some processes use the antisolvent feature of supercritical CO_2, for instance: Gas Antisolvent (GAS), Supercritical Antisolvent (SAS), Aerosol Solvent Extraction System (ASES), and Solution Enhanced Dispersion by Supercritical Fluids (SEDS). The differences between these processes are mostly related to the form of contact between solution and antisolvent and the physical state of them [11,12,13].

The development of formulation processes for multi-component systems using CO_2 antisolvent techniques requires knowledge of the phase behavior to select properly the optimal precipitation conditions, which enables to obtain particles with preferential size and morphology. Also, the interval of conditions where this system is a single phase and type of phase transitions are important for the efficiency of the process [13].

In this context, this work aims to investigate the high-pressure phase behavior of the quaternary systems of the carbon dioxide (1) + ethanol (2) + acetic acid (3) + solute (4) system, where the fourth component (solute) is methionine or ethyl cellulose. Descriptions of the equilibrium behavior of these quaternary mixtures were not found in the literature although this type of data is quite valuable for precipitation and encapsulation processes involving CO_2 as an antisolvent. The objective is to collect and model measured data in a range that could be applied directly to the encapsulation of methionine, using ethyl cellulose as an encapsulating agent and using the antisolvent gas process. In addition, the Peng-Robinson cubic equation of state was employed to represent the experimental phase equilibrium data for the studied systems.

3.2 EXPERIMENTAL

3.2.1. Material

DL-Methionine and ethyl cellulose were used as solutes, ethanol and acetic acid were used as organic solvents and carbon dioxide was used as an antisolvent. The components of the systems were obtained commercially, with purity at the

analytical level. The chemical names, molecular formula, molar mass, purity, critical properties (P_c and T_c), and acentric factor (ω) of the components used in this work are show in Table 3.

Table 3 – Molecular formula, molar mass, supplier, purity and characteristic parameters of substances used.

Compound	***CAS[a] No.***	***Molecular formula***	***Molar mass (g/mol)***	***Supplier***	***Mass fraction purity[b]***	***T_c/K***	***P_c/MPa***	***Ω***
DL-Methionine	59-51-8	$C_5H_{11}NO_2S$	149.2	Sigma-Aldrich	0.990	-	-	-
Ethyl cellulose	9004-57-3	$C_{20}H_{38}O_{11}$	454.5	Sigma-Aldrich	0.990	-	-	-
Ethanol[c]	64-17-5	C_2H_5OH	46.07[a]	Metaquímica	0.950	240.77	6.15[c]	0.649[c]
Acetic acid[d]	64-19-7	CH_3COOH	60.05	Metaquímica	0.990	592.70	5.79	0.447
CO_2[c]	124-38-9	CO_2	44.01[b]	White Martins S.A.	0.999	304.10[c]	7.38[c]	0.239[c]

[a]Chemical Abstract Service registry number. [b]Information provided by suppliers, [c]Provided by the reference [46], [d]Provided by the reference [47]. T_c, critical temperature; P_c, critical pressure; ω, acentric factor.

3.2.2 Phase equilibrium apparatus and measurements

Phase equilibrium data were obtained using the visual synthetic method. In this method, phase transitions are identified by the appearance of a bubble point, resulting from temperature or pressure variation in a visualization cell. Initially, precise amounts of the pure substances were introduced into the equilibrium cell, thus the general composition of the mixture is known. For illustration, a schematic diagram of the experimental apparatus is shown (Figures 10 and 11). Briefly, it consists of a variable-volume equilibrium cell (EC), equipped with sapphire windows (SW) for visualization of phase transitions. Connected to EC, a syringe pump (ISCO 260D model) is used to: (i) feed the system with a precise amount of liquid CO_2 and (ii) set the desired EC pressure by moving a floating piston (P) located inside EC. Both the experimental apparatus and the methodology were validated and described in detail in a variety of previous studies [13-17]. The equipment can be safely operated up to 27.50 MPa with a pressure expanded uncertainty of 0.01 MPa, provided by the indicator systems.

Figure 10 – Schematic diagram of the experimental unit for phase equilibrium determination.

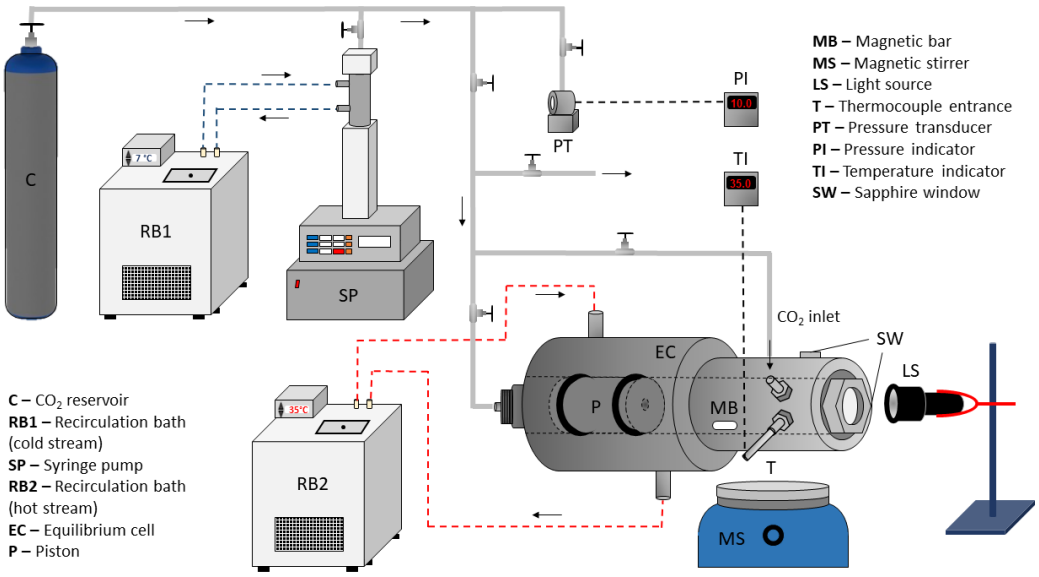

Source: provided by the reference [17].

Figure 11 – Balance unit.

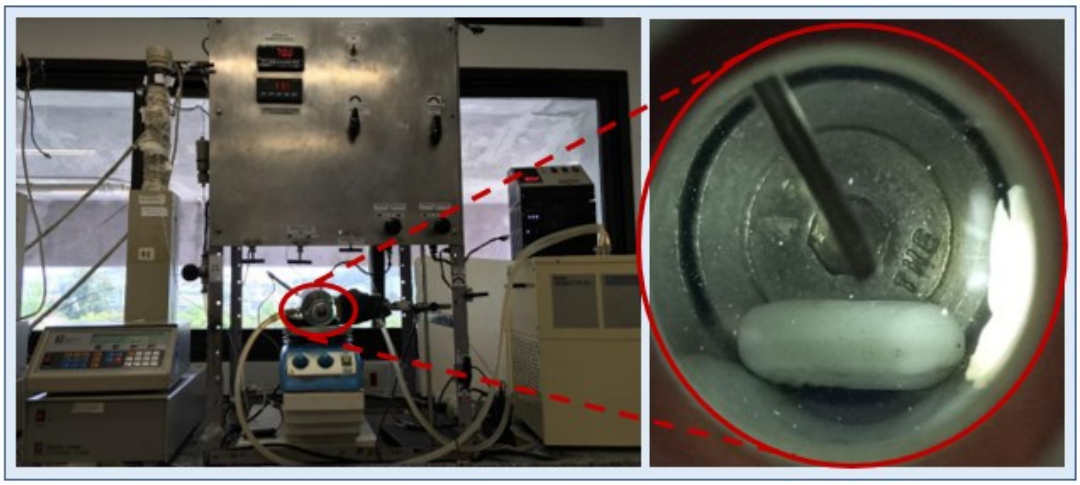

Source: the author (2021).

Systems investigated in this work consisted of the quaternaries CO_2 (1) + ethanol (2) + acetic acid (3) + methionine (4) and CO_2 (1) + ethanol (2) + acetic acid (3) + ethyl cellulose (4), Figure 12. Methionine and ethyl cellulose were previously solubilized at different concentrations (0.1 mg/mL [0.0110 % mass fraction] and 0.2 mg/mL [0.0221 % mass fraction] for methionine and 2.5 mg/mL [0.2757 % mass fraction] and 5.0 mg/mL [0.5514 % mass fraction] for ethyl cellulose) in a solution of ethanol and acetic acid with a 1:1 mass ratio of ethanol to acetic acid. Initially, with the aid of a Pasteur pipette, an approximate mass of 10 g of each solvent, ethanol and acetic acid, was weighed and stored in separately glass tubes. Then, the densities (specific mass) of the solvents were applied to convert these masses into volumes. The total volume of the solution, which will be inserted into the equilibrium cell, corresponds to the sum of the volume of ethanol with the volume of acetic acid. From this total volume and the concentration suggested for the study (5 mg/mL, for example), the mass of the solute (ethyl cellulose) was determined. Solvents and solutes were weighed with the analytical balance (Shimadzu, Model AUY220).

Figure 12 – Methodology layout.

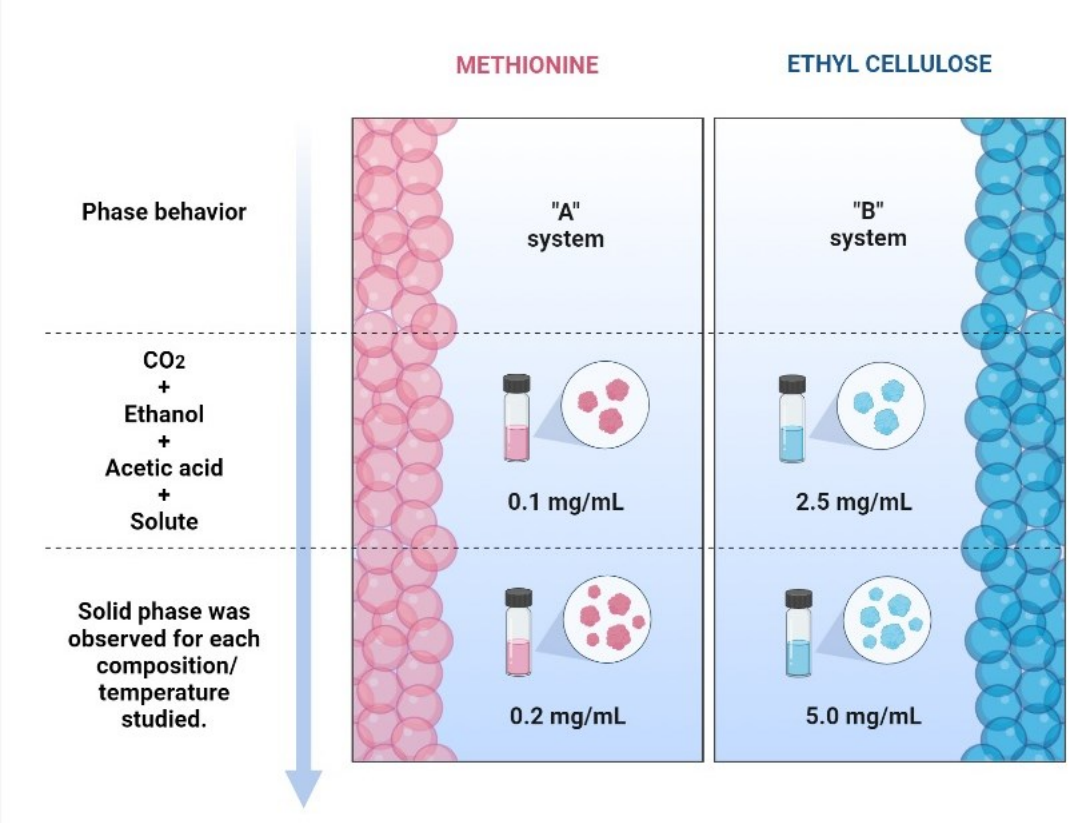

Source: the author (2022).

From the determination of the solute mass, the solutions were prepared differently for methionine and ethyl cellulose. When methionine was used, it was initially inserted into a glass tube containing acetic acid (a solvent with the highest affinity for this amino acid). This solution was then subjected to an ultrasound bath for 10 min and then heated (313.15 K) and stirred for 30-40 min. After this time and observing the complete solubilization of this solute in the acid medium, ethanol was added and heating and stirring continued for about 20-30 min, ensuring complete solubilization of methionine in the solvent mixture. With ethyl cellulose, the procedure was similar. However, the polymer was initially solubilized in the ethanol solvent (a solvent with the highest affinity for ethyl cellulose) and then acetic acid was added to the initial solution. This methodology was used for all concentrations and for all CO_2 mass fractions analyzed.

The low concentrations of methionine and ethyl cellulose are due to their low solubility in CO_2. System compositions were set by feeding the equilibrium cell with a precise amount of the solution of interest with the aid of an analytical balance

(Shimadzu AUY220 model, 0.0001 g precision). The amount of CO_2 for the composition of the system was calculated from the internal volume of the pump reservoir (0.01 mL precision), where the pressure and temperature are kept constant and the CO_2 mass is determined by means of density. The temperature control inside the cell took place through a K-type thermocouple, whose value is presented in the temperature indicator. The temperatures varied between 308.15 and 328.15 K (0.01 K precision) and the tests were analyzed from the lowest to the highest temperature. After stabilization of the temperature, measurements of the phase equilibrium (bubble point) were conducted by reducing gradually the pump pressure until the appearance of a small bubble, indicating second phase. The pressures varied between 6.19 and 11.45 MPa (0.01 MPa precision). Each measurement was repeated three times.

3.2.3 Thermodynamic modeling

The experimental data were correlated with the Peng-Robinson cubic equation of state using the Wong-Sandler mixing rule (PR-WS). The NRTL activity coefficient model was used to calculate the mole excess Gibbs energy, in which the following binary parameters were adjusted in the PR-WS model: *Δgij, Δgji*, *αij* and *kij*. The estimation of the binary interaction parameters was performed fitting the data with the PR-WS model by minimizing the objective function, OF (Eq. 1) of least squares of experimental pressures, using the Simplex method [18]. The saturation pressures of the system at vapor-liquid equilibrium data (VLE) were calculated by implementing a computational code in FORTRAN language [13,17,19]. The goodness of the fit was evaluated by average absolute deviation (AAD, Eq. 2) and root mean square deviation (rmsd, Eq. 3). A global temperature adjustament of the data was used to generate just one set of interaction parameters for the PR-WS.

$$OF = \sum_i^{Nobs}\left(P_i^{calc} - P_i^{exp}\right)^2 \quad (Equation\ 15)$$

$$AAD = \sum_i^{Nobs} \frac{\left|P_i^{calc} - P_i^{exp}\right|}{Nobs} \quad (Equation\ 16)$$

$$rmsd = \sqrt{\sum_i^{Nobs} \frac{\left(P_i^{calc} - P_i^{exp}\right)^2}{Nobs}} \quad (Equation\ 17)$$

The amount of the methionine and ethyl cellulose used in systems was small. Thus, due to the low concentration of solutes in the solutions and the high complexity in modeling systems with a fourth solid component, the effects of these solutes were ignored in the thermodynamic calculation of the vapor-liquid equilibrium. Furthermore, the acetic acid dimerization was neglected, where the dimer and monomer parameters were not considered in the modeling, approaching the concept of pure components.

3.3 RESULTS AND DISCUSSION

A mixture of solvents (ethanol and acetic acid) was carefully selected to mimic real conditions found on the formulation of methionine in ethyl cellulose matrix by CO_2 antisolvent methods. Because both components (methionine and ethyl cellulose) should be soluble in a common solvent or solvent mixture, preliminary studies were conducted to find a suitable solvent mixture to be further used in CO_2-based processes. In preliminary tests, the capacity of different solvents in dissolving ethyl cellulose and methionine was evaluated, by varying the solute concentrations and the ratio between the solvents used, when mixtures of solvents were tested. After some trials using diverse solvents mixtures, the mixture of ethanol and acetic acid at 1:1 mass ratio showed to be the most appropriated solvent because solubilized reasonable amounts of both components.

The experimental data for the quaternary systems combined with the type of transition observed in the experimental measurements are presented in Tables 2-5. The results in these tables are presented in terms of the mass fraction of CO_2 (w_1), pressure transition (P), and standard deviations (σ) of pressure for each temperature evaluated. In both methionine and ethyl cellulose containing systems, vapor-liquid equilibrium (VLE) or vapor-liquid equilibrium with presence of solids (SVLE) were observed.

Experimental data for the quaternary system CO_2 (1) + ethanol (2) + acetic acid (3) + methionine (4) at 0.1 mg/mL of methionine are shown in Table 4 and Figure 13. In this system, the influence of temperature on the appearance of solids was observed. At temperatures of 308.15, 318.15 and 328.15 K, the beginning of the occurrence of methionine precipitation was observed at CO_2 mass fractions of 0.8997, 0.9206, and 0.9383, respectively. This result is favorable for the application of different techniques involving supercritical antisolvent for methionine formulation, because

lower temperature and amount of CO_2 can be used to precipitate methionine. This especially important considering that methionine is a compound thermally sensitive.

Table 4 – Phase equilibrium data for the quaternary system CO_2 (1) + ethanol (2) + acetic acid (3) + methionine (4). w_1 denotes the mass fraction of CO_2 and w_2 denotes the mass fraction of the solution of ethanol + acetic acid + methionine, with 0.1 mg/mL [0.0110 % mass fraction] of methionine in the solvent solvent (1:1 mass ratio solution of ethanol to acetic acid).

T/K[1]	P/MPa	σ/MPa	Transition type	T/K	P/MPa	σ/MPa	Transition type
w_1 = 0.5954 (w_2 = 0.4046)[2]				w_1 = 0.8997 (w_2 = 0.1003)			
308.15	6.40	0.02	VLE (BP)	308.15	7.10	0.01	SVLE(BP)
318.15	7.53	0.03	VLE (BP)	318.15	8.81	0.01	VLE (BP)
328.15	8.93	0.02	VLE (BP)	328.15	10.68	0.02	VLE (BP)
w_1 = 0.6957 (w_2 = 0.3043)				w_1 = 0.9206 (w_2 = 0.0794)			
308.15	6.69	0.04	VLE (BP)	308.15	7.25	0.03	SVLE(BP)
318.15	7.70	0.03	VLE (BP)	318.15	9.05	0.03	SVLE(BP)
328.15	9.17	0.02	VLE (BP)	328.15	10.92	0.04	VLE (BP)
w_1 = 0.7954 (w_2 = 0.2005)				w_1 = 0.9383 (w_2 = 0.0617)			
308.15	6.93	0.10	VLE (BP)	308.15	7.35	0.02	SVLE(BP)
318.15	8.24	0.07	VLE (BP)	318.15	9.23	0.02	SVLE(BP)
328.15	9.82	0.03	VLE (BP)	328.15	11.06	0.01	SVLE(BP)
w_1 = 0.8479 (w_2 = 0.1521)				w_1 = 0.9521 (w_2 = 0.0479)			
308.15	7.02	0.03	VLE (BP)	308.15	7.49	0.02	SVLE(BP)
318.15	8.59	0.04	VLE (BP)	318.15	9.36	0.09	SVLE(BP)
328.15	10.20	0.03	VLE (BP)	328.15	11.20	0.04	SVLE(BP)

[1,2]Standard uncertainties u are u(T) = 0.01 K, and u(w) = 0.0001.

Figure 13 – Pressure-composition diagram for the quaternary system carbon dioxide (1) + ethanol (2) + acetic acid (3) + methionine (4), with a 1:1 mass ratio of ethanol to acetic acid and 0.1 mg/mL [0.0110 % mass fraction] of methionine for ethanol and acetic acid. Experimental BP measurements, solid phase boundary and comparison with PR-WS.

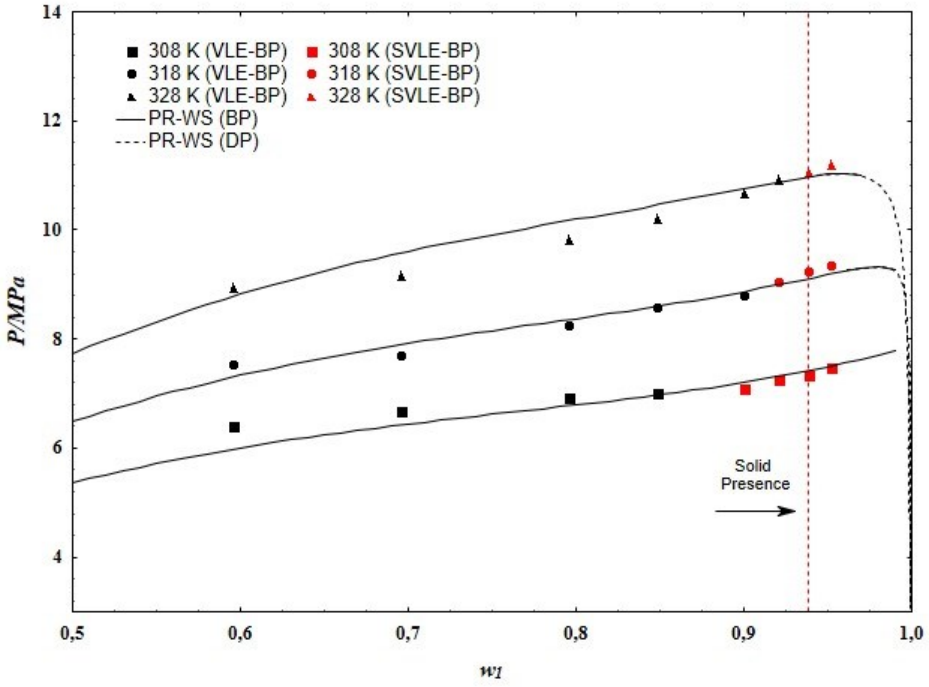

Source: the author (2022).

Figure 13 shows the *P-w* phase diagram which relates the pressure and composition of the system at different isotherms, along with the saturation curve correlated by PR-WS. The behavior of solid formation can be observed by dashed line, which indicates a region with coexistence of a solid phase in equilibrium with the vapor-liquid for all temperatures studies. From the use of CO_2 mass fractions greater than this dashed line, there was the presence of precipitated solid in the equilibrium cell. In the region nearby to the beginning of SVLE, it is possible to observe that the composition ranges are nearby. Thus, any change in composition can significantly influence the increase in the concentration of solids in solution [13,17].

Results for the system with a methionine concentration of 0.2 mg/mL are shown in Table 5 and Figure 14. Transition pressures were observed in the range of 6.19-11.42 MPa for temperature ranging from 308.15 to 328.15 K. In a mass fraction of CO_2 of 0.7091 in the equilibrium cell, the appearance of solids was observed at the temperatures of 308.15 and 318.15 K. However, when applying a higher temperature,

328.15 K, the methionine was solubilized and the absence of solids was observed in the system.

Table 5 – Phase equilibrium data for the quaternary system CO_2 (1) + ethanol (2) + acetic acid (3) + methionine (4). w_1 denotes the mass fraction of CO_2 and w_2 denotes the mass fraction of the ethanol + acetic acid + methionine solution, with 0.2 mg/mL [0.0221 % mass fraction] methionine in the solvent solvent (1:1 mass ratio solution of ethanol to acetic acid).

T/K[1]	P/MPa	σ/MPa	Transition type	T/K	P/MPa	σ/MPa	Transition type
w_1 = 0.6009 (w_2 = 0.3991)[2]				w_1 = 0.8006 (w_2 = 0.1994)			
308.15	6.19	0.04	VLE (BP)	308.15	7.00	0.10	SVLE(BP)
318.15	7.43	0.30	VLE (BP)	318.15	8.50	0.10	SVLE(BP)
328.15	8.82	0.20	VLE (BP)	328.15	9.80	0.20	SVLE(BP)
w_1 = 0.6991 (w_2 = 0.3009)				w_1 = 0.8501 (w_2 = 0.1499)			
308.15	6.69	0.20	VLE (BP)	308.15	7.12	0.17	SVLE(BP)
318.15	8.00	0.20	VLE (BP)	318.15	8.71	0.20	SVLE(BP)
328.15	9.26	0.40	VLE (BP)	328.15	10.33	0.20	SVLE(BP)
w_1 = 0.7091 (w_2 = 0.2908)				w_1 = 0.8997 (w_2 = 0.1003)			
308.15	6.75	0.06	SVLE(BP)	308.15	7.30	0.10	SVLE(BP)
318.15	8.11	0.17	SVLE(BP)	318.15	8.90	0.10	SVLE(BP)
328.15	9.38	0.04	VLE (BP)	328.15	10.85	0.10	SVLE(BP)
w_1 = 0.7251 (w_2 = 0.2749)				w_1 = 0.9250 (w_2 = 0.0750)			
308.15	6.79	0.06	SVLE(BP)	308.15	7.52	0.17	SVLE(BP)
318.15	8.20	0.26	SVLE(BP)	318.15	9.15	0.20	SVLE(BP)
328.15	9.49	0.26	SVLE(BP)	328.15	11.06	0.20	SVLE(BP)
w_1 = 0.7514 (w_2 = 0.2486)				w_1 = 0.9521 (w_2 = 0.0479)			
308.15	6.88	0.20	SVLE(BP)	308.15	7.73	0.10	SVLE(BP)
318.15	8.36	0.03	SVLE(BP)	318.15	9.46	0.20	SVLE(BP)
328.15	9.53	004	SVLE(BP)	328.15	11.42	0.10	SVLE(BP)

[1,2]Standard uncertainties u are u(T) = 0.01 K, u(w) = 0.0001.

Figure 14 – Pressure-composition diagram for the quaternary system carbon dioxide (1) + ethanol (2) + acetic acid (3) + methionine (4), with a 1:1 mass ratio of ethanol to acetic acid and 0.2 mg/mL [0.0221 % mass fraction] of methionine for ethanol and acetic acid. Experimental BP measurements, solid phase boundary and comparison with PR-WS.

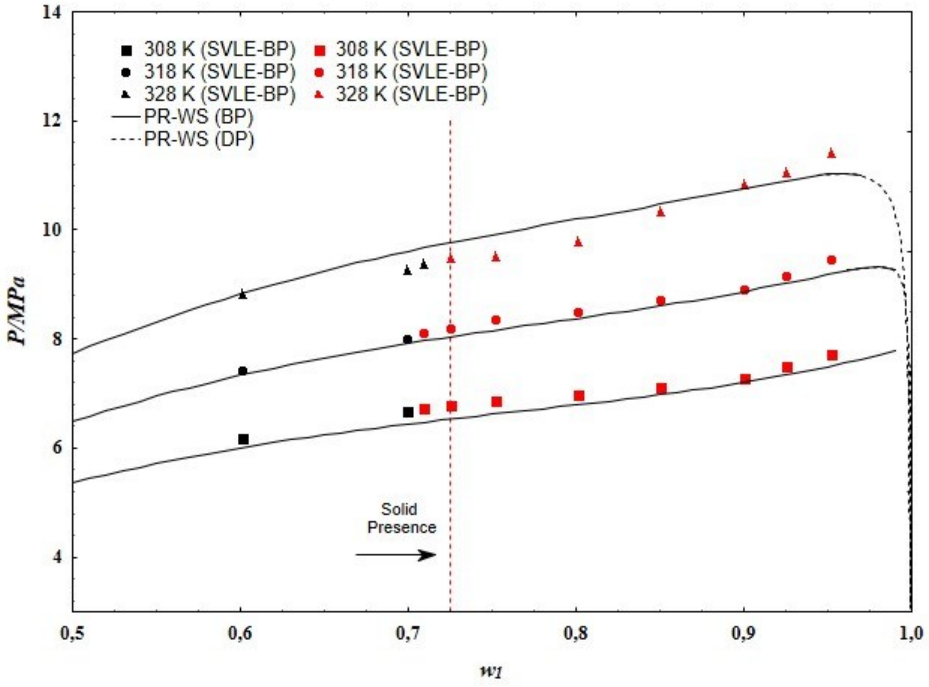

Source: the author (2022).

Comparing Figure 13 with Figure 14, it is verified that the increase in the concentration of methionine (from 0.1 to 0.2 mg/mL) provided an anticipation of the appearance of solids to lower fractions of CO_2, which can be explained by the antisolvent effect of the supercritical fluid used. The difference of line position is due to methionine concentration in the system. Methionine concentration is higher in Fig. 3. In this way, due to low solubility of methionine in CO_2, the border of area with solid phase was displaced to a lower value of mass fraction.

Results for the quaternary systems CO_2 (1) + ethanol (2) + acetic acid (3) + ethyl cellulose (4) at 2.5 and 5.0 mg/mL of ethyl cellulose are shown in Table 6 and Table 7, respectively. Comparing the mass fractions of CO_2 for the precipitation of solutes studied, it is verified that methionine precipitated in mass fractions of 0.9383 (0.1 mg/mL) and 0.7251 (0.2 mg/mL), while ethyl cellulose precipitated in fractions of 0.9530 (2.5 mg/mL) and 0.8997 (5.0 mg/mL). Therefore, ethyl cellulose showed a greater solubility in the fluid solution when compared to methionine.

Table 6 – Phase equilibrium data for the quaternary system CO_2 (1) + ethanol (2) + acetic acid (3) + ethyl cellulose (4). w_1 denotes the mass fraction of CO_2 and w_2 denotes the mass fraction of the ethanol + acetic acid + ethyl cellulose solution, with 2.5 mg/mL [0.2757 % mass fraction] of ethyl cellulose in the solvent solvent (1:1 mass ratio solution of ethanol to acetic acid).

T/K[1]	P/MPa	σ/MPa	Transition type	T/K	P/MPa	σ/MPa	Transition type
w_1 = 0.6999 (w_2 = 0.3001)[2]				w_1 = 0.8757 (w_2 = 0.1243)			
308.15	6.75	0.04	VLE (BP)	308.15	7.13	0.22	VLE (BP)
318.15	8.10	0.06	VLE (BP)	318.15	8.73	0.04	VLE (BP)
328.15	9.38	0.04	VLE (BP)	328.15	10.47	0.04	VLE (BP)
w_1 = 0.7248 (w_2 = 0.2752)				w_1 = 0.9068 (w_2 = 0.0932)			
308.15	6.80	0.04	VLE (BP)	308.15	7.48	0.05	VLE (BP)
318.15	8.19	0.04	VLE (BP)	318.15	9.00	0.04	VLE (BP)
328.15	9.53	0.02	VLE (BP)	328.15	10.90	0.04	VLE (BP)
w_1 = 0.7507 (w_2 = 0.2493)				w_1 = 0.9251 (w_2 = 0.0749)			
308.15	6.86	0.10	VLE (BP)	308.15	7.62	0.02	SVLE(BP)
318.15	8.28	0.10	VLE (BP)	318.15	9.16	0.01	VLE (BP)
328.15	9.69	0.20	VLE (BP)	328.15	10.98	0.01	VLE (BP)
w_1 = 0.8047 (w_2 = 0.1953)				w_1 = 0.9530 (w_2 = 0.0470)			
308.15	6.98	0.10	VLE (BP)	308.15	7.74	0.02	SVLE(BP)
318.15	8.48	0.10	VLE (BP)	318.15	9.41	0.01	SVLE(BP)
328.15	10.03	0.10	VLE (BP)	328.15	11.11	0.03	SVLE(BP)
w_1 = 0.8501 (w_2 = 0.1499)							
308.15	7.07	0.04	VLE (BP)				
318.15	8.64	0.02	VLE (BP)				
328.15	10.31	0.01	VLE (BP)				

[1,2]Standard uncertainties u are u(T) = 0.01 K, u(w) = 0.0001.

Table 7 – Phase equilibrium data for the quaternary system CO_2 (1) + ethanol (2) + acetic acid (3) + ethyl cellulose (4). w_1 denotes the mass fraction of CO_2 and w_2 denotes the mass fraction of the ethanol + acetic acid + ethyl cellulose solution, with 5.0 mg/mL [0.5514 % mass fraction] of ethyl cellulose in the solvent (1:1 mass ratio solution of ethanol to acetic acid).

T/K[1]	P/MPa	σ/MPa	Transition type	T/K	P/MPa	σ/MPa	Transition type
w_1 = 0.6038 (w_2 = 0.3962)[2]				w_1 = 0.8493 (w_2 = 0.1507)			
308.15	6.47	0.04	VLE (BP)	308.15	7.13	0.03	SVLE(BP)
318.15	7.57	0.03	VLE (BP)	318.15	8.61	0.02	SVLE(BP)
328.15	8.97	0.04	VLE (BP)	328.15	10.29	0.04	VLE (BP)
w_1 = 0.7109 (w_2 = 0.2891)				w_1 = 0.8752 (w_2 = 0.1248)			
308.15	6.74	0.02	SVLE(BP)	308.15	7.18	0.02	SVLE(BP)
318.15	8.10	0.01	VLE (BP)	318.15	8.75	0.04	SVLE(BP)
328.15	9.40	0.04	VLE (BP)	328.15	10.48	0.04	VLE (BP)
w_1 = 0.7249 (w_2 = 0.2751)				w_1 = 0.8997 (w_2 = 0.1003)			
308.15	6.78	0.03	SVLE(BP)	308.15	7.50	0.01	SVLE(BP)
318.15	8.15	0.02	VLE (BP)	318.15	8.90	0.03	SVLE(BP)
328.15	9.49	0.01	VLE (BP)	328.15	10.90	0.04	SVLE(BP)
w_1 = 0.7501 (w_2 = 0.2499)				w_1 = 0.9269 (w_2 = 0.0731)			
308.15	6.86	0.10	SVLE(BP)	308.15	7.64	0.02	SVLE(BP)
318.15	8.24	0.03	SVLE(BP)	318.15	9.23	0.04	SVLE(BP)
328.15	9.65	0.04	VLE (BP)	328.15	11.20	0.04	SVLE(BP)
w_1 = 0.8013 (w_2 = 0.1987)				w_1 = 0.9499 (w_2 = 0.0501)			
308.15	6.99	0.04	SVLE(BP)	308.15	7.73	0.01	SVLE(BP)
318.15	8.43	0.05	SVLE(BP)	318.15	9.51	0.10	SVLE(BP)
328.15	9.98	0.10	VLE (BP)	328.15	11.45	0.02	SVLE(BP)
w_1 = 0.8062 (w_2 = 0.1938)							
308.15	7.01	0.01	SVLE(BP)				
318.15	8.45	0.02	SVLE(BP)				
328.15	10.01	0.10	VLE (BP)				

[1,2]Standard uncertainties u are u(T) = 0.01 K, u(w) = 0.0001.

Figures 15 and 16 shows the phase equilibrium diagrams constructed using data from Table 6 and Table 7, respectively. Similar to the system involving methionine as a solute, in the system with ethyl cellulose, the increase in the concentration of ethyl cellulose provided an anticipation of the appearance of solids for lower CO_2 fractions. Its knowledge is critical for processes antisolvent, where solid precipitation is favored by higher antisolvent CO_2 mass fractions and/or high solute concentrations. The supercritical solvent acts like a dragging component on the solvents organic, drastically reducing the solubilization of methionine in the fluid medium. This effect was also verified in different studies that applied the fluid as an antisolvent [20-23].

Figure 15 – Pressure-composition diagram for the quaternary system carbon dioxide (1) + ethanol (2) + acetic acid (3) + ethyl cellulose (4), with a 1:1 mass ratio of ethanol to acetic acid and 2.5 mg/mL [0.2757 % mass fraction] of ethyl cellulose for ethanol and acetic acid. Experimental BP measurements, solid phase boundary and comparison with PR-WS.

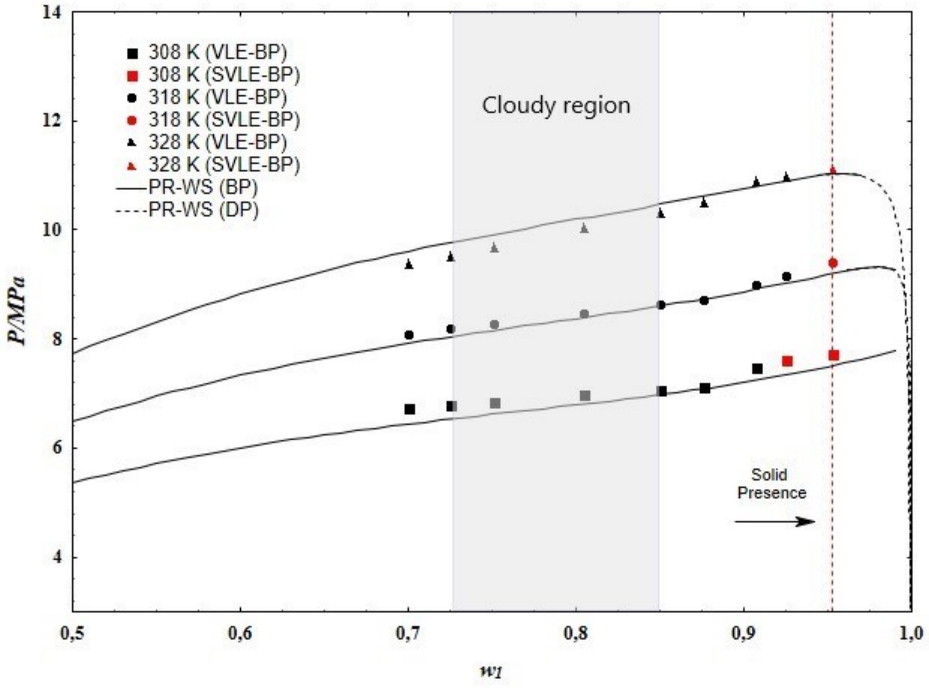

Source: the author (2022).

Figure 16 – Pressure-composition diagram for the quaternary system carbon dioxide (1) + ethanol (2) + acetic acid (3) + ethyl cellulose (4), with a 1:1 mass ratio of ethanol to acetic acid and 5.0 mg/mL [0.5514 % mass fraction] of ethyl cellulose for ethanol and acetic acid. Experimental BP measurements, solid phase boundary and comparison with PR-WS.

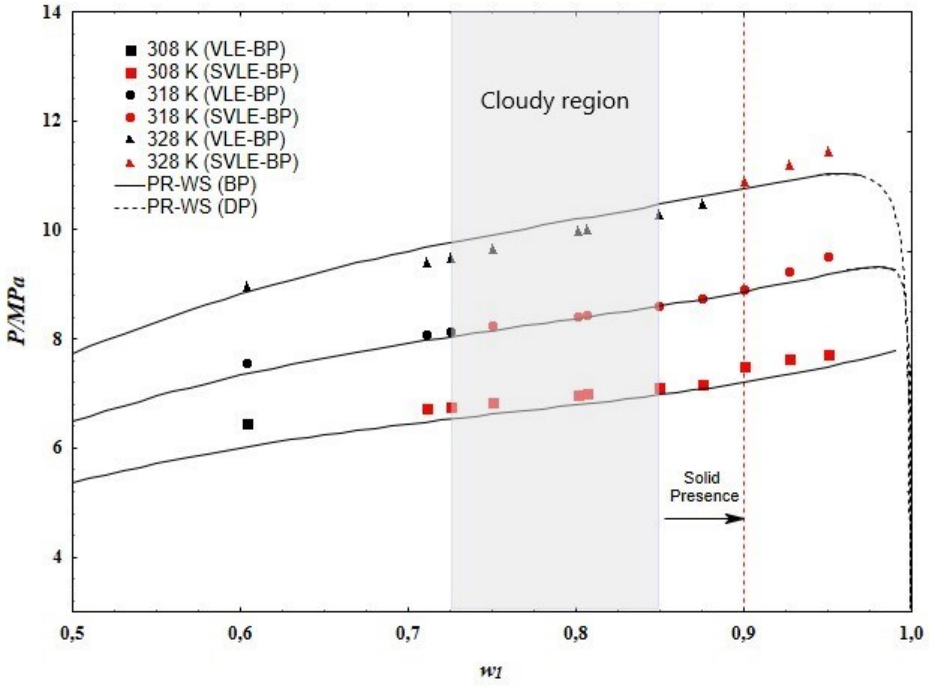

Source: the author (2022).

In ethanol + acetic acid systems, the addition of CO_2 affects the dielectric properties of the solvents and, therefore, the hydrogen bonds are weakened with an increase in the CO_2 content in the system [24]. Also, the addition of supercritical CO_2 can change the physicochemical properties of pure solvents, such as polarity and capacity to establish hydrogen bonds [25]. Duereh et al. [26] observed in their studies the variation of the dipolarity/polarizability parameters of the CO_2 and ethanol mixture and verified that the specific interactions between the components were affected by the CO_2 content, the dipole moment of the polar solvent and the density of the supercritical fluid (pressure and temperature). Yamamoto et al. [27] studied the CO_2/ethanol/acetic acid ternary system and quantified the hydrogen bond species between this carboxylic acid and the ethanol molecules. In both works, the authors confirmed that the greater the amount of CO_2 used in the system, the smaller the specific interactions between the solvents and the CO_2, consequently, the lower the

solubility between them. This effect of the CO_2 content and the changes in the properties of pure solvents were also observed in other works, [24, 25, 28].

Thus, knowing the implications caused by supercritical CO_2 in mixtures involving solvents, the addition of a solute with solubilization based on hydrogen bonds, such as methionine and ethyl cellulose, will possibly also suffer the effects caused by supercritical CO_2. This effect on the solute-solvent interaction will be even greater in ethyl cellulose, due to the hydrogen bonding sites inherent to cellulosic compounds and because it is used in greater amounts in the present work. El Seoud et al. [29] studied the physical dissolution of cellulose and observed that this type of solute requires the breaking of inter and intramolecular hydrogen bonds between the hydroxyl groups. Thus, considering similarity with ethyl cellulose, the interactions of this solute are favored in the CO_2/ethanol/acetic acid mixture, where the polar interactions promoted the formation of a single phase, providing a more soluble system and precipitation in higher CO_2 mass fractions, when compared to methionine, corroborating with Li and Mark [28].

Another trend that can be explained is related to temperature, since the increase in temperature favored the interactions involved in the quaternary systems studied. For example, in the quaternary system with 5.0 mg/mL of ethyl cellulose and in the CO_2 mass fraction of 0.7109, solids were only perceived at 308.15 K (lowest temperature evaluated), and then were solubilized at 318.15 K, due to the increase in solute-solvent interactions with increasing temperature [17]. The same behavior was found in systems with the presence of solids occurring only at the lowest temperatures evaluated [13,30,31].

In addition, another trend in the solute-solvent interaction is related to the concentration of the solutes involved. For more concentrated solutions, the amount of CO_2 required for the formation of a solid phase can be much smaller due to the proximity of the saturation of the solution [21,31], since this saturation is achieved by increasing the composition of the antisolvent CO_2, providing a sharp decrease in solute solubility from the saturation value in the pure solvent [13,17]. For example, in systems with concentrations of 2.5 mg/mL of ethyl cellulose, higher fractions of CO_2 are required for solids precipitation, when compared to more concentrated systems, with 5.0 mg/mL of the same solute. The same influence of solute concentration on the appearance of the solid phase was observed by other authors [13,17,21,32].

In the present work, the concept of a pseudoternary system was applied, which consists of neglecting the effect of the solute on equilibrium. However, both for methionine and for ethyl cellulose, the solute concentration changed the mass fraction of CO_2 in the appearance of the solid, indicating that the solutes remained solubilized in the mixture CO_2 + ethanol + acetic acid up to a certain condition. The increase in concentration favored precipitation due to the rapid appearance of solids. Thus, the behavior of solid formation can be compared to the displacement of the dashed line in Figures 13-16. This line indicates the area of the diagram related to the solid phase and the difference in its position is due to the concentration of the solute in the system. Due to the low solubility of the solute in CO_2, the boundary area with the solid phase was shifted to a lower value of mass fraction [31].

This factor is highly relevant in processes that involve precipitation, such as the antisolvent techniques. In this process, at the time of precipitation, the mixture of solvents has a greater solubility in CO_2 when compared to solutes. Thus, the CO_2 carry the solvent molecules, reducing the solute solubility in the fluid phase, causing its precipitation [13-15,17]. Therefore, studying the phase behavior is highly relevant for identifying the best precipitation conditions, ensuring that the conditions established for any supercritical antisolvent technique are adequate for the precipitation of solutes, preventing them from being carrying along with the CO_2 and solvents used.

The presence of acetic acid dimers made the medium cloudy, making it difficult to see the transition points [33,34,35]. In systems with ethyl cellulose, the influence of acetic acid dimers showed a greater intensity, where turbidity was verified in CO_2 mass fractions between 0.7248 to 0.8501 (2.5 mg/mL) and 0.7249 to 0.8493 (5.0 mg/mL). The cloud region can be seen in Figs. 15 and 16 for the concentrations of 2.5 and 5.0 mg/mL of ethyl cellulose, respectively. The turbidity region in the system does not correspond to a precondition for the presence of solids, but only an effect caused by the strong interactions of the acid group and polymer-polymer group in the studied systems [36].

The use of acetic acid in CO_2/ethanol/solute systems developed effects that are characteristic of these components, due to the presence of the acid group. The formation of dimers by the association of monomeric units is common in carboxylic acids, being their association relatively stable due to strong hydrogen bonds [36]. Carboxylic acids have a proton donating group (OH) and a proton acceptor group

(C=O), which favors this kind of association. In this way, there are interactions between each acetic acid molecule in one dimer and each acetic acid molecule in the other dimer, resulting in four attractive interactions like those between two monomers. This strong interaction can favor the appearance of turbid regions, which will depend on the components involved in the mixture and on the applied conditions, such as pressure and temperature [33,34,37].

When using ethyl cellulose as a solute, an intense cloud region was found in the quaternary systems. Ethyl cellulose forms intra and intermolecular hydrogen bonds, justified by the strong polymer-polymer interaction. Furthermore, this polymer is not soluble in pure CO_2 and ethanol is used as a co-solvent to achieve solubility between them. Thus, ethanol searches to increase the density of the solution, contributing with ethanol-ethyl cellulose hydrogen bonds and polar interactions, promoting the formation of a single phase. However, to reach adequate solubility, a large amount of ethanol is needed, indicating that CO_2 acts as an anti-solvent for this polymer [28,36,38,39]. In the present work, ethyl cellulose showed an increase in its solubility, which can be explained by the extra interactions provided by the acid group of acetic acid.

Figure 17 illustrates the experimental phase equilibrium data in P-T projection for CO_2/ethanol/acetic acid/solute systems, at different mass fractions of methionine (0.1 and 0.2 mg/mL) and ethyl cellulose (2.5 and 5.0 mg/mL). As shown in Figure 17, the P-T relationship is typical of Lower Critical Solution Temperature (LCST) behavior, in which the curves define a region where the components are soluble in any proportion (below the curves) and where occur two phases formation (above the curves). Also, it is possible to verify that an increase in temperature provided an augment in the pressure necessary for the homogenization of the system and consequently, an increase in the transition pressure values (BP). The main characteristics that define this behavior are interaction forces between the components of the mixture, which interfere in the expansion and exclusion of compounds, increasing the volume of the solution, which in turn depend on the nature of the molecules and molecular forces existing between them [40]. Thus, the most volatile compound (CO_2) expresses a tendency to expand faster than the other compounds in the system, providing an increase in the volume of the solution, requiring greater pressure for its complete solubilization [13,15,17,19,39].

Figure 17 – P-T diagrams for CO_2 + ethanol + acetic acid + solute systems. (a) 0.1 mg/mL [0.0110 % mass fraction] methionine, (b) 0.2 mg/mL [0.0221 % mass fraction] methionine, (c) 2.5 mg/mL [0.2757 % mass fraction] ethyl cellulose and (d) 5.0 mg/mL [0.5514 % mass fraction] ethyl cellulose, for different mass fractions (*w*) of CO_2.

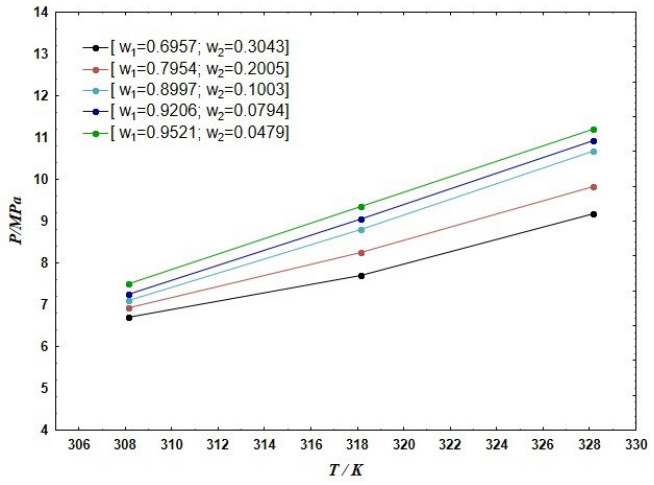

(a)

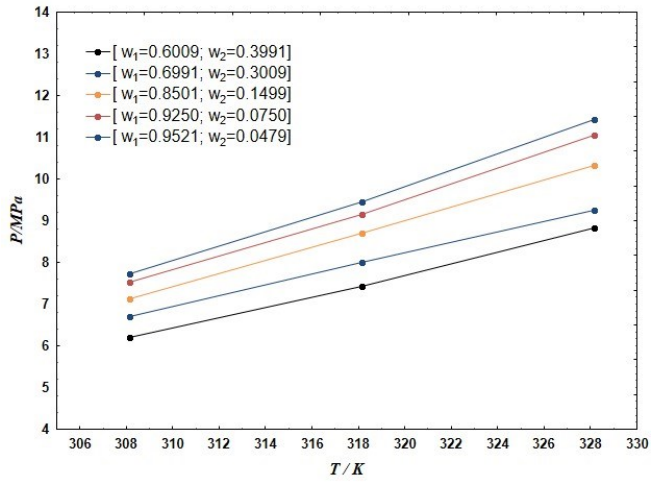

(b)

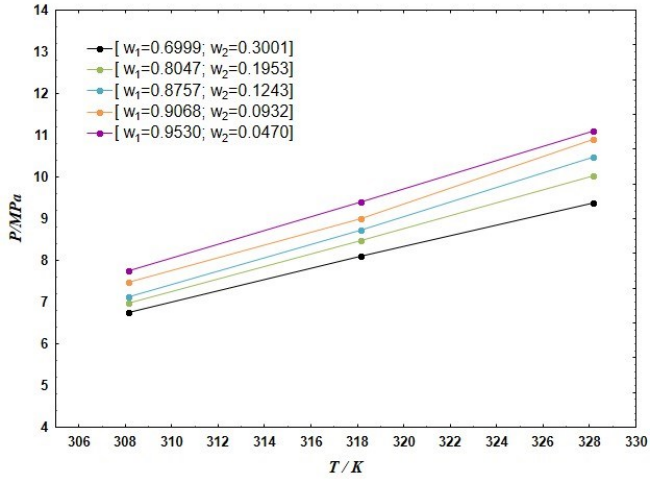

(c)

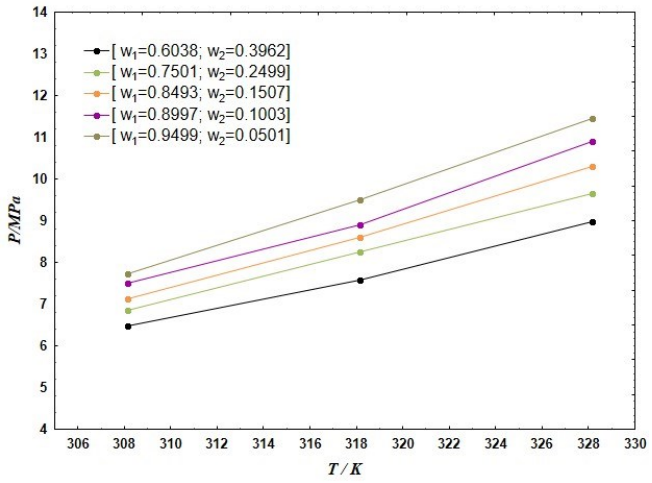

(d)

Source: the author (2022).

The experimental data obtained from the quaternary systems CO_2 (1) + ethanol (2) + acetic acid (3) + methionine (4), 0.1 mg/mL and 0.2 mg/mL for methionine, and CO_2 (1) + ethanol (2) + acetic acid (3) + ethyl cellulose (4), 2.5 mg/mL and 5.0 mg/mL for ethyl cellulose, were compared with data for binary systems (CO_2/ethanol and CO_2/acetic acid) available in the literature and illustrated in Figure 18. It is observed that the experimental and theoretical ELV data presented a relevant approximation, indicating that quaternary systems can be treated as pseudoternary, except when high solute concentrations are used.

Figure 18 – Pressure-composition diagram for the quaternary system carbon dioxide (1) + ethanol (2) + acetic acid (3) + methionine (4), 0.1 mg/mL [0.0110 % mass fraction] and 0.2 mg/mL [0.0221 % mass fraction] for methionine (MET), and carbon dioxide (1) + ethanol (2) + acetic acid (3) + ethyl cellulose (4), 2.5 mg/mL [0.2757 % mass fraction] and 5.0 mg/mL [0.5514 % mass fraction] for ethyl cellulose (ETHYL).

Comparison with literature data for the CO_2 + ethanol (EtOH) and CO_2 + acetic acid (AA) systems. (a) 308K, (b) 318K, (c) 328K.

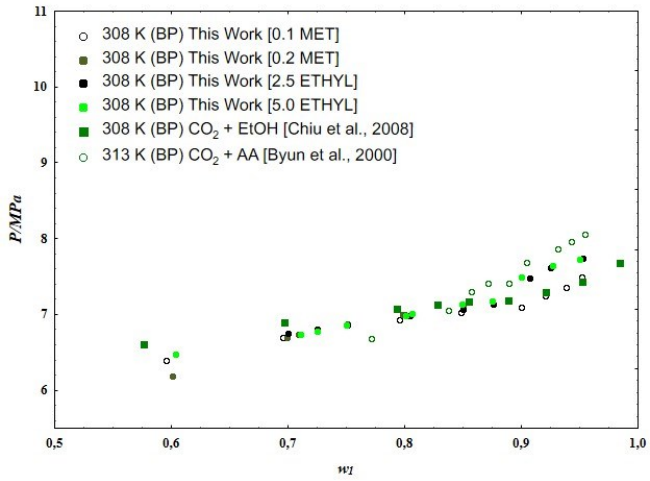

(a)

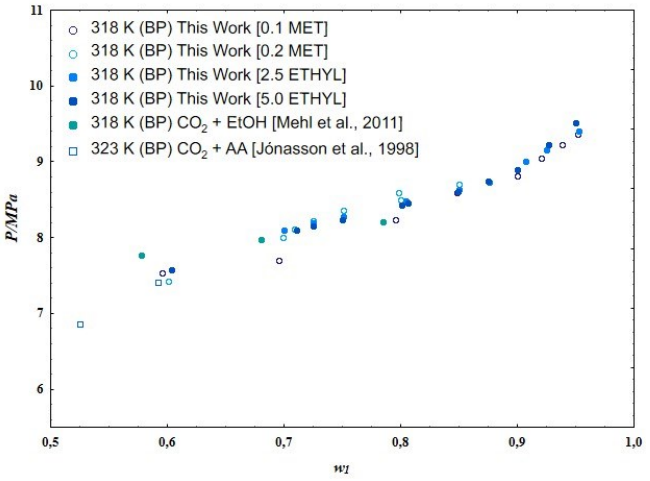

(b)

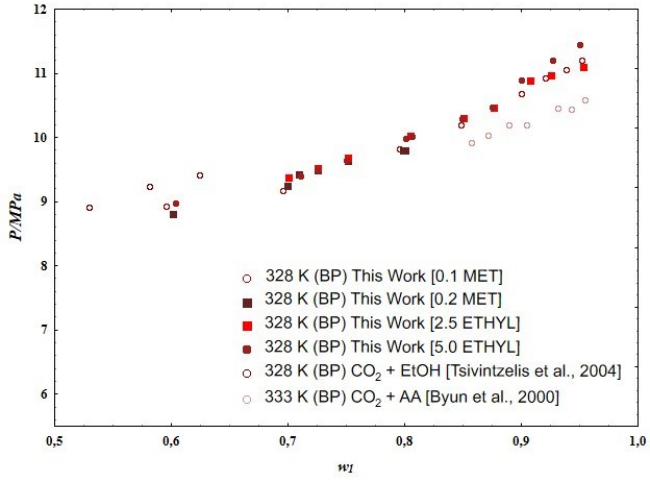

(c)

Source: the author (2022).

Regarding thermodynamic modeling, Table 8 presents the values of the binary interaction parameters (k_{ij} and l_{ij}) used in the PR-WS for pseudoternary system {CO_2

(1) + ethanol (2) + acetic acid (3)}. In addition, the deviations, rmsd (mean square deviation) and AAD (average absolute deviation), are also provided, indicating that the experimental data were satisfactorily adjusted.

Table 8 – Fitted interaction parameters of the PR-WS model used in this work.

T/K	*i-j*	Δg_{ij}/K	Δg_{ji}/K	α_{ij}	K_{ij}	*rmsd*/MPa	*AAD*/MPa
CO_2 (1) + Ethanol (2) + Acetic Acid (3)							
308-328	1 to 2	1268.92	1663.03	0.3129	0.3466	0.27	0.19
	1 to 3	1332.92	1652.13	0.3165	0.3464		
	2 to 3	2528.48	-1870.07	0.3905	0.2009		

Fitted parameters were $\Delta g_{ij} = \left(\lambda_{ij} - \lambda_{ii}\right)/R$

$AD = \sum_{i}^{nobs} \frac{\left|P_i^{Calc} - P_i^{Exp}\right|}{nobs}$ (absolute deviation)

$rmsd = \sqrt{\sum_{i=1}^{nobs} \frac{\left(P_i^{Calc} - P_i^{Exp}\right)^2}{nobs}}$ (root mean square deviation)

The Peng-Robinson equation presented a satisfactory adjustment to the experimental data, providing an excellent qualitative prediction of the vapor-liquid equilibrium boundary, despite disregarding the effects of acetic acid dimerization. Similar results were found in the literature [13,17,32-33,35,37].

The systems studied in the present work presented different associative interactions, which may complicate the application of thermodynamic models. Thus, for an effective modelling, the acetic acid dimerization was neglected as reported by Byun et al. [33]. Furthermore, due to the low concentration of solutes in the solutions, as well as the high complexity in modeling systems involving a fourth solid component, the effects of these solutes were also neglected and the system was considered pseudoternary, with only three components, CO_2/ethanol/acetic acid. However, despite not considering the dimerization and the presence of solutes in the systems,

the Peng-Robinson model was able to predict the vapor-liquid equilibrium boundaries [17,32,45].

Therefore, from the results obtained, the equation provided satisfactory results for systems containing low concentrations of methionine or ethyl cellulose, in the presence or absence of solids. Thus, in addition to providing pioneering data on the phase behavior of quaternary systems involving CO_2 + ethanol + acetic acid + (methionine or ethyl cellulose), the systems studied are relevant for the development of antisolvent processes with supercritical fluids for methionine formulation in ethyl cellulose matrixes.

3.4 CONCLUSIONS

The quaternary systems CO_2 + ethanol + acetic acid + methionine and CO_2 + ethanol + acetic acid + ethyl cellulose, at various solute concentrations, with solution of ethanol and acetic acid with a 1:1 mass ratio of ethanol to acetic acid at 308.15, 318.15 and 328.15 K was described by VLE and SVLE transitions. From the visual synthetic method, it was possible to present pioneering data on the behavior of the solutes of interest and the visualization of the effects of dimerization. The increase in solute concentration anticipated the presence of solids for smaller mass fractions of CO_2, where the solid phase was observed in mass fractions of 0.9383 (0.1 mg/mL) and 0.7251 (0.2 mg/mL) for methionine and 0.9530 (2.5 mg/mL) and 0.8997 (5.0 mg/mL) for ethyl cellulose, at the three temperatures evaluated (308.15-318.15-328.15 K). This behavior can be explained by the action of CO_2 as an antisolvent, where the increase in the fraction of CO_2 in the system increases this antisolvent effect. The Peng-Robinson equation of state satisfactorily represents the experimental phase transition data measured for the quaternary systems. Thus, knowing the phase equilibrium is essential for numerous supercritical carbon dioxide applications, especially involving mixtures of components. The experimental data reported in this study may facilitate optimization of the conditions for the production of particles of methionine and/or ethyl cellulose using the GAS technique.

3.5 REFERENCES

[1] M. Gierus. **Organic and inorganic sources of selenium in the nutrition of dairy cows: digestion, absortion, metabolism and requirements.** Cienc. Rural, 37 (2007), pp. 1212–1220. https://doi.org/10.1590/S0103-84782007000400052.

[2] H. N. Frota, R. B. Reis, B. N. Faria, S. G. Coelho, H. M. Saturnino. **Supplementation of lysine and methionine in association or not with soybean oil in dairy cow diets.** Arq. Bras. Med. Vet. Zootec., 66 (2014), pp. 1121-1128. https://doi.org/10.1590/1678-6471.

[3] National Research Council. **Nutrient requirements of dairy cattle.** Seventh revised edition (2001). Washington, DC: The National Academies Press. https://doi.org/10.17226/9825.

[4] S. C. Valadares Filho, D. S. Pina. **Fermentação ruminal.** In. T. T. Berchielli, A. V. Pires, S. G. Oliveira. Nutrição de ruminantes. 2 ed. Jaboticabal, FUNEP (2011), pp. 161-189.

[5] R. Djerafi, Y. Masmoudi, C. Crampon, A. Meniai, E. Badens. **Supercritical anti-solvent precipitation of ethyl cellulose.** J. Supercrit. Fluids, 105 (2015), pp. 92-98. http://dx.doi.org/10.1016/j.supflu.2015.02.033.

[6] R. Djerafi, A. Swanepoel, C. Crampon, L. Kalombo, P. Labuschagne, E. Badens, Y. Masmoudi. **Supercritical antisolvent co-precipitation of rifampicin and ethyl cellulose.** Eur. J. Pharm. Sci., 102 (2017), pp. 161-171. http://dx.doi.org/10.1016/j.ejps.2017.03.016.

[7] A. Montes, M. D. Gordillo, C. Pereyra, E. J. Martínez de la Ossa. **Co-precipitation of amoxicillin and ethyl cellulose microparticles by supercritical antisolvent process.** J. Supercrit. Fluids, 60 (2011), pp. 75-80. http://dx.doi.org/10.1016/j.supflu.2011.05.002.

[8] A. R. C. Duarte, M. D. Gordillo, M. M. Cardoso, A. L. Simplício, C. M. M. Duarte. **Preparation of ethyl cellulose/methyl cellulose blends by supercritical antisolvent precipitation.** In. J. Pharm., 311 (2006), pp. 50-54. https://doi.org/10.1016/j.ijpharm.2005.12.010.

[9] Z. Knez, E. Markocic, M. Leitgeb, M. Primozic, M. Knez Hrncic, M. Skerget. **Industrial applications of supercritical fluids: a review.** Energy, 77 (2014),

pp. 235-243. https://doi.org/10.1016/j.energy.2014.07.044.

[10] N. Esfandiari. **Production of micro and nano particles of pharmaceutical by supercritical carbon dioxide.** J. Supercrit. Fluids, 100 (2015), pp. 129-141. https://doi.org/10.1016/j.supflu.2014.12.028.

[11] W. L. Priamo, I. Dalmolin, D. L. Boschetto, N. Mezzomo, S. R. S. Ferreira, J. V. Oliveira. **Micronization processes by supercritical fluid technologies: a short review on process design (2008-2012).** Acta Sci., 35 (2013), pp. 695-709. https://doi.org/10.4025/actascitechnol.v35i4.18819.

[12] E. Reverchon, G. Della Porta, M. G. Falivene. **Process parameters and morphology in amoxicillin micro and submicro particles generation by supercritical antisolvent precipitation.** J. Supercrit. Fluids, 17 (2000), pp. 239-248. https://doi.org/10.1016/S0896-8446(00)00045-0.

[13] E. A. Rebelatto, G. P. S. Aguiar, A. L. Piato, J. P. Bender, M. Lanza, J. V. Oliveira **High-pressure phase equilibrium data for carbon dioxide + dichloromethane + acetone and carbon dioxide + dichloromethane + acetone + N-acetylcysteine (NAC).** Fluid Phase Equilib., 473 (2018), pp. 132-137. https://doi.org/10.1016/j.fluid.2018.06.008.

[14] E.A. Rebelatto, A.E. Polloni, K.S. Andrade, J.P. Bender, M.L. Corazza, M. Lanza, J.V. Oliveira. **High-pressure phase equilibrium data for systems containing carbon dioxide, Ω-pentadecalactone, chloroform and water.** J. Chem. Thermodyn., 122 (2018), pp. 125–132. https://doi.org/10.1016/j.jct.2018.03.008.

[15] D. A. Mayer, E. A. Rebelatto, P. M. Ndiaye, M. Lanza, D. de Oliveira, S. M. A. Guelli, U. de Souza, J. V. Oliveira. **High pressure phase equilibrium data for the ternary system containing carbon dioxide, dichloromethane, and ε-caprolactone.** J. Chem. Eng. Data, 64 (2019), pp. 2036-2044. https://doi.org/10.1021/acs.jced.8b01017.

[16] J.C. Nascimento, E.A. Rebelatto, D.A. Mayer, D.G.L. Girardi, P.M. Ndiaye, J.V. Oliveira, M. Lanza. **Phase behavior of carbon dioxide + chloroform + ω-pentadecalactone + poly(ω-pentadecalactone) system: Experimental data and PC-SAFT modeling.** Fluid Phase Equilib., 521 (2020). https://doi.org/10.1016/j.fluid.2020.112736.

[17] C. A. B. Filho, J. L. Dias, E. A. Rebelatto, J. V. Oliveira, S. R. Ferreira, M. Lanza.

Precipitation of quercetin and nicotinamide in carbon dioxide + ethanol + systems at high pressures: phase equilibrium data for antisolvent processes. Fluid Phase Equilib., 533 (2021), 112959. https://doi.org/10.1016/j.fluid.2021.112959.

[18] W.H. Press, S.A. Teukolsky, W.T. Vetterling, B.P. Flannery. **Numerical recipes in Fortran 90: the art of parallel scientific computing.** 2nd ed., Cambridge University Press, Cambridge (1992).

[19] E.A. Rebelatto, A.E. Polloni, K.S. Andrade, M.L. Corazza, J.P. Bender, M. Lanza, J.V. Oliveira. **Phase behaviour of pseudoternary system (carbon dioxide + ω-pentadecalactone + dichloromethane) at different dichloromethane to ω-pentadecalactone mass ratios.** J. Chem. Thermodyn., 126 (2018), pp. 55–62. https://doi.org/10.1016/j.jct.2018.06.019.

[20] J. Fages, H. Lochard, J. J. Letourneau, M. Sauceau, E. Rodier. **Particle generation for pharmaceutical applications using supercritical fluid technology.** Powder Technol., 141 (2004), pp. 219-226. https://doi.org/10.1016/j.powtec.2004.02.007.

[21] E. Franceschi, A. M. de Cesaro, M. Feiten, S. R. S. Ferreira, C. Dariva, M. H. Kunita, A. F. Rubira, E. C. Muniz, M. L. Corazza, J. V. Oliveira. **Precipitation of β-carotene and PHBV and co-precipitation from SEDS technique using supercritical CO_2.** J. Supercrit. Fluids, 47 (2008), pp. 259-269. https://doi.org/10.1016/j.supflu.2008.08.002.

[22] M. J. Cocero, A. Martín, F. Mattea, S. Varona. **Encapsulation and co-precipitation processes with supercritical fluids: fundamentals and applications.** J. Supercrit. Fluids, 47 (2009), pp. 546-555. https://doi.org/10.1016/j.supflu.2008.08.015.

[23] M. Kalani, R. Yunus. **Application of supercritical antisolvent method in drug encapsulation: a review.** Int. J. Nanomedicine, 6 (2011), pp. 1429-1442. https://doi.org/10.2147/IJN.S19021.

[24] J. Cui, M. Andersson, L. Klintberg, M. Sandahl, L. P. Cunico, C. Turner. **Measurement of relative static permittivity and solvatochromic parameters of binary and ternary CO_2-expansed green solvents**. J. Supercrit. Fluids, 171 (2021). https://doi.org/10.1016/j.supflu.2021.105196.

[25] V. T. Wyatt, D. Bush, J. Lu, J. P. Hallett, C. L. Liotta, C. A. Eckert. **Determination**

of solvatochromic solvent parameters for the characterization of gas-expanded liquids. J. Supercrit. Fluids, 36 (2005), pp. 16-22. https://doi.org/10.1016/j.supflu.2005.03.009.

[26] A. Duereh, Y. Sugimoto, M. Ota, Y. Sato, H. Inomata. **Kamlet-Taft dipolarity/polarizability of binary mixtures of supercritical carbon dioxide with cosolvents: measurement, prediction, and applications in separation processes.** Ind. Eng. Chem. Res., 59 (2020), pp. 12319-12330. https://doi.org/10.1021/acs.iecr.0c01251.

[27] M. Yamamoto, Y. Iwai, T. Nakajima, Y. Arai. **Fourier transform infrared study on hydrogen bonding species of carboxylic acids in supercritical carbon dioxide with ethanol.** J. Phys. Chem. A., 103 (1999), pp. 3525-3529. https://doi.org/10.1021/jp984604p.

[28] D. Li, A. Mark, M. C. **Hugh. Solubility behavior of ethyl cellulose in supercritical fluid solvents.** J. Supercrit. Fluids, 28 (2004), pp. 225-231. https://doi.org/10.1016/S0896-8446(03)00048-2.

[29] O. A. El Seoud, M. Kostag, K. Jedvert, N. I. Malek. **Cellulose in ionic liquids and alkaline solutions: advances in the mechanisms of biopolymer dissolution and regeneration.** Polymers, 11 (2019), 1917. https://doi:10.3390/polym11121917.

[30] P. Benelli, S. R. Rosso Comim, J. Vladimir Oliveira, R. C. Pedrosa, S. R. S. Ferreira. **Phase equilibrium data of guaçatonga (casearia sylvestris) extract + ethanol + CO_2 system and encapsulation using a supercritical anti-solvent process.** J. Supercrit. Fluids, 93 (2014), pp. 103-111. https://doi:10.1016/j.supflu.2014.02.007.

[31] W. M. Giufrida, L. F. Pinto, A. F. Zanette, F. A. P. Voll, M. H. Kunita, V. F. Cabral, L. Cardozo-Filho. **Liquid-vapor equilibrium data of CO2 + dichloromethane + medroxyprogesterone system.** Fluid Phase Equilib., 362 (2014), pp. 307-312. https://doi.org/10.1016/j.fluid.2013.10.037.

[32] O. V. Junior, L. F. Pinto, V. F. Cabral, W. M. Giufrida, L. C. Filho. Experimental measurements of the {CO2 (1) + acetone (2) + ivermectin (3)} system at high pressure. J. Chem. Eng. Data, 64 (2019), pp. 3786-3792. https://doi.org/10.1021/acs.jced.9b00072.

[33] H. S. Byun, K. Kim, A. Mark, M. Hugh. **Phase behavior and modeling of**

supercritical carbon dioxide – organic acid mistures. Ind. Eng. Chem. Res., 39 (2000), pp. 4580-4587. https://doi.org/10.1021/ie0001164.

[34] C. E. Schwarz, J. H. Knoetze. **Phase equilibrium measurements of long chain acids in supercritical carbon dioxide.** J. Supercrit. Fluids, 66 (2012), pp. 36-48. https://doi.org/10.1016/j.supflu.2011.12.011.

[35] A. Bamberger, G. Sieder, G. Maurer. **High-pressure phase equilibrium of the ternary system carbon dioxide + water + acetic acid at temperatures from 313 to 353 K.** J. Supercrit. Fluids, 32 (2004), pp. 15-25. https://doi.org/10.1016/j.supflu.2003.12.014.

[36] J. M. Prausnitz, R. N. Lichtenthaler, E. G. Azevedo. **Molecular thermodynamics of fluid-phase equilibria.** 3 ed. New Jersey: Prentice Hall (1999).

[37] A. Bamberger, G. Sieder, G. Maurer. **High-pressure (vapor+liquid) equilibrium in binary mixtures of (carbon dioxide + water or acetic acid) at temperatures from 313 to 353 K.** J. Supercrit. Fluids, 17 (2000), pp. 97-110. https://doi.org/10.1016/S0896-8446(99)00054-6.

[38] E. D. Becker. **Infrared studies of hydrogen bonding in alcohol-base systems.** Spectrochimica Acta, 17 (1961), pp. 436-447. https://doi.org/10.1016/0371-1951(61)80095-7.

[39] E. Kiran, H. Pohler. **Alternative solvents for cellulose derivatives: miscibility and density of cellulosic polymers in carbon dioxide + acetone and carbon dioxide + ethanol binary fluid mixtures.** J. Supercrit. Fluids, 13 (1998), pp. 135-141. https://doi.org/10.1016/S0896-8446(98)00090-4.

[40] S. Mawson, K. P. Johnston, J. R. Combes, J. M. De Simone. **Formation of Poly(1,1,2,2-tetrahydroperfluorodecyl acrylate) submicron fibers and particles from supercritical carbon dioxide solutions.** Macromolecules, 28 (1995), pp. 3182-3191. https://pubs.acs.org/doi/pdf/10.1021/ma00113a021.

[41] H. Y. Chiu, M. J. Lee, H. M. Lin. Vapor-liquid phase boundaries of binary mixtures of carbon dioxide with ethanol and acetone. J. Chem. Eng. Data, 53 (2008), pp. 2393-2402. https://doi.org/10.1021/je800371a.

[42] A. Mehl, F. P. Nascimento, P. W. Falcão, F. L. P. Pessoa, L. Cardozo-Filho. **Vapor-liquid equilibrium of carbon dioxide + ethanol: experimental measurements with acoustic method and thermodynamic modeling.** J. of

Thermodyn., (2011). https://doi.org/10.1155/2011/251075.

[43] A. Jónasson, O. Persson, P. Rasmussen, G. S. Soave. **Vapor-liquid equilibria of systems containing acetic and gaseous components. Measurements and calculations by a cubic equation of state.** Fluid Phase Equilib., 152 (1998), pp. 67-94.

[44] I. Tsivintzelis, D. Missopolinou, K. Kalogiannis, C. Panayiotou. **Phase compositions and saturated densities for the binary systems of carbon dioxide with ethanol and dichloromethane.** Fluid Phase Equilib., 224 (2004), pp. 89-96. https://doi.org/10.1016/j.fluid.2004.06.046.

[45] J. O. Valderrama. **The state of the cubic equations of state.** Ind. Eng. Chem. Res., 42 (2003), pp. 1603-1618. https://doi.org/10.1021/ie020447b.

[46] B.. Poling, J.M. Prausnitz, J.P. O'Connell. **The Properties of Gases and Liquids.** 5th ed., McGraw-Hill, New York (2001). https://doi.org/10.1021/ja0048634.

[47] C. L. Yaws. **Thermophysical properties of chemical and hydrocarbons.** New York: William Andrew Inc. (2009), p. 800.

CHAPTER 4 - ENCAPSULATION OF METHIONINE IN ETHYL CELLULOSE BY SUPERCRITICAL FLUID TECHNIQUE

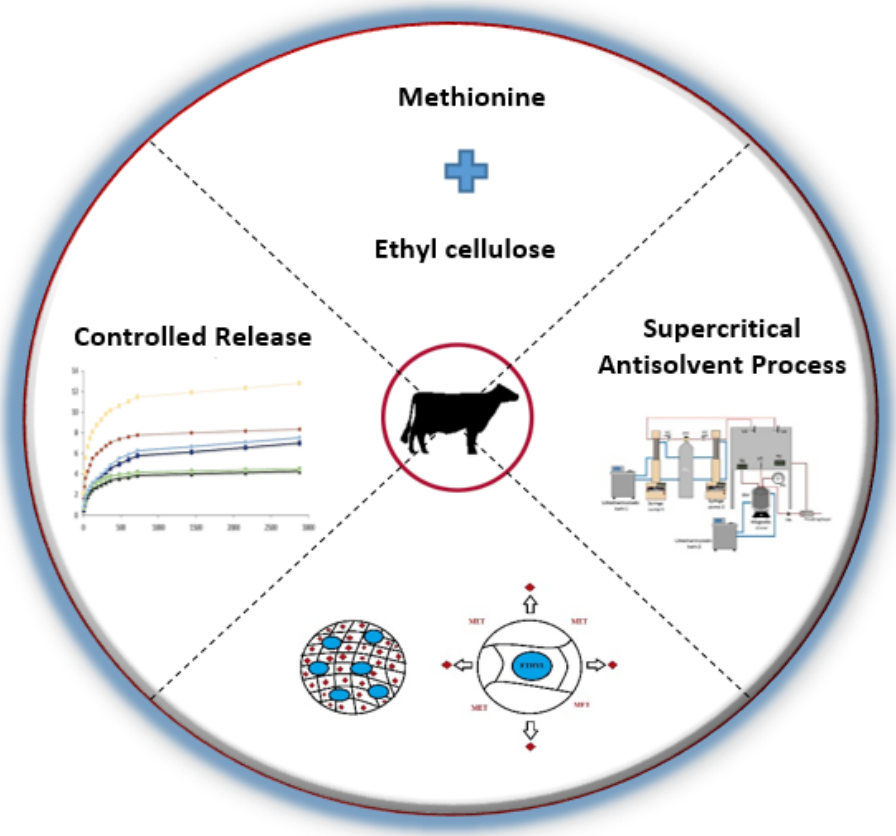

ABSTRACT

Methionine is an amino acid of great importance for lactating dairy cows, as it directly affects the quality and quantity of milk these animals produce. It needs to be supplied in the diets. However, the rumen constitutes an obstacle to the safe delivery of methionine, and techniques with supercritical fluids can be used to protect and control the release this amino acid. The main objective of this work was to investigate the encapsulation of methionine in ethyl cellulose with ethanol and acetic acid as a mixture solvent using the GAS technique. A central composite design 2^3 with three central points was used to evaluate the influence of methionine/polymer ratio (1:3, 1:2, and 1:1), temperature (308, 313, and 318 K), and pressure (10, 12, and 14 MPa) in terms of particle diameter, morphology of the particles, percentage of encapsulated material, encapsulation efficiency, and yield of precipitation. Encapsulation efficiencies as high as 99.72 % were obtained, for which the system methionine/polymer ratio showed a negative effect (95% confidence level). Particles showed irregular morphology with diameters from 29.93 to 68.89 μm. Thus, the co-precipitates presented excellent results regarding the methionine protection and controlled release possible.

Keywords: encapsulation; gas antisolvent; supercritical carbon dioxide; methionine; ethyl cellulose; co-precipitation.

4.1 INTRODUCTION

Methionine ($C_5H_{11}NO_2S$) is an essential amino acid, i.e., an amino acid that needs to be obtained from the diet because the organism cannot synthesize it. It is an important source of sulfur and acts in protein synthesis, strongly regulating animal metabolism [1,2]. Thus, methionine is widely used in medicine, food, cosmetics, and feed, mainly as a supplement for ruminant animals aiming to improve dairy production [3,4]. However, this amino acid suffers ruminal degradation when incorporated into the diet, becoming available in insufficient quantity and quality for absorption [4].

The formation of particles that protect the methionine can be an effective alternative to traditional free methionine supplementation [5]. Although many matrices achieve good stability in the rumen, they do not guarantee sufficient availability. Thus, formulated methionine should be prepared with smart materials (pH-sensitive), maintaining its integrity at ruminal pH and provoking its rupture at abomasal pH.

Although several polymers are used to protect the encapsulated material, cellulose derivatives are among the most commonly used for better drug delivery efficiency, reduced toxicity, provide a suitable medium for preserving the properties and the activity of the active substance and be easy to process. In this context, ethyl cellulose is featured because it is non-toxic, stable, pH-sensitive, and biocompatible [6-8]. The low solubility of ethyl cellulose in CO_2 and its relatively high solubility in organic solvents provide suitable conditions to employ high-pressure processes for particle formation and improved controlled delivery systems [9].

Supercritical fluid techniques can be used for encapsulation, micronization, and co-precipitation of different compounds, corresponding to an alternative to conventional methods [10,11]. The most used supercritical fluid is carbon dioxide (CO_2) because it is chemically inert, non-toxic, non-flammable, abundant in nature, cheap, recyclable, eco-friendly, and moderate critical properties – critical temperature = 31.1 °C, critical pressure = 7.38 MPa. In addition, CO_2 in a supercritical state exhibit certain properties of both gases and liquids, which means that this fluid has a lower viscosity and higher permeability than gas and can be used as a solvent, like a liquid [12-14].

The gas antisolvent methodology is formed by a solute, a solvent, and an anti-solvent and is based on the reduction of the solvent's solvation ability, causing supersaturation of the solution and resulting in the precipitation of particles [15]. Thus, when carbon dioxide is dissolved in the solvent, the solubility of the solvent is reduced,

causing solute transfer from the liquid phase to the solid phase in the form of precipitated particles [16]. Therefore, the solvent must be soluble in CO_2, but the solute should have low solubility or be practically insoluble in CO_2.

In this context, this work aims to study the influence of methionine/polymer ratio, temperature, and pressure on the co-precipitation of methionine in ethyl cellulose. The GAS encapsulation method using the ethyl cellulose biopolymer with supercritical carbon dioxide acting as an anti-solvent appears as a possible alternative for the protection, preservation of the properties, and controlling delivery of the methionine.

4.2 MATERIALS AND METHODS

4.2.1 Materials

DL-Methionine (MET) and ethyl cellulose (ETHYL) were used as solutes, ethanol and acetic acid were used as organic solvents, and carbon dioxide was used as an antisolvent. The DL-methionine and ethyl cellulose were purchased from Sigma-Aldrich (Steinheim, Germany), with 0.99 mass fraction purity. MET presented an average molar mass of 149.2 $g.mol^{-1}$, while ETHYL was 454.5 $g.mol^{-1}$. In addition, ethanol (95% purity) and acetic acid (99%) were purchased from Metaquímica (Jaraguá do Sul, Brazil), and carbon dioxide (99.9% in liquid phase) was provided by White Martins S/A (São Paulo, Brazil).

4.2.2 Co-precipitation process conditions

In this work, the influence of mass ratio between methionine (MET) and ethyl cellulose (ETHYL), temperature, and pressure was evaluated by a 2^3 design central composite (DCC) with three central points on the encapsulation percentage, encapsulation efficiency, and particle diameter. The parameters used are presented in Table 9. The total concentration was fixed at 6.67 $mg.mL^{-1}$, and the volume of the solvent mixture used was 15 mL (70 % ethanol – 10.5 mL and 30 % acetic acid – 4.5 mL) since these conditions provided better results in preliminary tests. Other process variables were fixed based on previous work by this same group [15,17- 22]. The antisolvent flow rate was 10 $mL.min^{-1}$, where the compressed CO_2 (20 MPa) was continuously pumped into the precipitation vessel, until reaching the processing

pressure and temperature. The volume of antisolvent used to dry the solvent was 800 mL.

Table 9 – Condition of process design by 2^3 central composite design with three central points. Experimental condition: total concentration fixed at 6.67 mg/mL, antisolvent flow rate of 10 mL min^{-1}, volume of solvent (70% ethanol and 30% acetic acid) was 15 mL, pump pressure of 200 bar, and antisolvent volume of 800 mL.

RUN	MET/ETHYL ratio (g MET : g ETHYL)	T (K)	P (MPa)
1	1:3	308	10
2	1:3	308	14
3	1:3	318	10
4	1:3	318	14
5	1:1	308	10
6	1:1	308	14
7	1:1	318	10
8	1:1	318	14
9 (1)	1:2	313	12
9 (2)	1:2	313	12
9 (3)	1:2	313	12

4.1.3 Gas antisolvent procedure

Figure 19 presents a schematic diagram of the experimental apparatus representing the GAS technique employed to co-precipitate methionine with ethyl cellulose. The methodology used to produce particles was based on research by Pessoa et al. [20] and Dias et al. [22]. The procedure started with the preparation of two solutions, solution A for MET and solution B for ETHYL. In solution A, the methionine was mixed in acetic acid, subjected to an ultrasonic bath for 10 min, and then heated with stirring into complete dissolution. Solution B was not subjected to the ultrasound, and ethyl cellulose was mixed in ethanol, heated, and stirred into complete dissolution. Then, solutions A and B were mixed and heated with stirring for 5 min for complete homogenization. The total concentration of the solution A + B was fixed at 6.67 $mg.mL^{-1}$, and different methionine-to-ethyl cellulose mass ratios were evaluated.

For each GAS assay, a different MET/ETHYL solution was placed in the chamber, and CO_2 was continuously pumped at a constant flow rate (10 mL.min^{-1}), under continuous magnetic stirring, until the planned pressure and temperature, Figure 20. When this condition operation was reached, the antisolvent flow was stopped, and the chamber continued to agitate the solution for 10 min. After this, washing step was started with the antisolvent flow at 10 mL.min^{-1}. The particles were collected manually.

Figure 19 – Schematic diagram of the experimental unit for GAS procedure.

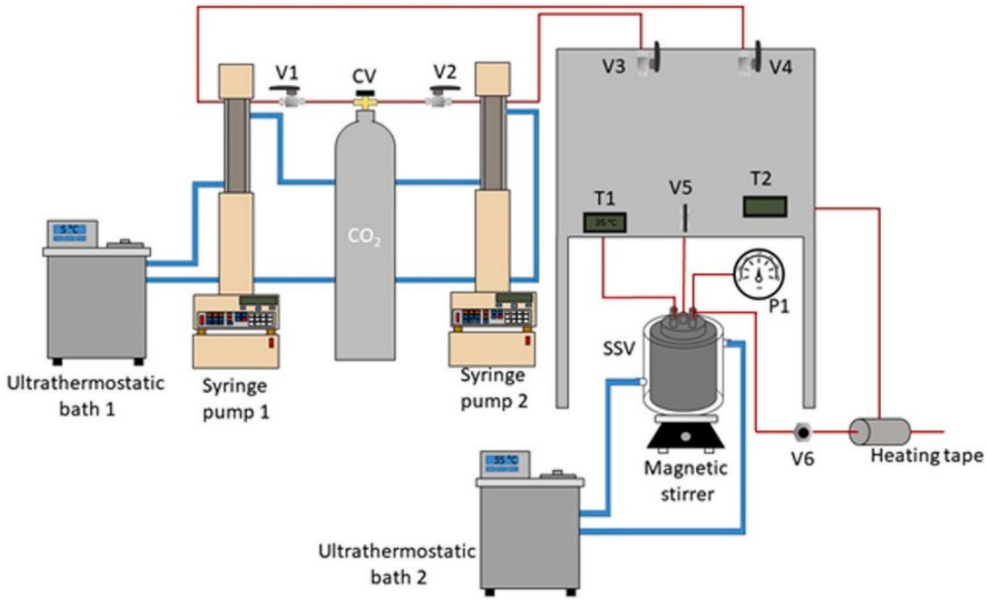

Source: Provided by the reference [13].

Figure 20 – GAS procedure summary.

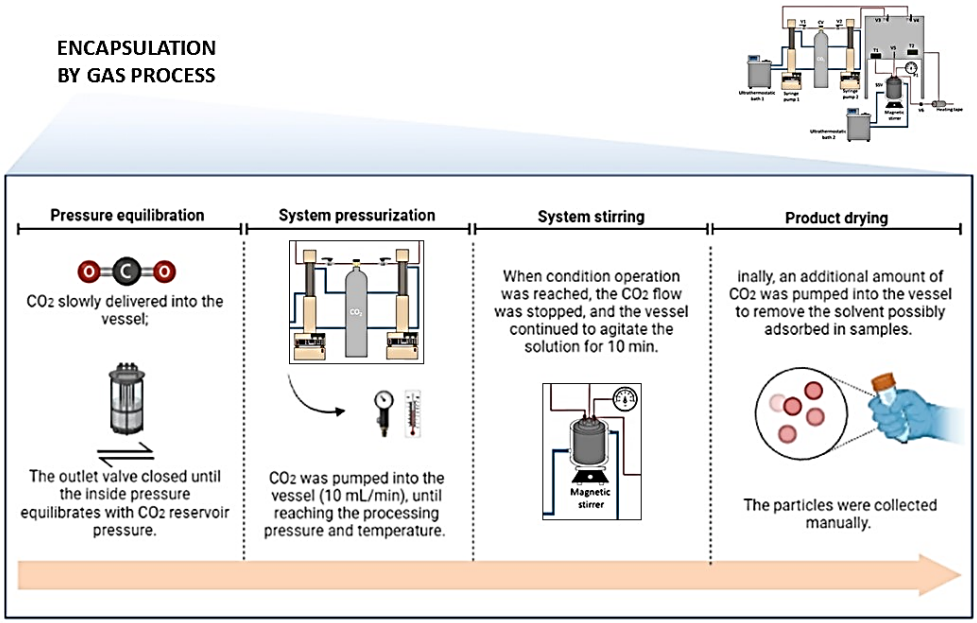

Source: the author (2022).

4.2.4 Percentage of encapsulation (PE), encapsulation efficiency (EE) and precipitation yield

The methodology used in this experiment was based on a spectroscopy method, where the percentage of encapsulation was calculated as described in the literature [6,23-25], with some adaptations. The co-precipitated particles were previously washed with excess distilled water to solubilize the MET and remove the non-encapsulated (free) methionine, Figure 21. As ethyl cellulose is insoluble in water, that solvent removes free MET mainly deposited on the surface of polymeric particles. After washing, the solution was filtered, and the retained material was dried under a controlled temperature (308 k). This dried material was subjected to steps 1 and 2.

Figure 21 – Sample preparation for the analysis of the percentage of encapsulation and encapsulation efficiency.

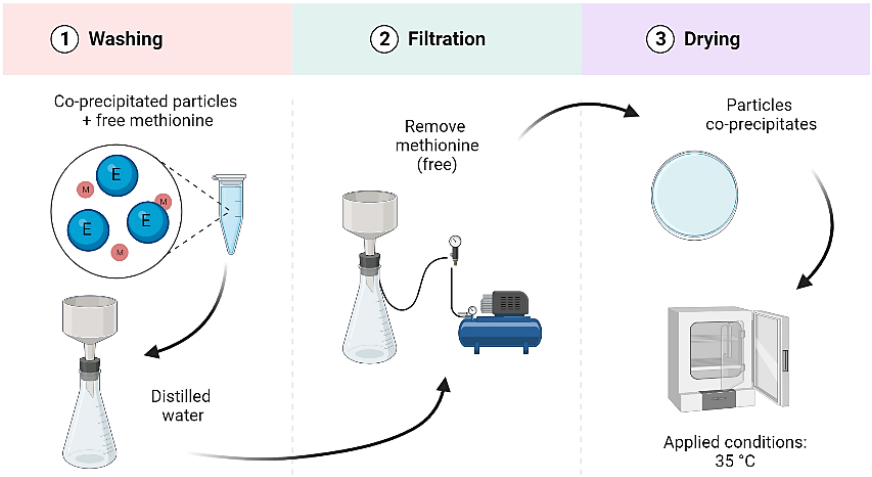

Source: the author (2022).

Step 1: Dried particles were added to a small volume of dichloromethane-ethanol (9 volumes of dichloromethane and 1 volume of ethanol). This mixture was heated (313 k) and stirred for 3 hours, where the polymer was dissolved, causing effective separation of methionine and ethyl cellulose. Figure 22. Then, this solution was centrifuged at 3.400 rpm for 20 min. Since methionine has no solubility in the dichloromethane-ethanol mixture, the supernatant was removed, and the retained methionine was dried under a controlled temperature (308 k). After evaporation of the solvent mixture, precipitated methionine was forwarded to step 2.

Figure 22 – Step 1: analysis of the percentage of encapsulation and encapsulation efficiency.

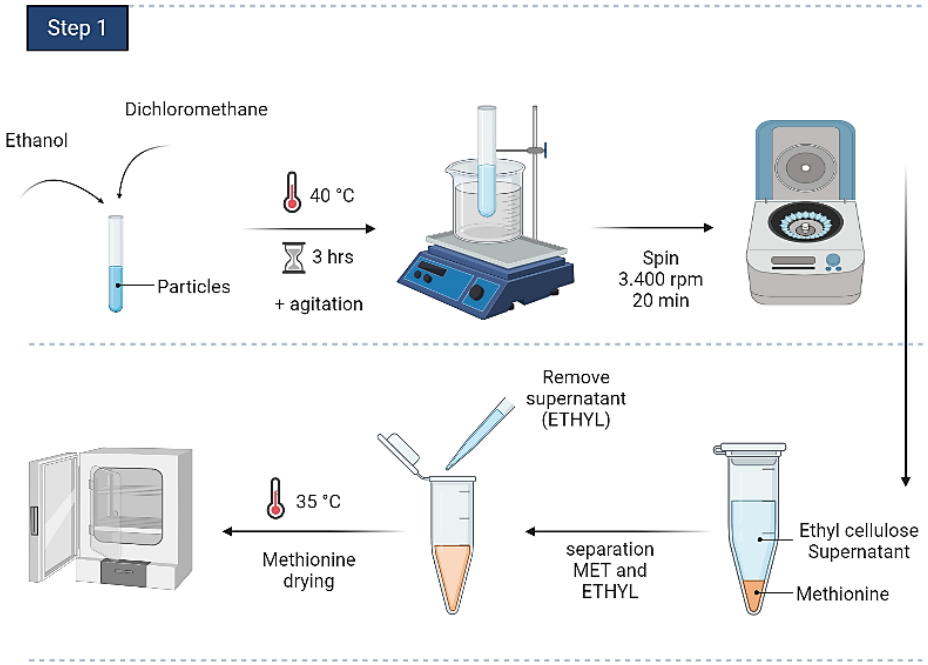

Source: the author (2022).

Step 2: A methionine solution was prepared by dissolving precipitated methionine in 2.5 mL of distilled water, Figure 23. In a tube, this solution was added to be tested. Then was added 0.5 mL of 5N NaOH (10 g of NaOH in distilled water, diluted to 50 mL) and 0.15 mL of 10% aqueous solution of sodium nitroprusside, with an interval of 1min for each addition. The tube was placed in a water bath at a temperature of 313 K and stirred for 10 min. Then, it was cooled in ice water for 2 min and added 2.5 mL of an HCl-H_3PO_4 mixture (9 volumes of concentrated HCl and 1 volume of H_3PO_4, for example, 45 mL HCL and 5 mL H_3PO_4) with shaking during the addition of the acid. The stirring continued for 1 min in an ice-water bath. Next, the solution was read in UV-VIS spectrophotometry (U-1900, Hitachi). The methionine concentration was measured at 520 nm at a previously established calibration curve (R^2 = 0.9979) with different concentrations (0.1 to 1.0 $mg.mL^{-1}$) of methionine.

Figure 23 – Step 2: analysis of the percentage of encapsulation and encapsulation efficiency.

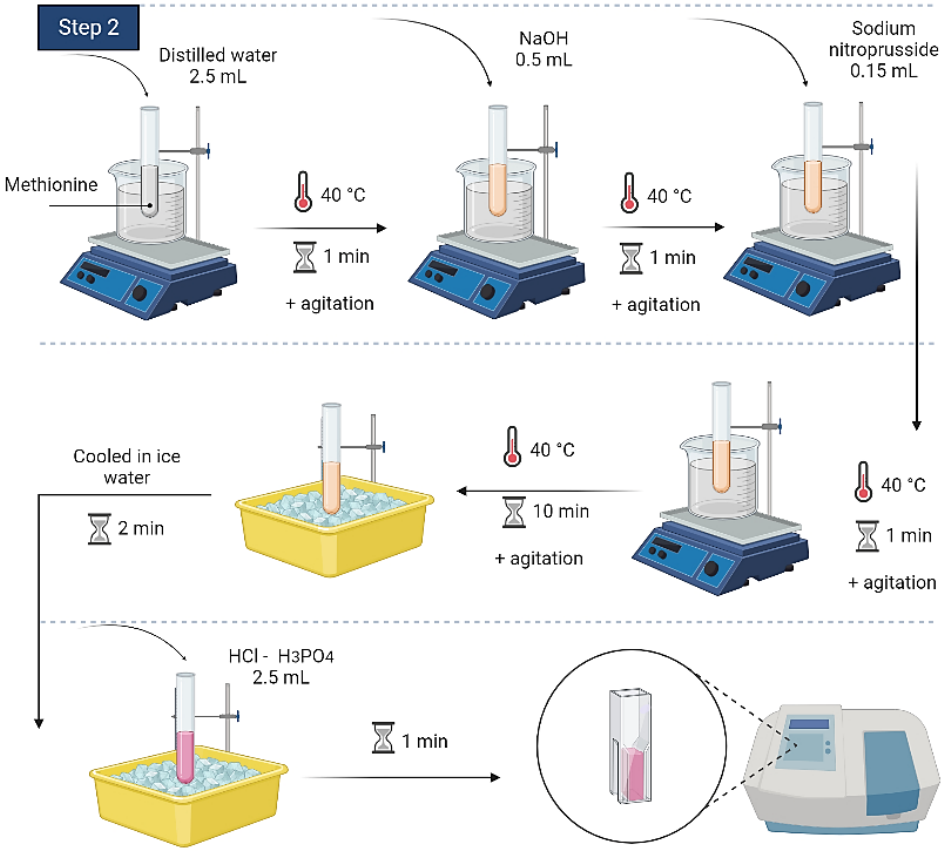

Source: the author (2022).

The precipitation yield (%), percentage of encapsulation (PE%), and encapsulation efficiency (EE%) in each run were evaluated by the following expressions:

$$Yield[\%] = \frac{mass\ of\ encapsulated\ (experimental)}{mass\ of\ methionine + mass\ of\ ethyl\ cellulose\ (theoretical)}\ x\ 100\ (Equation\ 18)$$

$$PE[\%] = \frac{mass\ of\ methionine\ encapsulated}{(mass\ of\ methionine + mass\ of\ ethyl\ cellulose)\ after\ filtration}\ x\ 100\ (Equation\ 19)$$

$$EE[\%] = \frac{percentage\ of\ methionine\ encapsulated}{theoretical\ loading\ percentage\ of\ methionine\ encapsulated}\ x\ 100\ (Equation\ 20)$$

The theoretical loading percentage of methionine encapsulated is the ratio between methionine and the total mass of methionine and ethyl cellulose used in the co-precipitation experiments.

4.1.5 Morphology and particle diameter determination

Particle shape and morphology were analyzed through scanning electron microscopy (SEM) using a JEOL JSM-6390LV. The images were performed with 15 kv acceleration and were used to determine mean particle diameters employing the ImagenJ software (developed by Wayne Rasband), in which for each sample the weighted average of the diagonal and vetical line of approximately 200 particles was measured. Furthermore, SEM was coupled with energy-dispersive X-rays to identify chemical elements of co-precipitates.

4.2.6 Powder X-ray diffraction (XRD)

The XRD patterns were collected to evaluate the crystallinity of the co-precipitated particles, which were collected by Rigaku MiniFlex600 powder diffractometer. Measurements were taken utilizing a copper X-ray source powered at 40 kV and 15 mA (Kα1 1.54059 Å) in θ-2θ scan mode. Scans were measured between 5° and 35° 2θ with a step size of 0.02° 2θ and with a scanning speed of 6°/min.

4.2.7 Fourier Transform Infrared Spectroscopy (FTIR)

The co-precipitated particles, unprocessed methionine, and unprocessed ethyl cellulose structures were observed using Fourier Transform Infrared Spectroscopy (FTIR) (Agilent Technologies – Cary 600 Series FTIR Spectrometer) to determine possible changes in the structures of the compounds caused by the GAS process. The samples were mixed with KBr powder and compressed to form a pellet. The KBr pellet was used to record the background reference spectrum. The spectra were recorded in the range of 400–4000 cm^{-1} at 4 cm^{-1} with 64 scans.

4.2.8. Calorimetric profiles with differential scanning calorimetry (DSC)

Differential scanning calorimetry (DSC) analyses were carried out on a differential scanning calorimeter (Jade DSC, Perkin Elmer, USA). Samples were placed in hermetically sealed aluminum pans and its was subjected to a first heating (50 °C – 260 °C), then it was cooled (5°C.min^{-1}) and subjected to a second heating (50 °C – 300 °C), under nitrogen flow (20 mL.min^{-1}) (Jade DSC, Perkin Elmer, USA).

4.2.9. Residual solvent

The methodology used was determined as described by Lima et al. [26]. All measurements were carried out using a 22.5 mL headspace vial, injecting 500 µL of vapor (Incubation Temperature (°C): 90 and Incubation Time (s): 420) into an automatic headspace sampler (GC sampler 80, Agilent), which was analyzed by a capillary gas chromatograph (GC) with a flame ionization detector (FID, GC-7890A Agilent). The GC conditions were as follows: DB-624 UI capillary column (60 m × 0.25 mm × 1.40 µm), flame ionization detector at 250 °C, injector temperature of 200 °C using a splitless mode (ethanol detection) and split mode 200:1 (acetic acid detection). The GC oven was programmed from 40 °C (held for 7 min) to 70 °C at 10 °C min^{-1} (held for 6 min), to 110 °C at 10 °C min^{-1} (held for 5 min) and to 220 °C at 20 °C min^{-1} (held for 5 min). Helium was used as the carrier gas with a constant flow of 2 mL.min^{-1}.

4.2.10. Statistical analysis

The study of process variables on the percentage of encapsulation, encapsulation efficiency, precipitation yield, and particle diameter were analyzed employing the software Statistica (Statsoft Inc., USA) since the work used a Central Composite Design. The results were analyzed by analysis of variance (ANOVA) with the Tukey test. Differences were considered to be statistically significant at a level of $p \leq 0.05$.

4.3 RESULTS AND DISCUSSION

This study investigated the feasibility of preparing methionine-loaded particles using the GAS process. The conditions employed in the co-precipitation experiments were chosen based on previous results to ensure that methionine (MET) and ethyl

cellulose (ETHYL) could be precipitated [27]. A mixture of solvents (ethanol and acetic acid) was carefully selected to mimic real conditions found on the formulation of methionine in ethyl cellulose matrix by CO_2 antisolvent methods. Because both components (methionine and ethyl cellulose) should be soluble in a common solvent or solvent mixture, preliminary studies were conducted to find a suitable solvent mixture to be further used in CO_2-based processes. This polymer was micronized individually and co-precipitate with other compounds in different studies in the literature [6,8-9,28-31].

4.3.1 Co-precipitation of methionine and ethyl cellulose

The co-precipitation results are shown in Table 10, which exhibits the experimental conditions adopted in this work, the powder characteristics in terms of yield and particle diameter, and methionine loading results from the co-precipitates, in terms of percentage of encapsulation (PE) and encapsulation efficiency of methionine (EE).

Table 10 – Experimental conditions co-precipitation of methionine with ethyl cellulose by GAS process.

Sample	Operating conditions			Powder characteristics		Co-precipitates particles	
	MET/ETHYL ratio[A]	T (K)[B]	P (MPa)[C]	Yield (%)	Dp[D]	PE (%)[E]	EE (%)[F]
RUN 1	1:3	308	10	$63.34^{b,c} \pm 0.02$	$57.73^{d} \pm 0.01$	$27.95^{c} \pm 0.01$	$95.20^{a,b} \pm 0.02$
RUN 2	1:3	308	14	$59.66^{c} \pm 0.01$	$55.71^{d} \pm 0.02$	$21.43^{d} \pm 0.01$	$84.08^{c,d} \pm 0.02$
RUN 3	1:3	318	10	$41.07^{e} \pm 0.01$	$68.89^{c} \pm 0.01$	$41.40^{a} \pm 0.02$	$99.72^{a} \pm 0.01$
RUN 4	1:3	318	14	$48.00^{d} \pm 0.03$	$57.30^{d} \pm 0.02$	$23.35^{c,d} \pm 0.01$	$93.23^{b} \pm 0.03$
RUN 5	1:1	308	10	$84.37^{a} \pm 0.01$	$31.79^{g} \pm 0.02$	$39.38^{a,b} \pm 0.03$	$78.84^{d} \pm 0.01$
RUN 6	1:1	308	14	$80.62^{a} \pm 0.01$	$29.93^{g} \pm 0.01$	$34.36^{b} \pm 0.02$	$68.53^{e} \pm 0.01$
RUN 7	1:1	318	10	$67.37^{b} \pm 0.02$	$48.88^{e} \pm 0.01$	$43.24^{a} \pm 0.01$	$85.73^{c} \pm 0.02$
RUN 8	1:1	318	14	$58.68^{c} \pm 0.01$	$39.39^{f} \pm 0.01$	$25.45^{c,d} \pm 0.01$	$58.54^{f} \pm 0.02$
RUN 9 (1)	1:2	313	12	$66.03^{b} \pm 0.01$	$47.02^{e} \pm 0.03$	$26.75^{c,d} \pm 0.02$	$79.94^{d} \pm 0.03$
RUN 9 (2)	1:2	313	12	$62.88^{b,c} \pm 0.01$	-	$24.04^{c,d} \pm 0.01$	$86.79^{c} \pm 0.01$
RUN 9 (3)	1:2	313	12	$58.36^{c} \pm 0.03$	-	$27.40^{c} \pm 0.01$	$82.36^{c,d} \pm 0.01$
MET[G]	-	-	-	-	714.62^{b}	-	-
ETHYL[H]	-	-	-	-	1037.93^{a}	-	-

[A]Methionine/ethyl cellulose mass ratio; [B]T – Temperature (K); [C]P – Pressure (MPa); [D]Dp – Mean particle diameter (μm); [E]PE – Percentage of encaspulation; [F]EE – Encapsulation efficiency; [G]MET – Unprocessed methionine; [H]ETHYL – Unprocessed ethyl cellulose.

Mean ± standard deviation; the same lowercase letters do not indicate a significant difference ($p < 0.05$).

The results showed that the precipitation yield was significantly improved by increasing the MET/ETHYL ratio and reducing the temperature, where the highest yield was 84.37% (RUN 5 – 1:1 ratio, 308 K and 10 MPa). On the other hand, decreasing the MET/ETHYL ratio and lowering pressures increased the EE of the process. The highest EE was 99.72% for RUN 3, for which the highest amount of polymer was used in the process (1:3 ratio) and the lowest pressure (10 MPa).

Figures 24a and b (Pareto diagrams) confirmed that the MET/ETHYL ratio influenced precipitation yield (positive effect) and the EE (negative effect), respectively. An increase in the ratio of MET to ETHYL in the mixed solvent of ethanol and acetic acid means a decrease in the amount of ETHYL, i.e., a reduction of the solution viscosity in the antisolvent process. Franceschi et al. [32] and Hu et al. [33] reported that low viscosity can imply a decrease in shear forces, where the diffusion of the organic solvent is more effective, causing an increase in the mass transfer rate, generating a change in the precipitation yield and entrapment efficiency.

Figure 24 – (a) Pareto chart showing the effects of the variables on the precipitation yield; (b) Pareto chart showing the effects of the variables on the EE.

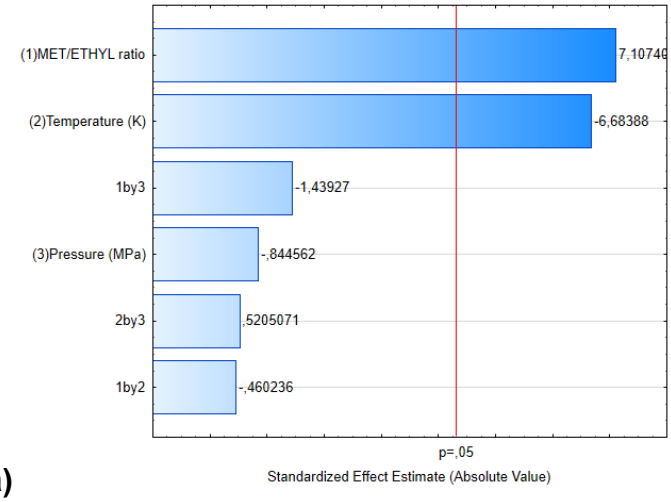

(a)

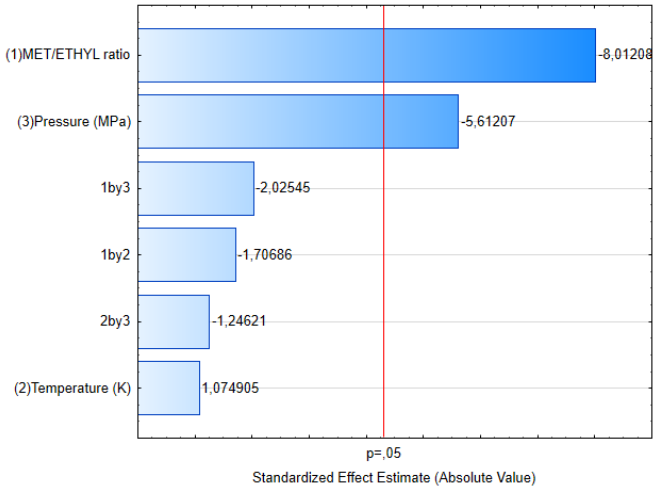

(b)

Source: the author (2022).

Regarding the negative influence in the EE, decrease in the MET/polymer ratio, i.e., greater quantities of ethyl cellulose, indicates lower supersaturation of the methionine in the organic solution, where a lower amount of the MET led to higher entrainment of solvents with the fluid phase. This effect can be observed by comparing RUN 1 (1:3 ratio) with RUN 5 (1:1 ratio), where the efficiency decreases from 95.20 to 78.84 %, applying 308 K and 10 MPa, corroborating with Djerafi et al. [6] and Hu et al. [33].

The influence of the temperature was studied at 308, 313, and 328 K, fixing all the other operating parameters. From the data in Table 10 and Figure 24a, temperature showed a negative effect, where the lowest yield results were at higher temperatures. Jin et al. [34] suggested that higher temperatures may reduce CO_2 density, resulting in the decreased solubility of the solvent in supercritical CO_2 and the solute's lower solvation power, which induces lower supersaturation of solute in the mixed solvent. Furthermore, Machado et al. [13] and Djerafi et al. [31] observed that higher temperatures are associated with increases in aerodynamic forces (destabilizing effects), impairing the precipitation process when some polymers, especially amorphous ones, are used. So, induced by CO_2 supercritical, polymers reduce the glass transition temperature due to the plasticizing effect of CO_2-solvent at high pressure. Therefore, lower temperatures are required to obtain precipitates through the GAS process.

Regarding the pressure, as shown by the Pareto graph (Figure 24b), it had a significant negative effect on the encapsulation efficiency (95% confidence level).

Comparing RUN 2 (14 MPa) with RUN 1 (10 MPa), the efficiency decreases from 95.20 to 84.08 %, both applying a MET/ETHYL ratio of 1:1 and temperature of 308 K. Thus, pressure increase results in lower encapsulation efficiency. Increasing the system pressure, methionine solubility in CO_2 also increases, which favors carrying the compound out of the precipitation chamber and, consequently, reduces the encapsulation efficiency [18].

The morphology of unprocessed methionine (MET), unprocessed ethyl cellulose (ETHYL), and co-precipitated particles are shown in Figure 25. While the MET and ETHYL present irregular structures, similar to literature data [30,31,35], all the co-precipitated particles exhibit a spherical shaped aggregate structure, with small connections between them [18]. These particles are very interesting for modulating release systems due to their greater surface area and, consequently, a larger contact surface concerning particle volume, leading to a probable increase in bioavailability of a compost impregnated in the system [9,36-37].

The morphology of the co-precipitates was strongly influenced by the methionine/polymer ratio. The presence of plates observed in the experiments with the MET/ETHYL ratio 1:1 (RUNs 5,6,7 and 8) could be attributed to a lower polymer fraction and supersaturation of methionine, occasioned by the higher concentration of this amino acid in the organic solution. Thus, the co-precipitated particles show characteristics of plaque similar to unprocessed methionine. This drug/polymer ratio effect was also observed by Djerafi et al. [6]. The authors studied the supercritical antisolvent co-precipitation of rifampicin and ethyl cellulose in different process conditions. In the formulation with a lower amount of polymer, i.e., higher drug concentrations in the organic solution, most rifampicin diffused in the continuous supercritical phase and did not co-precipitate with the polymer. Therefore, the co-precipitates showed a morphology with plate crystals characteristic of rifampicin.

Figure 25 – Morphology and Energy-dispersive X-ray spectroscopy of the particles obtained in the co-precipitation runs 1–9, and unprocessed methionine (MET) and ethyl cellulose (ETHYL).

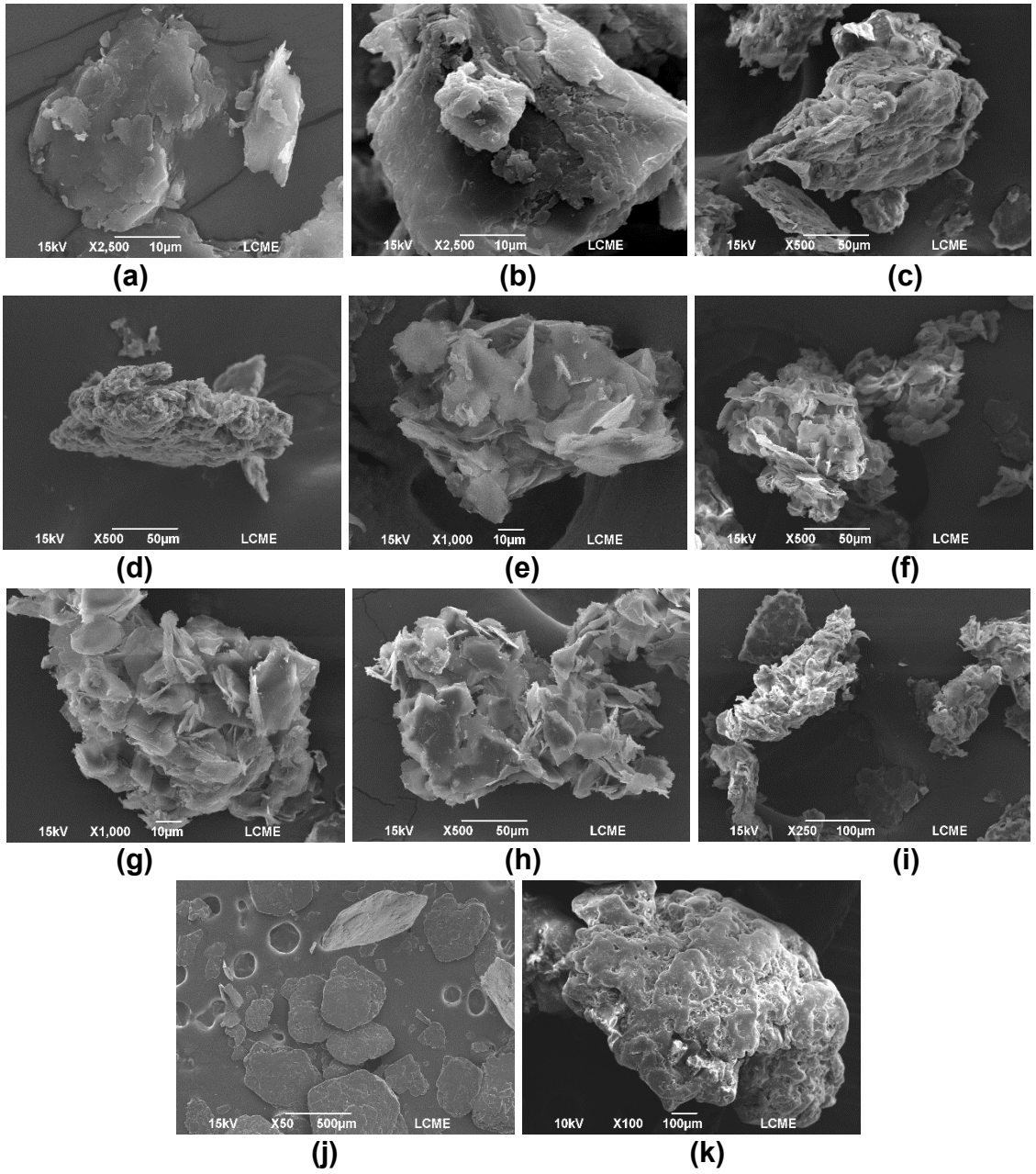

Samples	Carbon (atom%)	Oxygen (atom%)	Sulfur (atom%)
RUN 1	76.75 ± 1.93	17.49 ± 2.10	5.75 ± 0.16
RUN 2	69.38 ± 0.27	27.34 ± 0.80	3.28 ± 0.60
RUN 3	69.61 ± 1.04	25.63 ± 2.54	4.75 ± 1.62
RUN 4	70.35 ± 4.01	26.97 ± 5.12	2.67 ± 1.61
RUN 5	72.21 ± 1.34	22.32 ± 0.78	6.49 ± 0.88
RUN 6	72.64 ± 3.65	19.86 ± 5.17	7.49 ± 1.53
RUN 7	70.75 ± 0.83	20.51 ± 1.40	8.73 ± 1.72
RUN 8	69.96 ± 0.12	22.55 ± 0.93	7.49 ± 0.82
RUN 9	71.07 ± 1.31	24.61 ± 1.79	5.63 ± 1.14
MET	60.87 ± 1.86	21.49 ± 4.63	17.64 ± 0.73
ETHYL	65.97 ± 0.51	34.02 ± 0.51	-

Source: the author (2022).

To confirm that MET is present in the co-precipitated, SEM was coupled with energy-dispersive X-rays to identify chemical elements, and the results are shown in Figure 25. The aspect that differentiates methionine from ethyl cellulose is sulfur, where this element can indicate the location of the MET in the co-precipitated particles. Therefore, it has been verified that sulfur element is present in all the encapsulated particles, showing the encapsulation efficiency corroborating with Montes et al. [8].

Figure 26 shows the influence of the process parameters on the particle diameter of the co-precipitates, where the MET/ETHYL ratio (1), temperature (2), pressure (3), the interaction between variables 1 and 2, and variables 2 and 3 were considered to be statistically significant at a level of $p \leq 0.05$. The particle diameter distribution is shown in APPENDIX C.

The MET/ETHYL ratio revealed a negative effect on the particle diameter parameter, i.e., a decrease in the MET/polymer ratio (greater quantity of ethyl cellulose) provided co-precipitates with larger diameters. This effect was expected since an increase in the concentration of the polymer in the formulation would lead to an increase in the size of the dispersed droplets, which in turn would result in the formation of precipitated with larger particles diameters [23,30].

Concerning the temperature effect, co-precipitated particle diameters have been lower in the RUNs at lower temperatures. For example, when the temperature of the experiments was increased from 308 to 318 K, with constants pressure (10MPa) and MET/ETHYL ratio (1:3), the diameter of the co-precipitates increased from 57.73 to 68.89, respectively. A similar result was found by Montes et al. [8] when a supercritical antisolvent process obtained composite microparticles of ampicillin and ethyl cellulose. This temperature effect was also observed by Cocero and Ferrero [38]

where the authors verified that higher temperatures mean a greater agglomeration of the particles formed, which may be due to a more favorable redissolution of the precipitates at higher temperatures, providing particles with larger sizes at the end of the process.

The results of Figure 26 also revealed that the mean particle diameter decreased with increasing pressure, in which the coalescence phenomenon can explain. This phenomenon is controlled by the precipitation pressure, i.e., coalescence decrease with increasing pressure. This evidence demonstrates that coalescence is produced by the interaction of the liquid solvent dissolved in the supercritical antisolvent and the solute particles. The increase in pressure increases the strength of the solvated complex formed between liquid solvent and CO_2, thus reducing the ability of the solvent to interact with the solute particles. It is possible to take advantage of coalescence to produce larger or smaller aggregates, as drug-specific formulations require [7].

Figure 26 – Pareto chart showing the effects of the variables on the particle diameter.

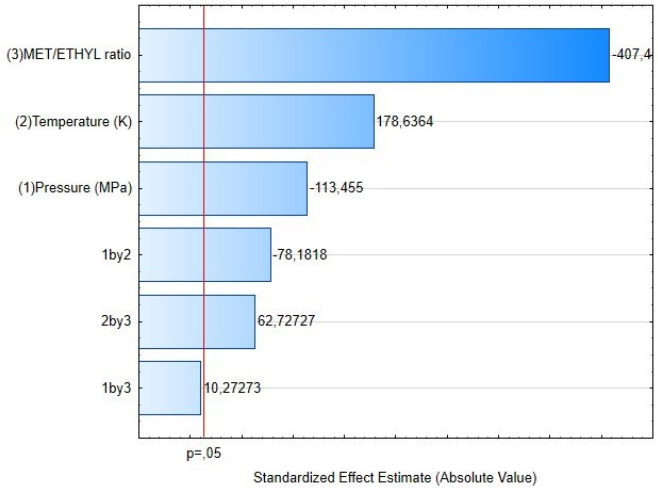

Source: the author (2022).

4.3.2 X-ray diffraction (XRD)

XRD measurements were performed to evaluate the crystallinity of embedded MET. The obtained diffractograms are illustrated in Figure 27. The unprocessed methionine (MET) diffractogram showed peaks of high intensity in the diffractogram at 2θ of 5.6°, 22.4° and 33.8°, similar to Li et al. [3]. The unprocessed ethyl cellulose

(ETHYL) showed peaks at 2θ of 12.5° and 20.3°, corroborating with Lokhande et al. [23].

Figure 27 – X-ray diffraction of the particles obtained in the co-precipitation runs 1–9, and unprocessed methionine (MET) and ethyl cellulose (ETHYL).

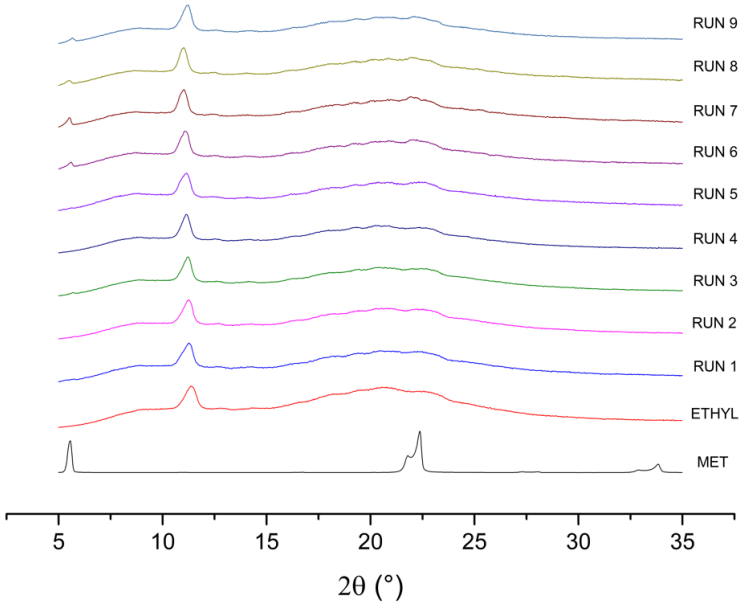

Source: the author (2022).

Encapsulated particles showed similar predominant peaks to ETHYL. Although some peaks MET were observed in RUNs 6, 7, 8, and 9, in which the polymer was in a lower proportion, this behavior was also observed by Garcia-Casas et al. [39]. Despite this finding, the XRD analyses verified the absence of characteristic MET peaks. This may be due to interference of ETHYL molecules arrangement in MET molecules during precipitation. Thus, methionine is possibly dispersed at a molecular level in a polymer matrix or ethyl cellulose molecules arrangement in methionine molecules during precipitation caused amorphous nature, accentuating the characteristic peaks of ETHYL [23].

4.3.3 Fourier transform infrared spectroscopy (FTIR)

In the present work, methionine/ethyl cellulose co-precipitates were subjected to FTIR, and the spectra obtained were compared to that of unprocessed MET and ETHYL in Figure 28. The unprocessed MET spectrum showed intense bands due to

NH_3, where at 2943, 1580, 1450, and 1340 cm^{-1} corresponded to C–H, N–H, C–H, and O–H stretchings, respectively. Characteristics NH_3^+ bands are due to the asymmetric and symmetric bending, typical bands that characterize MET and also observed by Mahotra [5] and Ramachandran [40]. ETHYL infrared spectrum showed principal peaks between 1000 to 3500 cm^{-1}. Of these 3472 and 1119 cm^{-1} were due to O–H and C–O stretchings, respectively [23]. The typical characteristic bands of methionine and ethyl cellulose are demarcated with shading in Figures 28a and b.

Figure 28 – Fourier transform infrared spectroscopy of the particles obtained in the co-precipitation runs 1–9, and unprocessed methionine (MET) and ethyl cellulose (ETHYL). 1: O-H stretching; 2: C-O stretching; 3: N-H bending; 4: C-H bending.

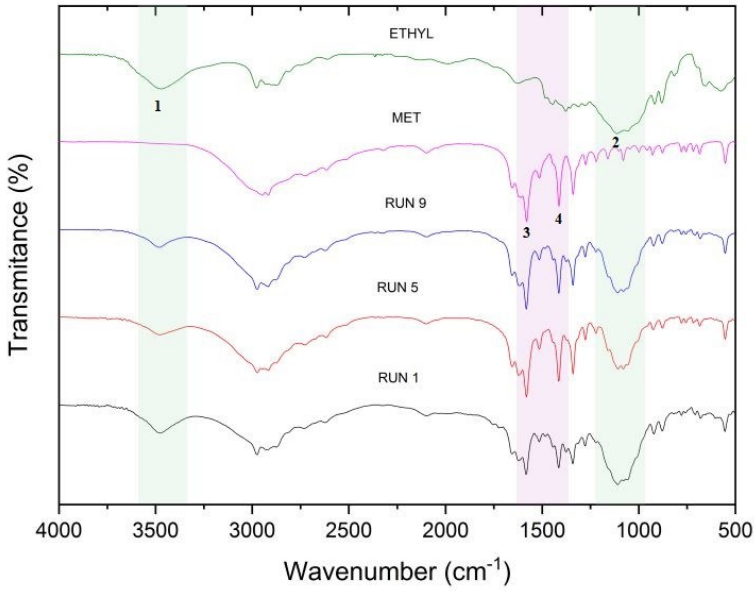

(a)

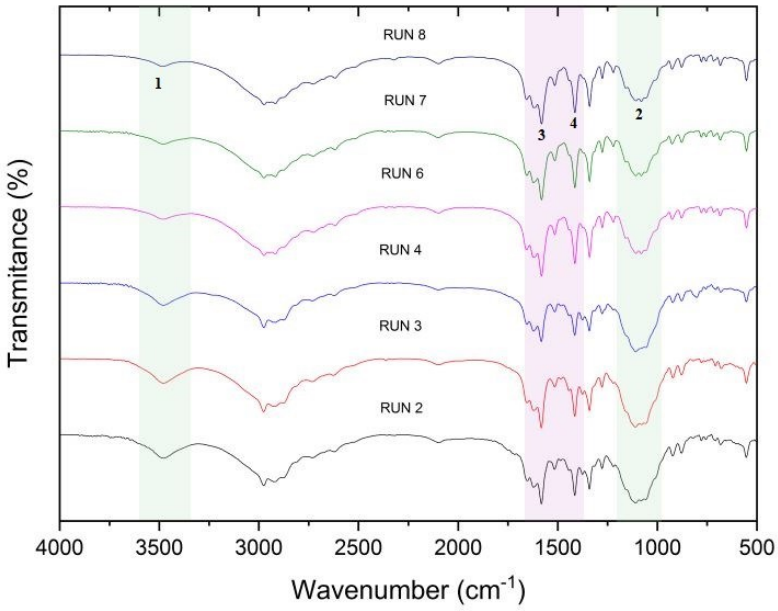

(b)

Source: the author (2022).

These characteristic ETHYL and MET peaks are present in all encapsulated particles, thus confirming the presence of MET and the lack of chemical changes in the co-precipitation process [39]. Furthermore, the peaks not significantly shifted to lower or higher intensity than the MET peak indicating that the MET molecules were not excessively degraded during the GAS process, confirming the successful encapsulation of the methionine.

4.3.4 Differential scanning calorimetry (DSC)

DSC was performed to provide qualitative information about the physical state of methionine in the co-precipitates compared to that of unprocessed MET. The DSC curve of methionine shows a sharp endothermic peak at 278.96 °C, similar to Mahotra et al. [5] and Neto et al. [35]. The unprocessed ETHYL was also analyzed with DSC, and an endotherm-melting peak ascribed to the crystalline part of the polymer was observed at 193.14 °C, corroborating with Djerafi et al. [6].

The thermograms of MET, ETHYL, and co-precipitates are shown in Figure 29. For all the co-precipitates, a peak was observed between 160 and 200 °C. The greater the amount of ETHYL used in the process, the closer the peak of the co-precipitates was to the unprocessed polymer. For example, RUN 1 (ratio 1:3) showed a peak of 178.00 °C, closer than RUN 2 (ratio 1:1), with a value of 162.36 °C.

Therefore, the ethyl cellulose unaffected by the supercritical co-precipitation with methionine.

Figure 29 – Differential scanning calorimetry of the particles obtained in the co-precipitation runs 1–9, and unprocessed methionine (MET) and ethyl cellulose (ETHYL).

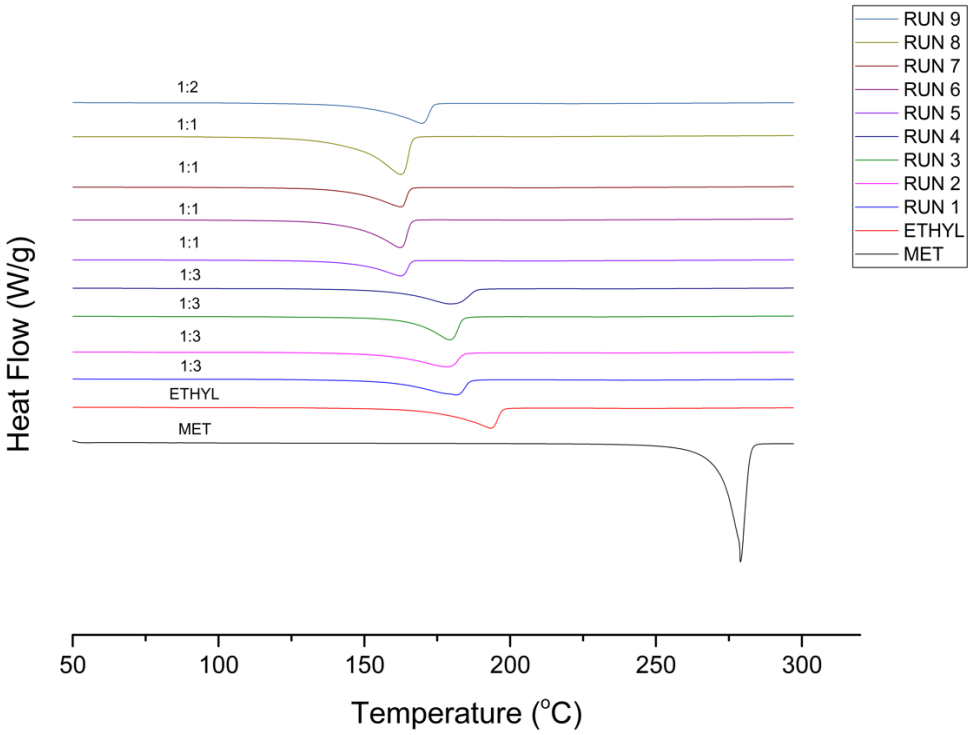

Source: the author (2022).

Small endothermic depression can be observed in RUN 1 (239.59 °C, ratio 1:3), RUN 5 (252.11 °C, ratio 1:1), and RUN 9 (245.17 °C, ratio 1:2), showed in Figures 30a, b, and c, respectively. Thus, indicating the presence of methionine and the successful encapsulation of methionine in the ethyl cellulose [5].

Figure 30 – Differential scanning calorimetry of the particles obtained in the co-precipitation. (a) RUN 1, (b) RUN 5, and (c) RUN 9.

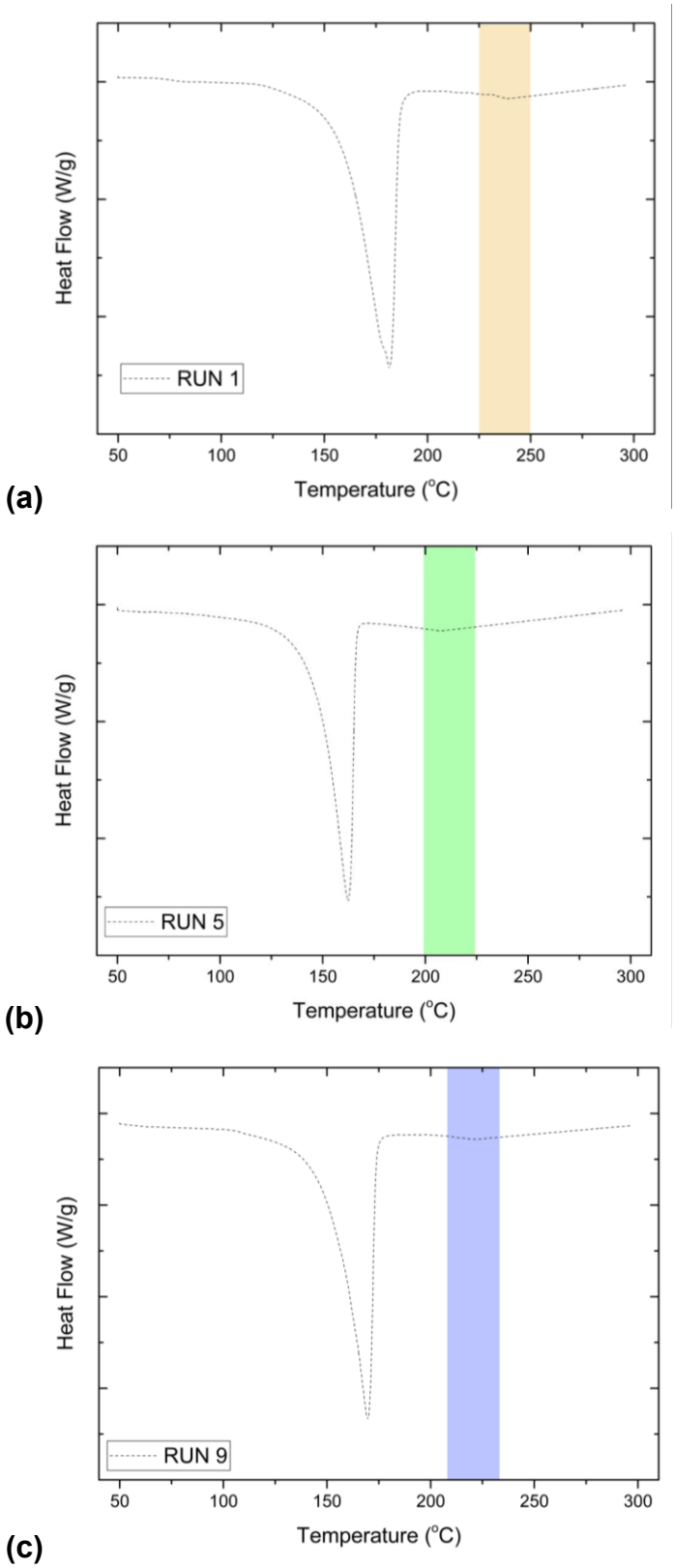

Source: the author (2022).

4.3.5. Residual solvent

According to Food and Drug Administration (FDA) guidelines, ethanol and acetic acid are class 3 solvents; therefore, their maximum acceptable concentration in the final product is 5000 ppm or 50 mg. A headspace sampler, coupled with a gas chromatograph, was used to verify the solvent residue content in GAS-produced precipitates. The analysis revealed that the solvent residue was around 45.06 ppm and 0.03 mg for ethanol and acetic acid, respectively, in all the samples.

4.4 CONCLUSIONS

The co-precipitates obtained using the ethyl cellulose as an encapsulating agent presented excellent results regarding the protection of methionine. The gas antisolvent technique was adequate, providing precipitation yield values reaching 84 % and encapsulation efficiency values above 99%, where MET/ETHYL ratio presented a positive effect on the yield and a negative effect on the EE. The SEM showed particle diameters from 29.93 to 68.89 μm, where the particle diameter obtained in the precipitates were significantly smaller than those of the corresponding unprocessed materials. The MET/ETHYL ratio revealed a negative effect on the particle diameter, i.e., a decrease in the MET/polymer ratio (greater quantity of ethyl cellulose) provided co-precipitates with larger diameters. This negative effect also was observed by pressure. The temperature showed a positive effect, thus, when the experiments temperature was increased the particle diameter of the co-precipitateds increased. About the characterizations of the co-precipitates, XRD analyses verified the absence of characteristic peaks of the MET due to interference of ETHYL molecules arrangement in MET molecules during precipitation, FTIR confirmed the presence of MET and the lack of chemical changes in the co-precipitation process, and DSC showed that ethyl cellulose unaffected by the supercritical co-precipitation. Thus, the co-precipitates presented excellent results regarding the methionine protection and controlled release possible, showing strong potential for a release into the abomasum and greater absorption at the intestinal level, thereby reducing the disadvantages incurred with the direct use of this amino acid.

4.5 REFERENCES

[1] Gierus, M. (2007). **Fontes orgânicas e inorgânicas de selênio na nutrição de vacas leiteiras: digestão, absorção, metabolismo e exigências.** Ciência Rural, 37, 1212-1220. https://doi.org/10.1590/S0103-84782007000400052.

[2] Frota, H. N., Reis, R. B., Faria, B. N., Coelho, S. G., & Saturnino, H. M. (2014). **Suplementação de lisina e metionina em associação ou não com o óleo de soja na dieta de vacas leiteiras.** Arquivo Brasileiro de Medicina Veterinária e Zootecnia, 66, 1121-1128. https://doi.org/10.1590/1678-6471.

[3] Li, Z., Ma, Y., Lin, J., Gao, Z., Wu, S., Li, W., ... & Wang, J. (2022). **The polymorph and crystal habit control of dl-methionine assisted by ultrasound.** Journal of Crystal Growth, 596, 126818. https://doi.org/10.1016/j.jcrysgro.2022.126818.

[4] National Research Council. (2001). **Nutrient requirements of dairy cattle:** 2001. National Academies Press. https://doi.org/10.17226/9825.

[5] Mahotra, M., Yu, H., Xu, Q., Liew, W. C., Kharel, S., Tan, L. S. E., & Loo, J. S. C. (2022). **Solid lipid microparticles as leaching free, slow-release encapsulation system for methionine in aquaculture**. Aquaculture. https://doi.org/10.1016/j.aquaculture.2022.738342.

[6] Djerafi, R., Swanepoel, A., Crampon, C., Kalombo, L., Labuschagne, P., Badens, E., & Masmoudi, Y. (2017). **Supercritical antisolvent co-precipitation of rifampicin and ethyl cellulose.** European Journal of Pharmaceutical Sciences, *102*, 161-171. https://doi.org/10.1016/j.ejps.2017.03.016.

[7] REVERCHON, E., PORTA, G. D., ROSA, I. De, SUBRA, P., LETOURNEUR, D. (2000). **Supercritical antisolvent micronization of some biopolymers**. J. Supercrit. Fluids, 18, pp 238-245. https://doi.org/10.1016/S0896-8446(00)00069-3.

[8] Montes, A., Gordillo, M. D., Pereyra, C., & De La Ossa, E. M. (2011). **Co-precipitation of amoxicillin and ethyl cellulose microparticles by supercritical antisolvent process.** The Journal of Supercritical Fluids, 60, 75-80. https://doi.org/10.1016/j.supflu.2011.05.002

[9] Duarte, A. R. C., Gordillo, M. D., Cardoso, M. M., Simplício, A. L., & Duarte, C. M. (2006). **Preparation of ethyl cellulose/methyl cellulose blends by supercritical antisolvent precipitation**. International Journal of

Pharmaceutics, *311*(1-2), 50-54. doi:10.1016/j.ijpharm.2005.12.010.

[10] Prosapio, V., De Marco, I., Scognamiglio, M., & Reverchon, E. (2015). **Folic acid–PVP nanostructured composite microparticles by supercritical antisolvent precipitation.** Chemical Engineering Journal, *277*, 286-294. https://www.sciencedirect.com/science/article/pii/S1385894715006488.

[11] Junior, O. V., Cardoso, F. A. R., Giufrida, W. M., de Souza, M. F., & Cardozo-Filho, L. (2020). **Production and computational fluid dynamics-based modeling of PMMA nanoparticles impregnated with ivermectin by a supercritical antisolvent process.** Journal of CO_2 Utilization, *35*, 47-58. https://www.sciencedirect.com/science/article/pii/S2212982019301751

[12] Campardelli, R., & Reverchon, E. (2017). **Instantaneous coprecipitation of polymer/drug microparticles using the supercritical assisted injection in a liquid antisolvent.** The Journal of Supercritical Fluids, *120*, 151-160. https://www.sciencedirect.com/science/article/pii/S0896844616304351

[13] Machado, A. P. D. F., Rueda, M., Barbero, G. F., Martín, Á., Cocero, M. J., & Martínez, J. (2018). **Co-precipitation of anthocyanins of the extract obtained from blackberry residues by pressurized antisolvent process**. The Journal of Supercritical Fluids, *137*, 81-92. https://doi.org/10.1016/j.supflu.2018.03.013.

[14] Yan, T., Tao, Y., Wang, X., Lv, C., Miao, G., Wang, S., ... & Wang, Z. (2021). **Preparation, characterization and evaluation of the antioxidant capacity and antitumor activity of myricetin microparticles formated by supercritical antisolvent technology.** The Journal of Supercritical Fluids, *175*, 105290. https://www.sciencedirect.com/science/article/pii/S0896844621001303

[15] Sakata, G. S., Ribas, M. M., Dal Magro, C., Santos, A. E., Aguiar, G. P., Oliveira, J. V., & Lanza, M. (2021). **Encapsulation of trans-resveratrol in poly (ε-caprolactone) by GAS antisolvent.** The Journal of Supercritical Fluids, *171*, 105164. https://doi.org/10.1016/j.supflu.2021.105164

[16] Esfandiari, N., & Sajadian, S. A. (2022). **CO_2 Utilization as Gas Antisolvent for the Pharmaceutical Micro and Nanoparticle Production: A Review.** Arabian Journal of Chemistry, 104164. https://doi.org/10.1016/j.arabjc.2022.104164

[17] Boschetto, D. L., Aranha, E. M., de Souza, A. A. U., Souza, S. M. G. U., Ferreira, S. R., Priamo, W. L., & Oliveira, J. V. (2014). **Encapsulation of bixin in PHBV using SEDS technique and in vitro release evaluation.** Industrial Crops and

Products, 60, 22-29. https://doi.org/ 10.1016/j.indcrop.2014.05.050.

[18] Dal Magro, C., Aguiar, G. P., Veneral, J. G., dos Santos, A. E., de Chaves, L. M., Oliveira, J. V., & Lanza, M. (2017). **Co-precipitation of trans-resveratrol in PHBV using Solution Enhanced Dispersion by Supercritical Fluids technique**. The Journal of Supercritical Fluids, 127, 182-190. http://dx.doi.org/10.1016/j.supflu.2017.03.025.

[19] Aguiar, G. P. S., Arcari, B. D., Chaves, L. M., Dal Magro, C., Boschetto, D. L., Piato, A. L., ... & Oliveira, J. V. (2018). **Micronization of trans-resveratrol by supercritical fluid: Dissolution, solubility and in vitro antioxidant activity.** Industrial Crops and Products, 112, 1-5. https://doi.org/10.1016/j.indcrop.2017.11.008.

[20] Pessoa, A. S., Aguiar, G. P. S., Oliveira, J. V., Bortoluzzi, A. J., Paulino, A., & Lanza, M. (2019). **Precipitation of resveratrol-isoniazid and resveratrol-nicotinamide cocrystals by gas antisolvent**. The Journal of Supercritical Fluids, 145, 93-102. https://doi.org/ 10.1016/j.supflu.2018.11.014.

[21] Ribas, M. M., Sakata, G. S., Santos, A. E., Dal Magro, C., Aguiar, G. P. S., Lanza, M., & Oliveira, J. V. (2019). **Curcumin cocrystals using supercritical fluid technology**. The Journal of supercritical fluids, 152, 104564. https://doi.org/10.1016/j.supflu.2019.104564.

[22] Dias, J. L., Rebelatto, E. A., Hotza, D., Bortoluzzi, A. J., Lanza, M., & Ferreira, S. R. (2022). **Production of quercetin-nicotinamide cocrystals by gas antisolvent (GAS) process.** The Journal of Supercritical Fluids, 188, 105670. https://doi.org/10.1016/j.supflu.2022.105670.

[23] Lokhande, A. B., Mishra, S., Kulkarni, R. D., & Naik, J. B. (2013). **Preparation and characterization of repaglinide loaded ethylcellulose nanoparticles by solvent diffusion technique using high pressure homogenizer.** Journal of pharmacy research, 7(5), 421-426. http://dx.doi.org/10.1016/j.jopr.2013.04.049.

[24] McCarthy, T. E., & Sullivan, M. X. (1941). **A new and highly specific colorimetric test for methionine**. J. biol. Chem, 141(3), 871.

[25] Horn, M. J., Jones, D. B., & Blum, A. E. (1946). **Colorimetric determination of methionine in proteins and foods**. J. biol. Chem, 166, 313-320.

[26] Lima, N. K., Lopes, A. R., Guerrero Jr, P. G., Yamamoto, C. I., & Hansel, F. A. (2018). **Determination of volatile organic compounds in eucalyptus fast**

pyrolysis bio-oil by full evaporation headspace gas chromatography. Talanta, 176, 47-51. https://doi.org/10.1016/j.talanta.2017.08.008.

[27] Laurintino, T. N. S., Rebelatto, E. A., Dias, J. L., Oliveira, J. V., & Bolzan, A. (2022). **Precipitation of methionine and ethyl cellulose in carbon dioxide+ ethanol+ acetic acid systems at high pressures: phase equilibrium data for the GAS antisolvent process.** Fluid Phase Equilibria, 113650. https://doi.org/10.1016/j.fluid.2022.113650.

[28] Lan, C. H. E. N., & Zhepeng, L. I. U. (2008). **Microparticle Formation of Ethyl Cellulose Using Compressed CO2 Antisolvent Precipitations.** Tarım Makinaları Bilimi Dergisi, 4(3), 313-317. https://dergipark.org.tr/tr/download/article-file/119103.

[29] Li, B. G., Zhang, Y., Zhang, W. J., & Hua, Z. Z. (2008). **Supercritical CO_2 spray drying of ethyl cellulose (EC) for preparing microparticles**. Drying Technology, 26(4), 464-469. https://doi.org/10.1080/07373930801929441.

[30] Montes, A., Gordillo, M. D., Pereyra, C., De los Santos, D. M., & De La Ossa, E. M. (2014). **Ibuprofen–polymer precipitation using supercritical CO_2 at low temperature**. The Journal of Supercritical Fluids, 94, 91-101. http://dx.doi.org/10.1016/j.supflu.2014.07.001.

[31] Djerafi, R., Masmoudi, Y., Crampon, C., Meniai, A., & Badens, E. (2015). **Supercritical anti-solvent precipitation of ethyl cellulose**. The Journal of Supercritical Fluids, 105, 92-98. http://dx.doi.org/10.1016/j.supflu.2015.02.033.

[32] Franceschi, E., De Cesaro, A.M., Feiten, M., Ferreira, S.R.S., Dariva, C., Kunita, M.H., Rubira, A.F., Muniz, E.C., Corazza, M.L., Oliveira, J.V., 2008. **Precipitation of bcarotene and PHBV and co-precipitation from SEDS technique using supercritical CO_2**. Journal of Supercritical Fluids 47, 259–269. https://doi.org/10.1016/j.supflu.2008.08.002.

[33] Hu, D., Lin, C., Liu, L., Li, S., & Zhao, Y. (2012). **Preparation, characterization, and in vitro release investigation of lutein/zein nanoparticles via solution enhanced dispersion by supercritical fluids.** Journal of food engineering, 109(3), 545-552. doi:10.1016/j.jfoodeng.2011.10.025.

[34] Jin, H. Y., Xia, F., & Zhao, Y. P. (2012). **Preparation of hydroxypropyl methyl cellulose phthalate nanoparticles with mixed solvent using supercritical**

antisolvent process and its application in co-precipitation of insulin. Advanced Powder Technology, 23(2), 157-163. doi:10.1016/j.apt.2011.01.007.

[35] de Carvalho Neto, J. P., Bezerra, L. R., da Silva, A. L., de Moura, J. F. P., Pereira Filho, J. M., da Silva Filho, E. C., ... & Oliveira, R. L. (2019). **Methionine microencapsulated with a carnauba (Copernicia prunifera) wax matrix for protection from degradation in the rumen.** Livestock Science, 228, 53-60. https://doi.org/10.1016/j.livsci.2019.07.024.

[36] Reverchon, E., Adami, R., Caputo, G., & De Marco, I. (2008). **Spherical microparticles production by supercritical antisolvent precipitation: interpretation of results**. The Journal of Supercritical Fluids, 47(1), 70-84. https://doi.org/10.1016/j.supflu.2008.06.002.

[37] Aguiar, G. P., Magro, C. D., Carvalho, G. O., Santos, A. E., Lanza, M., & Oliveira, J. V. (2021). **Co-precipitation of anthocyanin in PHBV by the SEDS technique**. Journal of Food Science and Technology, 58(11), 4217-4224. https://doi.org/10.1007/s13197-020-04895-4

[38] Cocero, M. J., & Ferrero, S. (2002). **Crystallization of β-carotene by a GAS process in batch effect of operating conditions**. The journal of supercritical fluids, 22(3), 237-245. https://doi.org/10.1016/S0896-8446(01)00125-5.

[39] García-Casas, I., Montes, A., Pereyra, C., & De La Ossa, E. M. (2017). **Co-precipitation of mangiferin with cellulose acetate phthalate by Supercritical antisolvent process.** Journal of CO_2 Utilization, 22, 197-207. http://dx.doi.org/10.1016/j.jcou.2017.10.003.

[40] Ramachandran, E., & Natarajan, S. (2006). **Gel growth and characterization of β-DL-methionine.** Crystal Research and Technology: Journal of Experimental and Industrial Crystallography, 41(4), 411-415. DOI 10.1002/crat.200510595.

CHAPTER 5 – FINAL CONSIDERATIONS AND FUTURE STUDIES

Encapsulate methionine in ethyl cellulose by the GAS technique, using carbon dioxide as an antisolvent and ethanol and acetic acid as solvents, was successfully performed. The high-pressure liquid-vapor equilibrium for the quaternary systems CO_2 (1) + ethanol (2) + acetic acid (3) + solute (4) (methionine or ethyl cellulose) provided pioneering data on the behavior of the solutes and the visualization of the effects of dimerization. The influence of the interaction of the compounds involved in the systems and the interference of different concentrations of solutes on the behavior of phases were observed. The increase in solute concentration anticipated the presence of solids for smaller mass fractions of CO_2, where the solid phase was observed in mass fractions of 0.9383 (0.1 mg/mL) and 0.7251 (0.2 mg/mL) for methionine and 0.9530 (2.5 mg/mL) and 0.8997 (5.0 mg/mL) for ethyl cellulose, at the three temperatures evaluated (308.15-318.15-328.15 K). The thermodynamic modeling satisfactorily fitted the experimental phase transition data.

The encapsulating methionine in ethyl cellulose using the GAS technique provided pioneering and excellent results regarding the protection of methionine. The pressure, temperature, and mass ratio between methionine influenced the process, where temperature affected the precipitation yield and pressure affected encapsulation efficiency. MET/ETHYL ratio presented a positive effect on the yield and a negative effect on the EE. The GAS antisolvent technique was adequate, providing precipitation yield values reaching 84 % and encapsulation efficiency values above 99%. The characteristics of the particles formed in terms of morphology, size of particles, X-ray diffraction (XRD), Fourier transform infrared spectroscopy (FTIR), and differential scanning calorimetry (DSC) confirmed the presence of MET and the lack of chemical changes in the co-precipitation process. The particle sizes obtained in the precipitates were significantly smaller than those of the corresponding unprocessed materials. Thus, the co-precipitates presented excellent results regarding the protection of methionine and controlled release possible.

Future work in vivo release can be carried out to verify the reproducibility and bioavailability of methionine co-precipitates and confirm the milk production benefits in dairy cows. Furthermore, the mathematical modeling of release profiles can contemplate adequate representations of the release mechanisms involved in the process.

Furthermore, the effects of methionine supplementation on human health can be studied. Methionine is an essential sulfur-containing amino acid and plays a vital role in the production of important molecules such as antioxidants (e.g., glutathione, cystathionine), other non-essential amino acids (e.g., carnitine, cysteine, taurine, and creatine), methyl donors (e.g., S-adenosyl methionine) and phospholipids (e.g., phosphatidylcholine). Thus, methionine supplementation can modulate metabolism, oxidative stress, and inflammation in the organism showing therapeutic potential for treating diabetes and non-alcoholic fatty liver diseases, for example.

APPENDIX A – CALIBRATION CURVE CONSTRUCTED BY SPECTROPHOTOMETER (520 nm).

Figure 31 – Calibration curve for methionine quantification for analysis of encapsulation percentage and encapsulation efficiency.

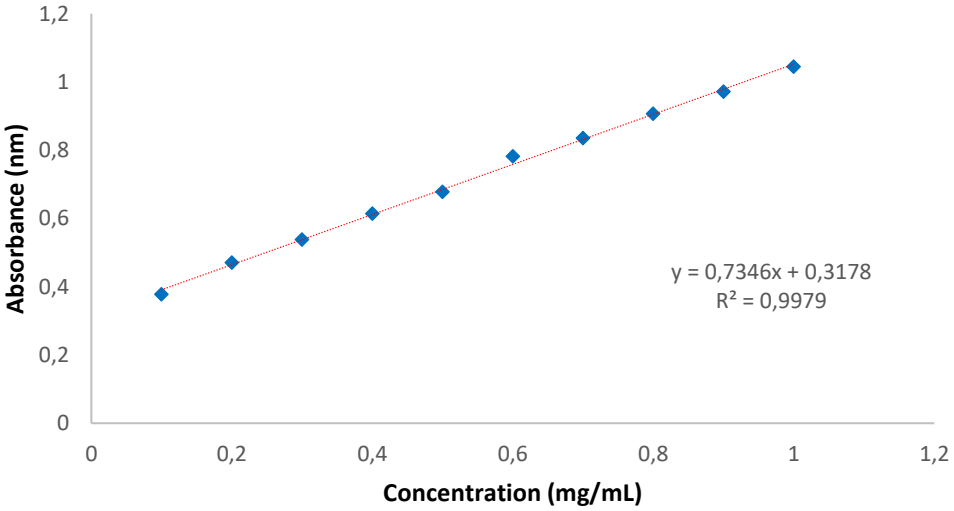

APPENDIZ B – CALIBRATION CURVES CONSTRUCTED BY CG-FID.

Figure 32 – Calibration curve for quantification of residual ppm of ethanol.

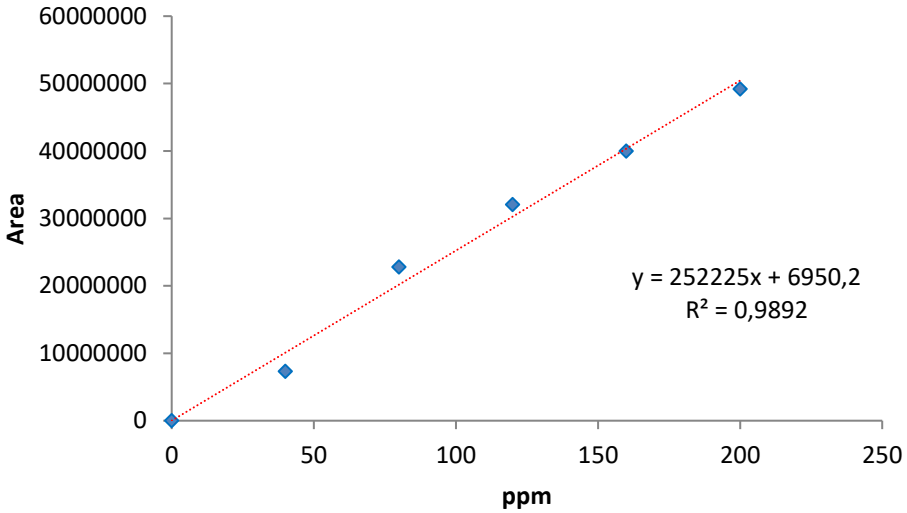

Figure 33 – Calibration curve for quantification of residual ppm of acetic acid.

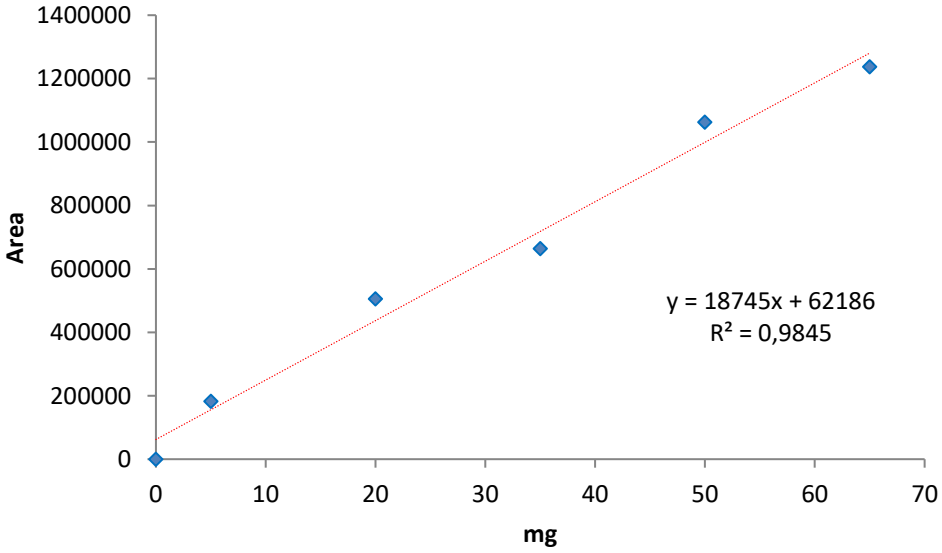

APPENDIZ C – DIAMETER DISTRIBUTION.

Figure 34 – Diameter distribution: RUN 1.

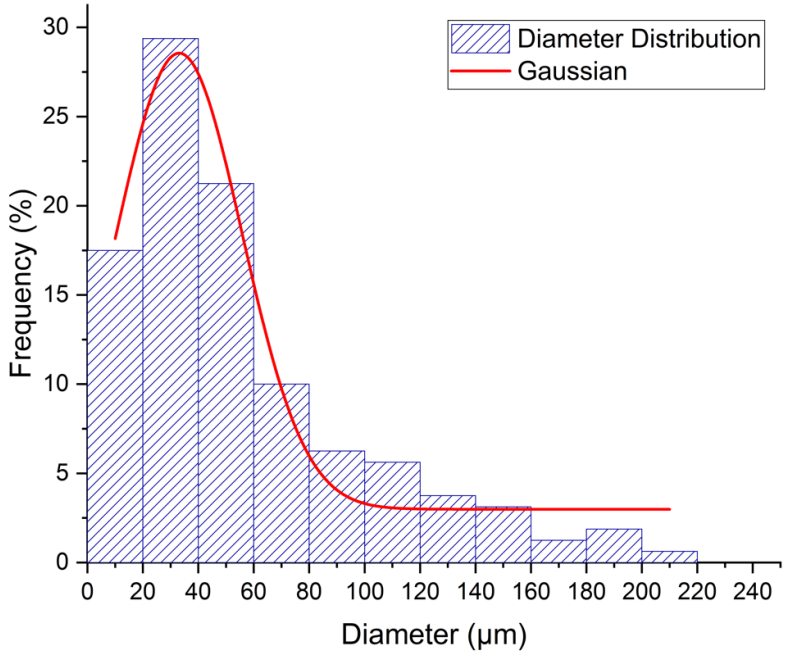

Figure 35 – Diameter distribution: RUN 2.

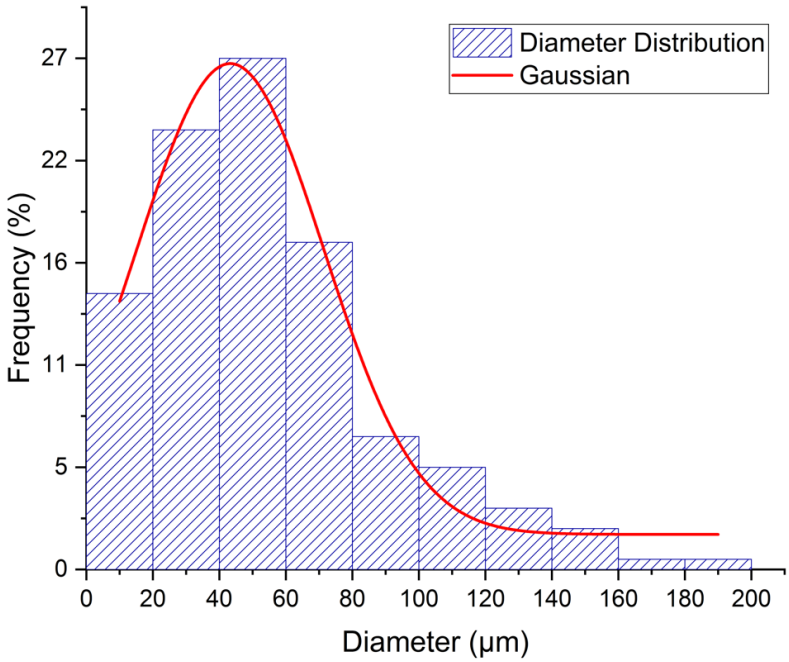

Figure 36 – Diameter distribution: RUN 3.

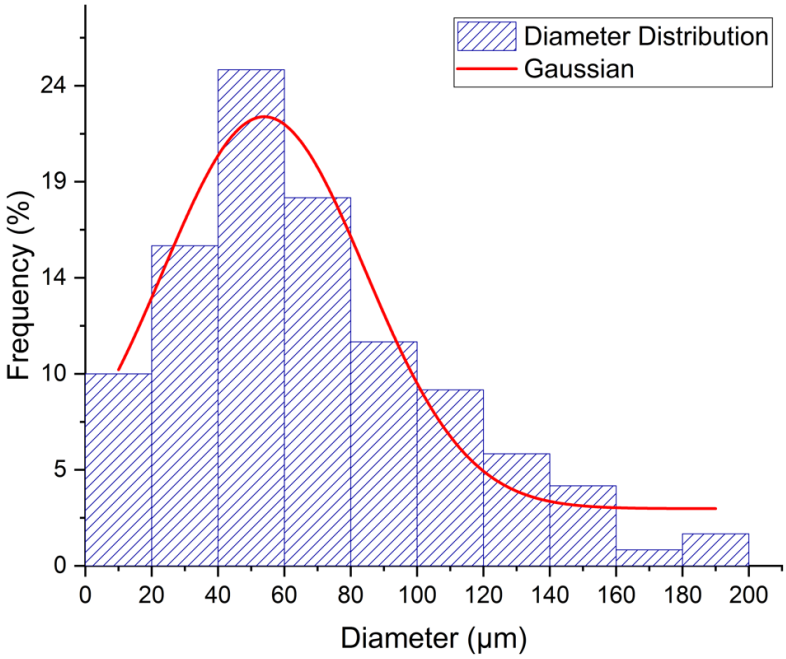

Figure 37 – Diameter distribution: RUN 4.

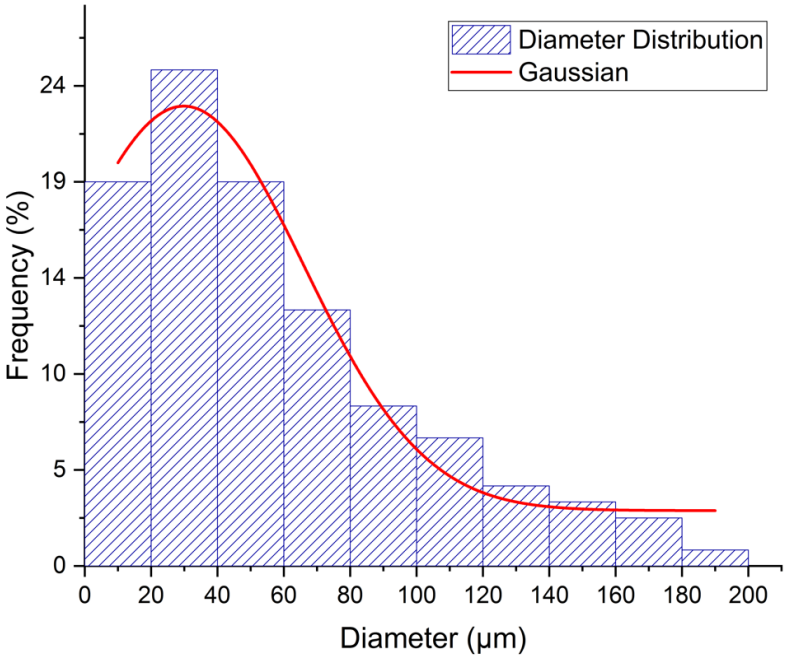

Figure 38 – Diameter distribution: RUN 5.

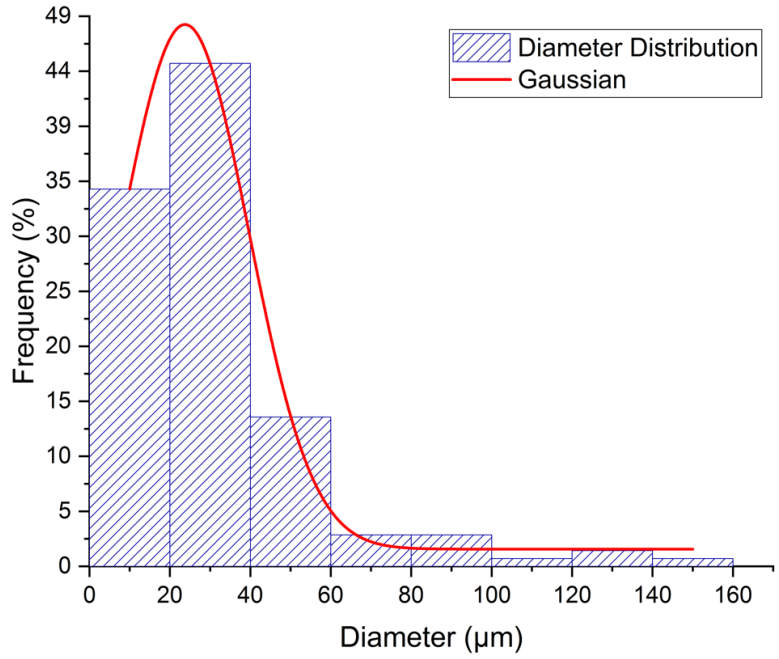

Figure 39 – Diameter distribution: RUN 6.

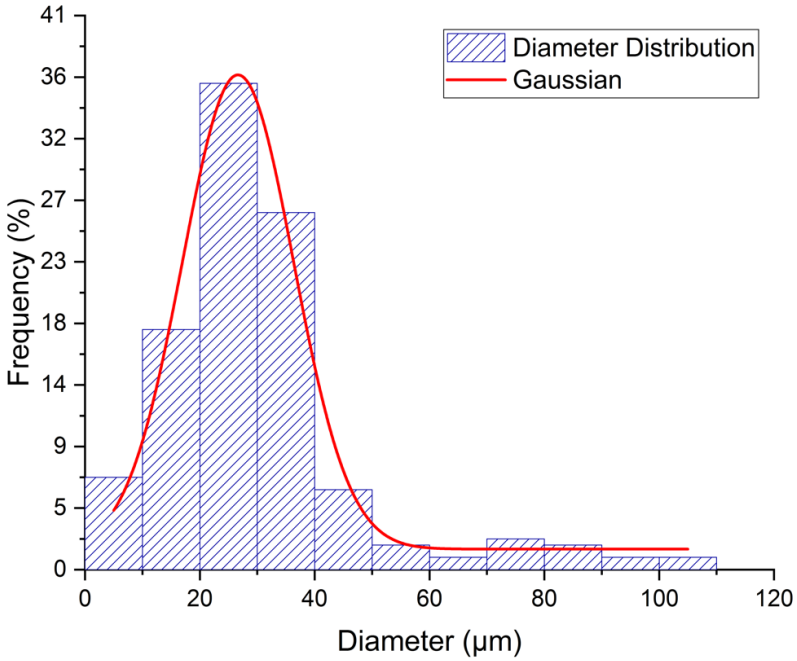

Figure 40 – Diameter distribution: RUN 7.

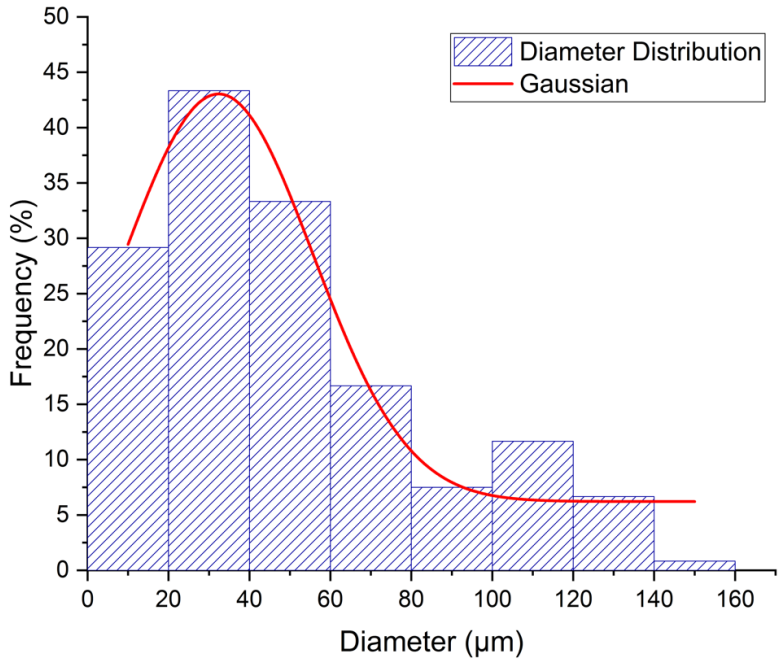

Figure 41 – Diameter distribution: RUN 8.

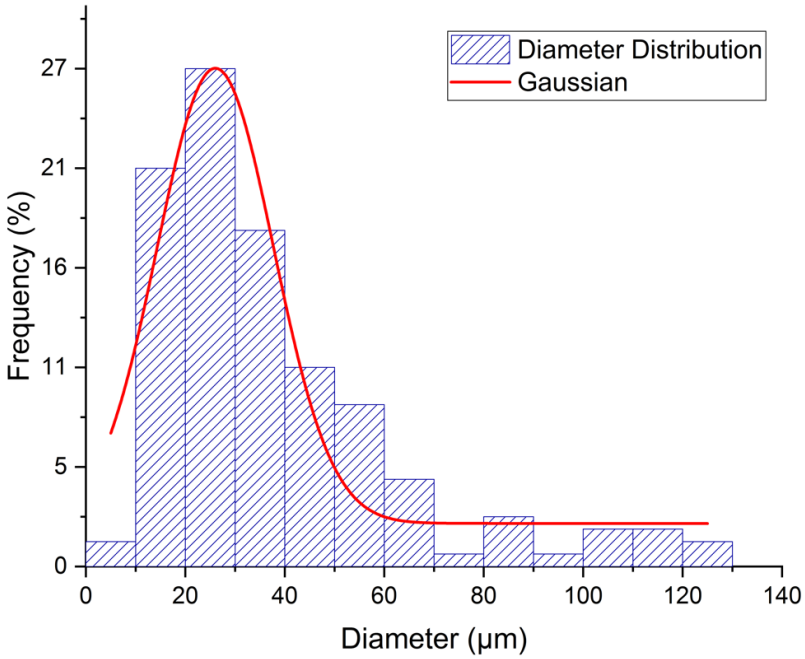

Figure 42 – Diameter distribution: RUN 9.

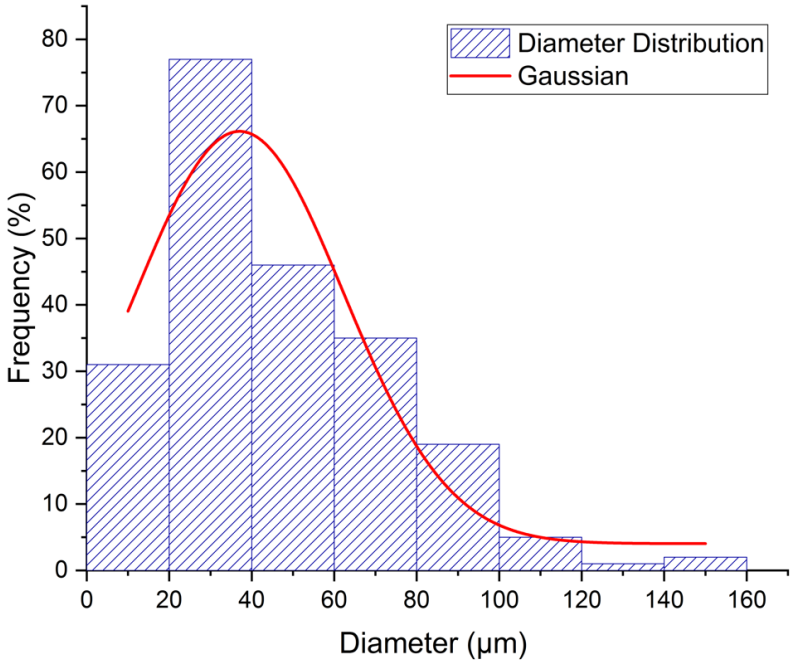

Figure 43 – Diameter distribution: MET.

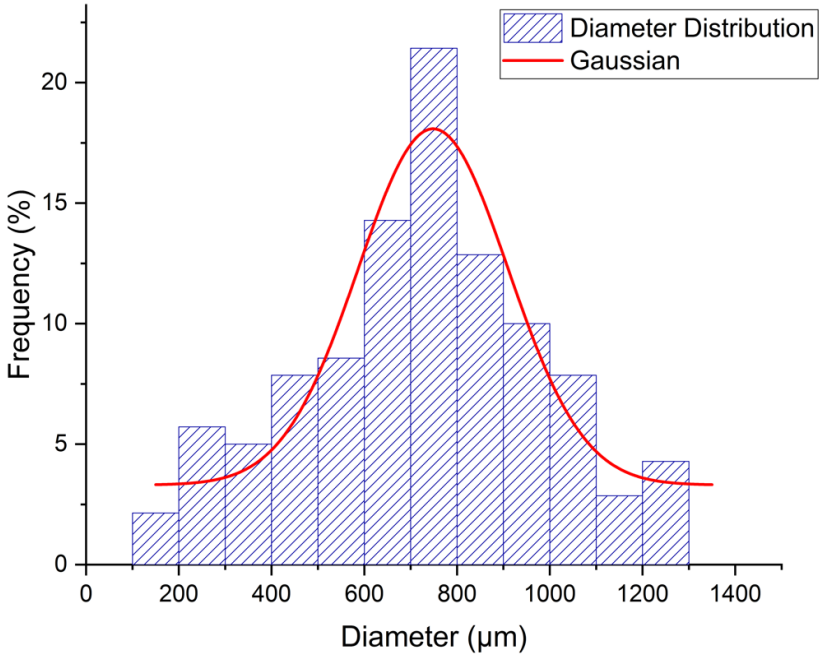

Figure 44 – Diameter distribution: ETHYL.